The Role of PTP4A3 Phosphatase in Microvascular Endothelial and Tumor Cells

Kelley Elizabeth McQueeney

Columbia, SC

Masters of Science in Biological and Physical Sciences, University of Virginia, Charlottesville, VA

Bachelors of Science in Biochemistry, Clemson University,
Clemson, SC

A Dissertation Presented to the Graduate Faculty of the University of Virginia in Candidacy for the Degree of Doctor of Philosophy

Department of Pharmacology

University of Virginia

February 2018

John S. Lazo, Ph.D.
Elizabeth R. Sharlow, Ph.D.
Thurl E. Harris, Ph.D.
Christopher A. Moskaluk, M.D., Ph.D.
David L. Brautigan, Ph.D.
Amy H. Bouton, Ph.D.

ABSTRACT

Cancer is a disease caused by errant cell signaling. Targeting the enzymes that control reversible phosphorylation is one strategy for correcting this aberration. The intracellular protein tyrosine phosphatase PTP4A3 is overexpressed in multiple human cancers and this correlates with poor patient prognosis and reduced survival. PTP4A3 also seems to regulate key malignant processes such as invasion, migration, and angiogenesis, suggesting a pivotal role in both cancer and endothelial signaling pathways. In the work presented here, I describe: (1) the creation and characterization of paired colorectal cancer cell lines expressing or lacking PTP4A3 protein, (2) the discovery and evaluation of JMS-053, the most potent PTP4A3 inhibitor known to date, and (3) the interrogation of PTP4A3 function in endothelial cells. In brief, the genetic loss of PTP4A3 or phosphatase inhibition by JMS-053 in tumor cells resulted in reduced colony formation, spheroid formation, migration, and adhesion. These phenotypes led me to uncover a previously unknown effect of this intracellular phosphatase on the expression of cellular adhesion proteins, most notably *Emilin 1,* which may be important for colorectal cancer. In addition, I show a role for PTP4A3 in promoting VEGF signaling, endothelial cell motility via Src activation and vascular permeability via RhoA activation. Thus, this dissertation presents novel concepts and reagents that facilitated the discovery of a relationship between PTP4A3 phosphatase activity and genes controlling extracellular matrix interactions, along with a contribution to endothelial cell barrier function through enhanced VEGF signaling. This suggests PTP4A3 inhibition may suppress tumor progression through actions on tumor and endothelial cells.

ACKNOWLEDGMENTS

I would like to express my gratitude to everyone involved in the completion of this dissertation. My time here has been the most professionally challenging and gratifying experience of my life. I consider myself fortunate to have conducted my graduate work at the University of Virginia.

The support and guidance of my mentor, Dr. John S. Lazo, has been paramount to my scientific development and personal growth. Dr. Lazo was earnestly dedicated to my training and has been an exemplary mentor. He was constantly willing to give his time in activities ranging from spending hours on a phone, going line by line through manuscript drafts to sitting shoulder to shoulder in the hood isolating endothelial cells. He has gone above and beyond in every aspect of his mentorship. I am unendingly grateful for everything that he has taught me. Dr. Lazo gave me reassurance when experimental challenges or unfavorable grant reviews shook my confidence. He taught me to be appreciative of the learning experience that failure provides. Upon joining Dr. Lazo's laboratory, I was privileged to work with Dr. Elizabeth R. Sharlow. Dr. Sharlow, one of the most skillful scientists I have ever met. Her door was always open. From Dr. Sharlow I have received invaluable scientific and professional counsel that I will carry with me into the next stages of my career.

Dr. Thurl Harris was one of the first University of Virginia faculty members I had the chance to know personally. His enthusiasm for science, kindness, and easygoing attitude quickly established him as both a scientific mentor and an unceasing advocate for my success. I have become accustomed to walking into Dr. Harris' office to ask for help with an experiment and, following a discussion of our shared assessment of the strength

of schedule (or lack thereof) in the SEC, walking out with detailed notes on how to execute my scientific plans. His co-mentorship has meant more to me than I can express and I am so thankful and proud to have been under his advisement.

The members of my thesis dissertation committee have been instrumental in my success as a graduate student and are all outstanding in their own regard. I found my committee meetings to be a constant source of motivation, comfort, and reassurance. Drs. Amy Bouton, David Brautigan, and Chris Moskaluk were all engaged and helpful during our regular meetings, but, supplemental to this, they each went above and beyond in making themselves available to me throughout my pre-doctoral career. Dr. Amy Bouton, in addition to her help with various scientific aspects of my project, was indispensable in the preparation and submission of my NIH fellowship. She is a fierce advocate for students and improves the graduate student experience not only through her overarching role in the BIMS program, but through personal interactions, which I feel fortunate to have been granted.

Dr. David Brautigan established himself as someone I could count on to provide me with relevant papers, useful reagents, or a general offer to come and discuss the best way to approach the question at hand. His fervid interest in advancing scientific discovery is evident in the time and energy he dedicates to the training of young scientists. I am pleased to have been one of these young scientists and for the opportunity to learn from him. Dr. Chris Moskaluk, too, exceeded the requisites that accompany the position of committee member. Despite his busy schedule, he always made time to meet with me if I requested help. These individuals have provided me with considerate, constructive evaluations that have vastly improved my research project.

I would also like to thank the members of the Lazo lab throughout the years. Specifically, Steph, Ana, Jennifer, Alex, Paula, and Bella. Aside from being excellent scientists, these individuals all made early mornings and late nights in lab a little bit more fun. Lastly, I would like to thank my friends and family for their love and boundless support of my enterprises. No matter what I do, they enthusiastically encourage my pursuits and I am eternally grateful.

TABLE OF CONTENTS

LIST OF FIGURES

LIST OF TABLES

ABBREVIATIONS

AOM	Azoxymethane
APC	Adenomatous polyposis coli
CDC25	Cell division cycle 25 family phosphatase
CRC	Colorectal cancer
DiFMUP	6,8-difluoro-4-methylumbelliferyl phosphate
DMEM	Dulbecco's minimum essential medium
DMSO	Dimethyl sulfoxide
DUSP	Dual-specificity phosphatase
EC_{50}	Effective concentration at 50% maximal response
ECM	Extracellular matrix
EGFR	Epidermal growth factor receptor
ERK	Extracellular signal-regulated kinase
FBS	Fetal bovine serum
GFP	Green fluorescent protein
HMVEC	Human microvascular endothelial cell
HUVEC	Human umbilical vascular endothelial cells
IC_{50}	Inhibitory concentration at 50% maximal response
KRT8	Cytokeratin 8

JSM-038
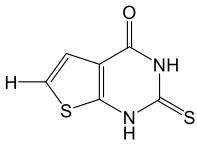
JMS-050
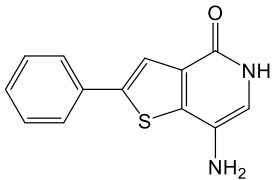
JMS-053
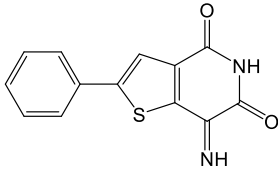
LPS	Lipopolysaccharide

MEF2C	Myocyte Enhancer Factor 2C
MMP	Matrix metalloproteinase
mTOR	Mechanistic target of rapamycin
MUC2	Mucin 2
MVEC	Primary human lung microvascular endothelial cells
NF-κB	Nuclear factor-κB
p130Cas	Crk-associated substrate
PBS	Phosphate buffered saline
PI3K	Phosphoinositide 3 kinase
PTEN	Phosphatase and tensin homologue
PTP	Protein tyrosine phosphatase
RFU	Relative fluorescence units
SD	Standard deviation of the mean
SEM	Standard error of the mean
SHP2	Src homology-2 domain containing phosphatase
STAT3/5	Signal transducer and activator of transcription
TEER	Trans-endothelial electrical resistance
TCGA	The Cancer Genome Atlas
TGFβ	Transforming growth factor beta
VEGF	Vascular endothelial growth factor

CHAPTER 1:   INTRODUCTION

1.1   Background and goals

1.1.1 Identification of problem: Well-credentialed targets needed for colorectal cancer therapies

The ensuing literature review will first present the pertinent information with regard to the protein tyrosine phosphatase (PTP) superfamily, PTP4A family phosphatases, and PTP4A3 phosphatase function and regulation. Then, I will discuss therapeutic strategies for the treatment of cancer in the form of currently approved angiogenesis inhibitors, PTP-targeted therapies seeking approval, and the available inhibitors of PTP4A3, which may guide the development of clinically beneficial small molecule PTP4A3 inhibitors. Finally, my overall hypothesis and the aims of my project will be discussed as a foundation for the studies that will be presented in this dissertation.

As a global regulator of cell activity, protein modifications by phosphorylation and dephosphorylation are central to cancer biology and treatment. Efforts to exploit changes in protein phosphorylation networks that drive tumor formation and progression led to an eruption of interest in kinases as potential molecular targets. Despite significant advances in our comprehension of cancer's molecular basis and the success of targeted kinase inhibitors, resistance to these therapies is increasingly problematic. Most cancers still remain largely fatal. Far less effort has been dedicated to manipulating the activity of phosphatases[1]. Members of the PTP superfamily have a central role in controlling the phosphorylation status and function of many eukaryotic proteins. Thus, it is unsurprising

that PTPs would be key participants in cancer[2]. Nonetheless, phosphatases were

previously thought to be "undruggable targets" and only recently has this notion begun to

erode[3,4]. With the transition of phosphatases from "undruggable" to "undrugged", a

concerted effort should be placed on the validation of phosphatases that are strongly

implicated in cancer.

1.1.2 Cancer impact: Colorectal cancer lethality

Cancer is the second leading cause of death in the United States. The National

Cancer Institute reports that in 2016 alone, approximately 1.7 million new cases of cancer

will be diagnosed[5]. In the United States, colorectal cancer (CRC) ranks as the third most

commonly diagnosed cancer and second leading cause of cancer death[6]. The 5-year

survival rate for localized CRC stages is 90%, but drops to 14% in patients with advanced

disseminated CRC, which is not amenable to surgery[7]. Recently, there has been a sharp

increase in the number of young adults diagnosed with a more advanced disease stage[8].

Thus, there is an urgent need for new molecular targets and therapies for CRC.

1.1.3 Goal of research

Protein Tyrosine Phosphatase 4A3 (PTP4A3) is a promising therapeutic target

because multiple human cancers have high expression of PTP4A3[9]; elevated PTP4A3

expression correlates with increased tumor invasiveness[10], and ectopic PTP4A3

expression enhances tumor cell migration and invasion *in vitro*[11]. There is a growing

body of evidence that PTP4A3 is a viable target to approach in the treatment of

CRC[9,10,12]. Moreover, PTP4A3 overexpression is observed in the tumor endothelium[13], and results in enhanced endothelial tube formation and migration *in vitro*[14], which suggests a role in tumor angiogenesis. Despite PTP4A3's strong association with malignancy and tumor progression, the mechanism by which it accomplishes this is unclear and it lacks potent, selective, phosphatase inhibitors to complete its pharmacological validation.

1.2 Protein Tyrosine Phosphatases and the Protein Tyrosine Phosphatase 4A family.

1.2.1 Protein Tyrosine Phosphatases (PTPs)

The PTP superfamily consists of 116 phosphatases that have been documented or are predicted, based on sequence homology, to catalyze the hydrolytic cleavage of phosphate groups on macromolecules; frequently from tyrosine, serine, and/or threonine residues on proteins[15,16]. The PTPs were initially classified based on the sequence of the active site, with the active site of first PTP to be isolated, PTP1B, serving as a means to classify proteins with unknown functions[17-19]. The PTP superfamily phosphatases require a Cys residue to act as the nucleophilic catalytic amino acid in the active site for hydrolysis of the phosphate group[15].The active site sequence of these Cys-based PTPs, referred to as the P-loop, contains the catalytic cysteine followed by a variable sequence of five amino acids and ended with an arginine residue (**C**xxxxx**R**)[12,15,20]. PTPs are differentiated into three classes, Class I: PTP family, Class II: low molecular weight

PTPs, and Class III: Cell division cycle 25s (CDC25s), and six sub-classes (Figure 1-1).

Subclass I-VI is composed of: VH1-like phosphatases, dual specificity phosphatases

(DUSPs), phosphoinositide phosphatases, PTP-like phytases, INPP4 phosphatases, and

TMEM55 phosphatases (Figure 1-1).

These PTPs regulate numerous cellular functions such as migration, immune

response, survival, proliferation and differentiation[12,21-23]. It is, therefore, explicable that

alterations in PTPs are often linked to human diseases, and specifically cancer. There is

evidence that PTPs can function as tumor suppressors including: phosphatase and tensin

homologue (PTEN), which dephosphorylates the lipid phosphatidylinositol 3,4,5-

trisphosphate and counteracts phosphatidylinositol 3 kinase (PI3K) signaling that can

dysregulate cell cycle progression and increase proliferation[24-27]; protein tyrosine

phosphatase receptor J, which directly dephosphorylates receptor tyrosine kinases that

can cause unconstrained growth and invasion[28,29], and DUSP6, which directly

dephosphorylates extracellular signal-regulated kinase (ERK) that can lead to enhanced

proliferation[30]. There is also a growing list of oncogenic PTPs including: Src homology-2

domain containing phosphatase (SHP2), which increases Ras dephosphorylation and

enhanced tumor growth and metastasis[31-35]; PTP1B, which is required for HER2-induced

breast cancer[36-40]; protein tyrosine phosphatase receptor ζ, which enhances stem cell-like

properties in glioblastoma causing increased tumorigenicity[41-43]; and PTP4A3, which will

be discussed in depth below[9,44-46]. Despite these observations, pharmacological validation

of many PTPs as therapeutic targets has been restricted by a scarcity of selective, potent,

cell active inhibitors or activators. As more PTP inhibitors and activators are discovered,

they will likely offer new insights into the consequences of perturbations in PTP activity

on normal physiological function as well as human disease.
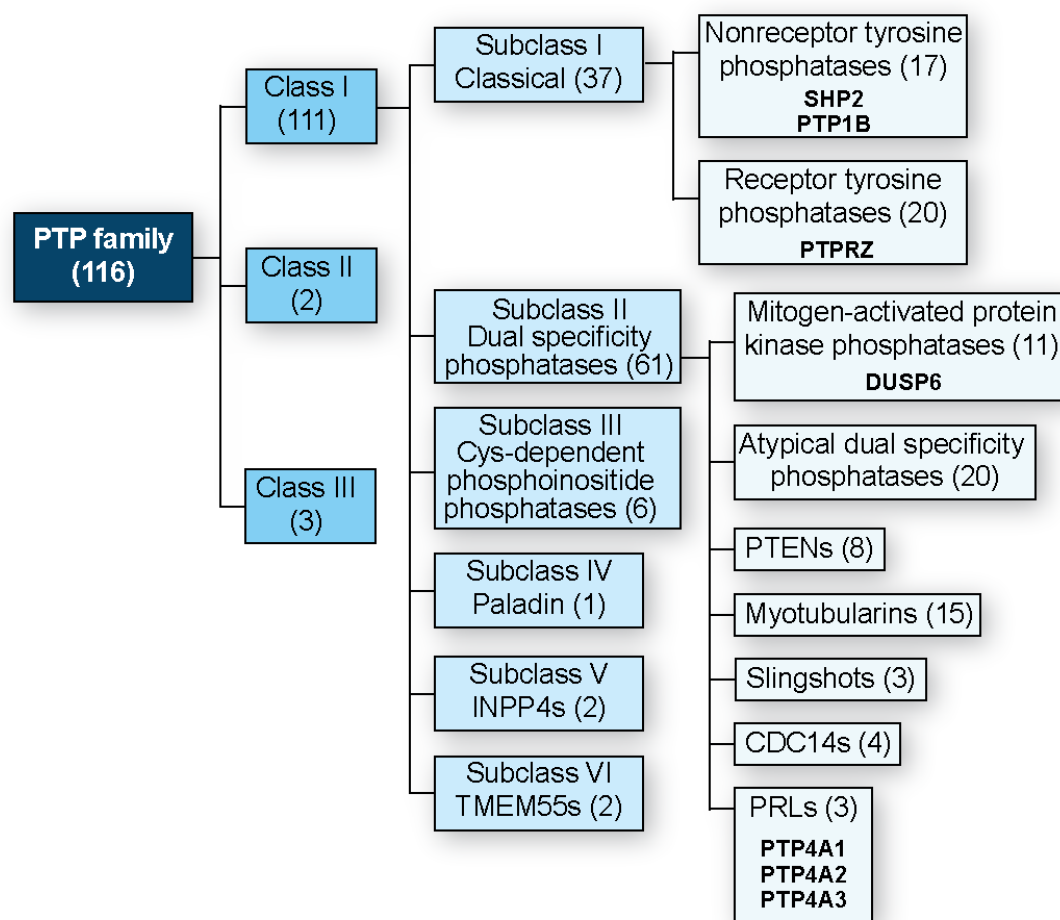
Figure 1-1 Human PTP classification.

The number of members belonging to each boxed family are indicated in parentheses.

Different colors represent different sub-classifications of the PTP family. Specific PTPs

mentioned in the text are emphasized in bold within the family to which they belong.

Figure inspired by Lazo et al.[47].

1.2.2 PTP4A family phosphatases

The PTP4A family of phosphatases, consisting of PTP4A1, -2 and -3, are members of Class I, subclass II (VH1-like DUSPs) Cys-based PTPs (Figure 1-1) and are the sole PTPs to contain a prenylation motif, facilitating PTP4A localization to the plasma membrane and early endosomes[48]. The seminal member of the PTP4A family, PTP4A1 (PRL-1), was first described as a gene whose expression increased in mitogen-stimulated cells following a partial hepatectomy in rodents[49], which is where the moniker Phosphatase of Regenerating Liver (PRL) family phosphatases derives its origin. PTP4A2 and -3 were later identified based on high degree of sequence identity, but unlike PTP4A1, high expression of PTP4A3 is not noted in regenerating liver cells[50].

All three members of the family (PTP4A1, PTP4A2, and PTP4A3) share a relatively small size (~22 kDa), high sequence identity (87 and 76% identity with PTP4A1 for PTP4A2 and PTP4A3, respectively), and the unique CAAX box, which facilitates the prenylation of the enzymes[48]. Figure 1-2 illustrates the amino acid sequence identity of the three family members and highlights the notable structural features. The key catalytic components, i.e., the P-loop (active site CxxxxxR) and the WPD-loop, are identical in PTP4A1-3. The removal of a phosphate group requires the insertion of the substrate phosphoamino acid into the catalytic pocket proximal to the Cys of the P-loop at the pocket's base. The nucleophilic attack of the active site Cys on the substrate phosphorus then breaks the phosphorus-oxygen bond and forms a covalent thiophosphate intermediate[51]. The Asp residue in the WPD loop then acts as the general acid required to donate a proton to the phenolic oxygen of the tyrosine residue of the substrate, facilitating transfer of the phosphate. The phosphate group is then transferred to

a water molecule by again using the WPD-loop Asp, which now functions as a general

base. It should be noted, however, that the shallow depth of the catalytic pocket and the

structural similarities to DUSPs such as PTEN, CDC14, and MKP indicate that the

PTP4A family may also be capable of dephosphorylating Ser and Thr residues as well[52].

Interestingly, in PTP4A3 the thiophosphate intermediate is extremely long lived and

results in the accumulation of PTP4A3 containing the phosphorylated catalytic Cys[53,54].

All three family members also contain a redox sensitive Cys residue that facilitates the

formation of a disulfide bridge with the catalytic Cys (Figure 1-2), further reducing their

enzymatic efficacy.

The PTP4A family members are thought to form trimers, which is important for

their cellular activity[12]. The proposed trimeric interface is identical between PTP4A1,

whose X-ray crystal structure initially suggested a trimeric structure[55-57], and PTP4A3.

The sequence of PTP4A2 in this region, however, differs by one amino acid (Figure 1-2).

It has also been suggested that the hydrophobic forces associated with the prenylation on

the CAAX box contributes to PTP4A oligomerization[58]. The prenylation, specifically

farnesylation, causes the localization of the protein to the plasma membrane and the

membrane of early endosomes[48], as well as the Golgi apparatus[59]. The polybasic region

proceeding the CAAX box was proposed to be a nuclear localization sequence in the

absence of prenylation, but upon treatment with farnesyl transferase inhibitors the protein

was found in neither the nuclear nor the plasma membrane fraction and instead in the

cytoplasm[57].

PTP4A1 and PTP4A2 appear to be expressed ubiquitously across all tissues[60],

while PTP4A3 is expressed at lower levels in most tissue and confined primarily to the

heart, skeletal muscle, brain, and vascular system[61]. Mice that lack PTP4A1 or PTP4A2 are grossly normal[46,62], however mice deficient in PTP4A2 experience placental insufficiency, impaired spermatogenesis, and defective hematopoietic stem cell renewal[63,64]. Moreover, transgenic mice engineered to overexpress PTP4A2 and activated rat c-Neu oncogene in mammary tissue exhibit accelerated development of mammary tumors[65]. Similar to results seen upon PTP4A1 and PTPA2 deletion, PTP4A3 targeted deletion produces viable mice with no gross abnormalities[46]. Significantly, fewer tumors were observed in a colitis-induced CRC model using azoxymethane (AOM) and dextran sodium-sulfate (DSS) treatment in PTP4A3 deficient mice compared to their wildtype littermates[46].
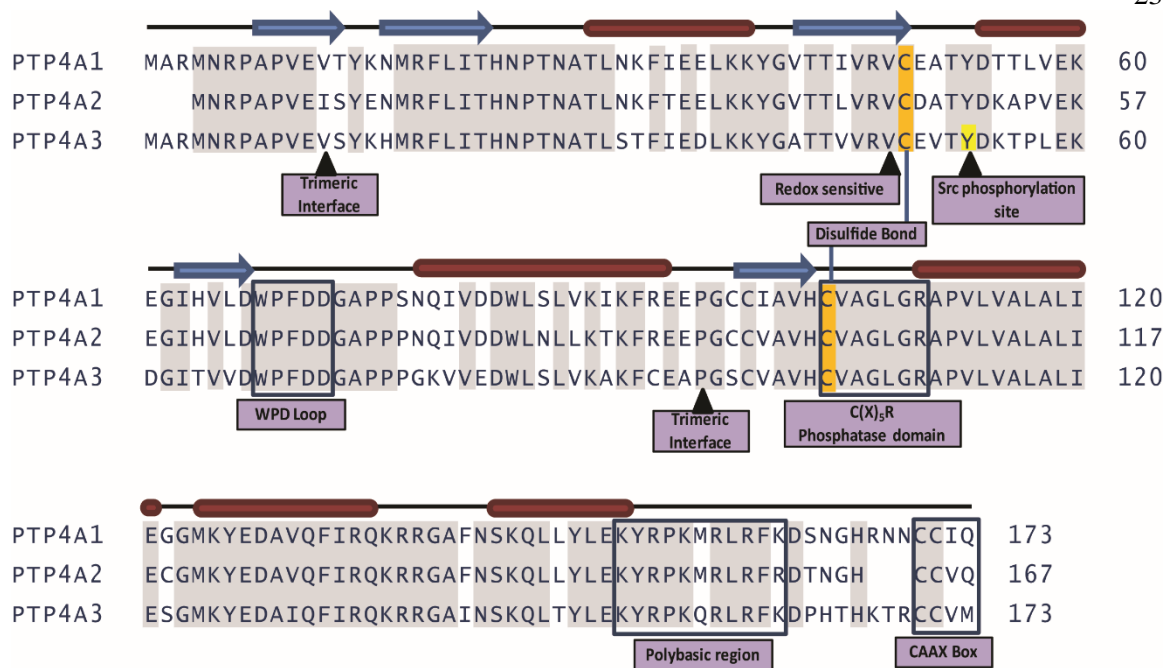
Figure 1-2 Human PTP4A family amino acid sequence alignment and common features of PTP4A1/2/3.

Identical amino acids are indicated in gray. Shown are common features or domains of PTP4A family members. Src phosphorylation site Y53 (highlighted in yellow) appears to be specific to PTP4A3. Blue arrows indicate β-strands and red bars indicate α-helical regions. The redox sensitive Cys residues are highlighted in orange. Figure from Sharlow *et al.*[51].

1.2.1 PTP4A family association with cancer

PTP4A1, 2, and 3 overexpression has been associated with numerous cancer types, highlighted in Figure 1-3. Interest in the family's association with cancer was first stimulated in 2001 when, in a set of 144 dysregulated genes, *Ptp4a3* was found to be the only gene consistently upregulated in metastatic liver lesions from CRC patients as measured by serial analysis of gene expression[9]. It was later found that not only liver metastases, but lung, brain, ovary, and lymph node metastatic lesions also exhibited high PTP4A3 expression and the level of PTP4A3 expression at the primary CRC tumor correlated with an increased instance of these lesions[66]. The findings with regard to PTP4A3 motivated subsequent studies looking at the expression of PTP4A1 and PTP4A2 in cancers. PTP4A2 overexpression in prostate cancer was identified shortly after the initial PTP4A3 findings[67]. Continued efforts have demonstrated increased expression of PTP4A family members in other malignancies (Figure 1-3) including melanoma, leukemia, ovarian, breast and lung cancer[68-72].

All three PTP4A family members are reported to promote the maintenance of the neoplastic phenotype, including survival, proliferation, invasion, migration, and angiogenesis[11,14,73-75]. This is in part due to the activation of growth and migration promoting signaling pathways such as ERK1/2, PI3K/AKT, Src, and Rho GTPase[21,46,51,76]. Unfortunately, the underlying mechanisms by which overexpression of the PTP4A family promotes cancer is poorly understood, due in part to the ambiguity surrounding the identity of the substrate(s) for any of the family members.
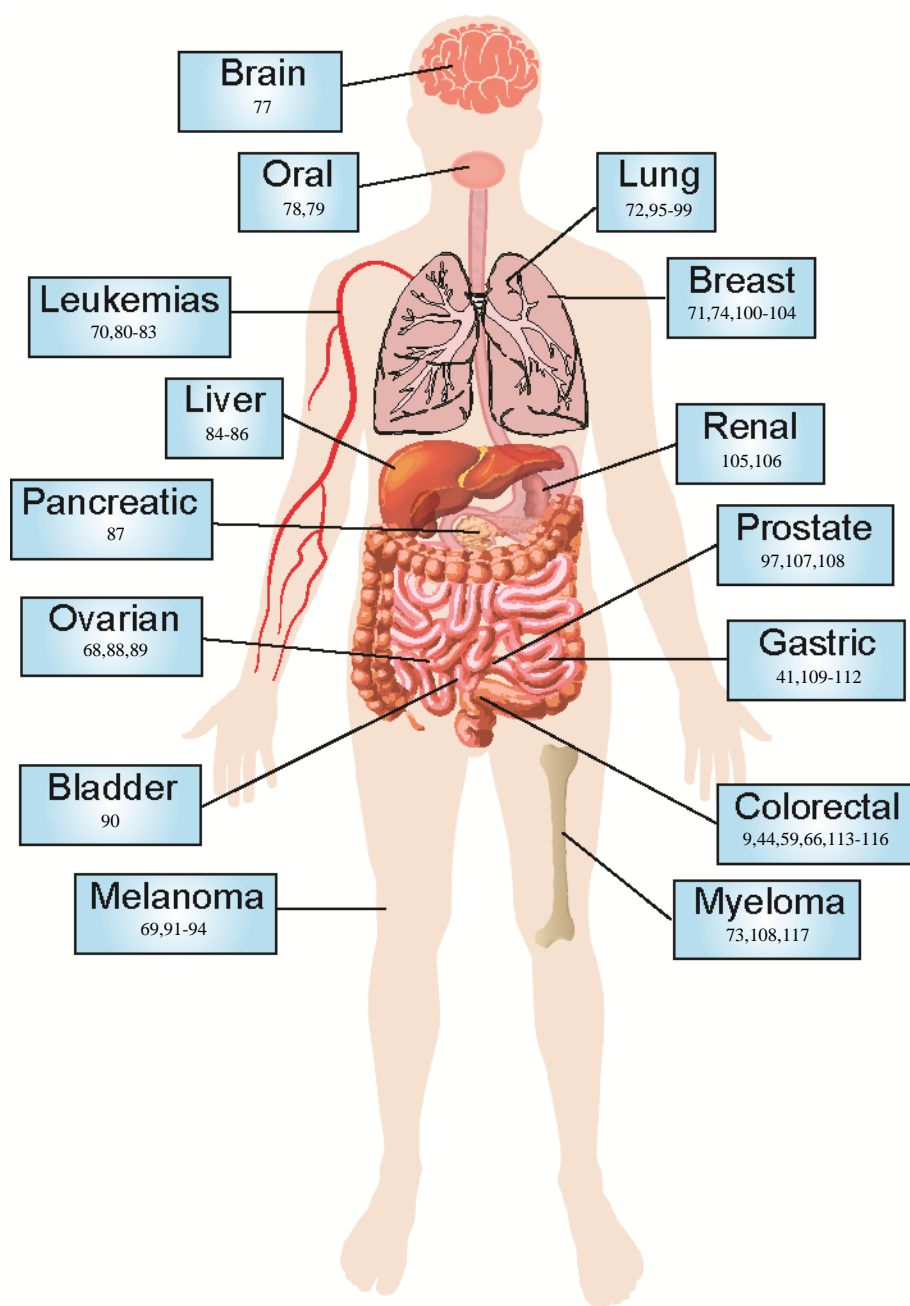
Figure 1-3 PTP4A3 expression in human cancers.

The figure demonstrates the cancer types in which PTP4A3 is reported to be

overexpressed. The associated references are listed in the boxes below the cancer type.

1.2.2 PTP4A3 regulation and signaling mechanisms in cancer

Increased expression of PTP4A3 in malignant cells, at both the gene and protein level, appears to be attributable to multiple mechanisms. For example, changes in PTP4A3 expression in CRC may be caused by the loss of transforming growth factor beta (TGFβ) signaling[118], which is frequently observed in human CRC[119]. In the absence of TGFβ, SMAD3/4 fails to inhibit PTP4A3 gene transcription. PTP4A3 transcription regulation is also controlled by the tumor suppressor p53, which activates its expression[120]. Thus, the C2H2-type zinc finger family protein Snail binds the PTP4A3 promoter and drives transcription in CRC cells[121]. In acute myelogenous leukemia and myeloma cells, the signal transducer and activator of transcription 3 (STAT3) can also increase PTP4A3 gene transcription[70,73,83]. PTP4A3 may be participating in a positive feedback loop with both Snail and STAT3, as it has been shown that increased PTP4A3 expression decreases E-cadherin expression resulting in increased Snail protein in CRC cells and phosphorylated STAT3[121]. In myeloma cells, the PTP4A3-mediated increase in STAT3 phosphorylation facilitates the formation of dimers and translocation of STAT3 to the nucleus, which is important because many of the STAT3 target genes are implicated in tumorigenic processes such as migration, invasion and proliferation[73,122,123].

Post-transcriptionally, poly C-binding protein 1 (PCBP1) can downregulate PTP4A3 translation by binding to the 5'-UTR region of the mRNA transcript[124]. The degradation of PTP4A3 is also post-translationally regulated[125]. This was first shown in HCT116 CRC cells and MCF-7 breast cancer cells through the binding of FK506-binding protein 38 (FKBP38) to PTP4A3, which leads to the proteasomal degradation of PTP4A3[126]. It was later shown in CRC cell lines that the deubiquitinating enzyme

ubiquitin specific protease 4 (USP4), which is also known to regulate the stability of p53 and TGFβ, interacts with and deubiquitinates PTP4A3[127]. In addition, in CRC patient samples there is a positive correlation between PTP4A3 and USP4 protein expression levels indicating that the stabilization of PTP4A3 by USP4 may be occurring *in vivo*[127].

There are numerous reports of PTP4A3 promoting pro-oncogenic signaling pathways and in some cases this effect may depend on more than increases in transcription or translation. PTP4A3, but not PTP4A1 or PTP4A2, is phosphorylated on Tyr53 (Figure 1-2) in CRC cells and this phosphorylation is executed by Src protein tyrosine kinase[50,76]. This may indicate the existence of a positive feedback loop for Src activation in malignant cells, as PTP4A3 is known to activate Src through inhibition of its regulatory protein tyrosine kinase C-terminal Src kinase (Csk)[11]. This Csk inhibition appears to occur due to increased elongation initiation factor 2 (eIF2) Ser51 phosphorylation (as seen in Figure 1-4 in which the red line originating from PTP4A3 represents inhibition of phosphorylation), which facilitates the translation of Csk, and is phosphatase-dependent, as the Cys104Ser catalytic PTP4A3 mutant did not elicit the response[11,128]. Notably, it has been proposed that eIF2 is a direct substrate of PTP4A3, based on reduced Tyr phosphorylation in HCT116 CRC cells ectopically overexpressing PTP4A3, but there is an absence of any additional direct *in vitro* evidence and the reduced phosphorylation could be an indirect effect[129].
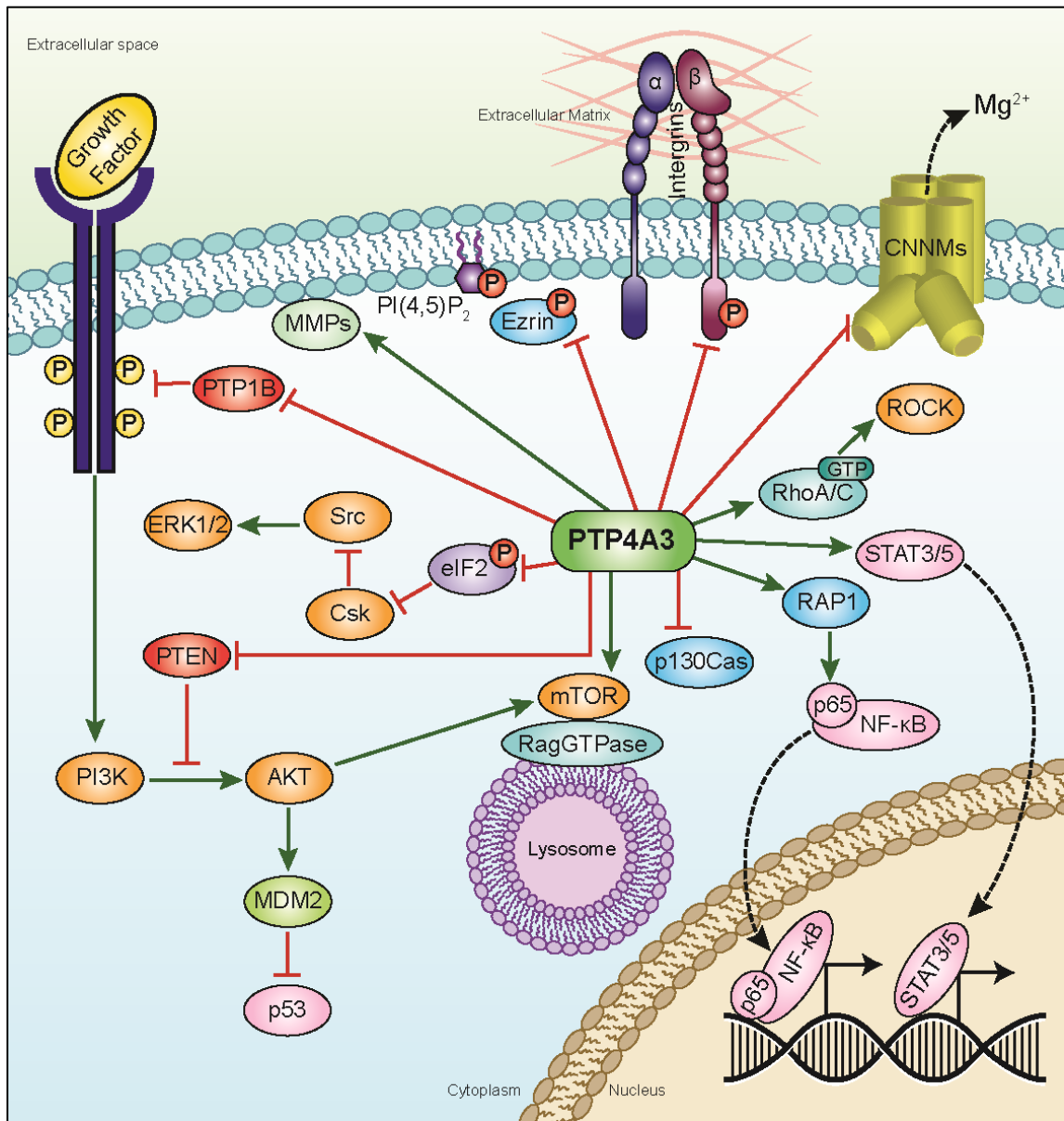
Figure 1-4 The impact of PTP4A3 on cell signaling.

A summary of the impact of PTP4A3 in malignant cells as determined by ectopic

PTP4A3 overexpression, PTP4A3 knockdown, and the use of PTP4A3 inhibitors

chronicled in the literature. It is recognized that cross-talk occurs between many of the

included molecules (for instance c-Src phosphorylation of STAT3 or p130Cas). The

figure is only meant to illustrate direct reported effects of PTP4A3. Potential PTP4A3

substrates presented in the literature are highlighted by the addition of a red "P" attached

to the molecule; green arrow = activation of function/expression, red line = inhibition of

function/expression, black dashed line = change in localization. With the exclusion of

PTP4A3, depicted in green, molecules are colored based on the family to which they

belong. Orange = kinases, pink = transcription factors, red = phosphatases, blue = adaptor

proteins, and teal = GTPases. Abbreviations listed on pages 12-13.

PTP4A3 regulation of Src family kinases is observed in multiple cancer types, including myeloma, breast, and CRC, and it has been suggested that Src tyrosine kinase is the primary intracellular signaling molecule responsible for the PTP4A3-induced changes in signal transduction[101,117,130,131]. In multiple myeloma cells interleukin-6 stimulates an increase in PTP4A3 expression that leads to activation of both Src and Src family kinases LYN and HCK[73,117]. In CRC cells, PTP4A3 overexpression induces Src activation, which results in EGFR hyper-activation[130].

Rho GTPases have a well-defined role in the regulation of cytoskeletal dynamics. These, in turn, impact cell cycle progression and proliferation, migration, invasion, and metastasis, which are all key aspects of cancer initiation and progression (reviewed in[132,133]). PTP4A3's impact on Rho GTPases was first shown in SW480 CRC cells, in which overexpression of PTP4A3 increases the amount of GTP-bound RhoA and RhoC that then require Rho effector Rho kinase (ROCK) to drive increased cell migration and invasion[134]. Phosphorylation of PTP4A3 at Tyr53 by Src kinase is required to promote RhoC activation by PTP4A3 as demonstrated by mutation of the Tyr residue and the use of a Src inhibitor[76]. Similarly, in triple negative breast cancer excess PTP4A3, concomitant with the increase in Src activation, promotes RhoA activation leading to actin filament rearrangement and enhanced invasion[101].

PTP4A3 activates the PI3K/AKT pathway, which plays a vital role in cell growth and survival and is frequently hyper-activated in cancer. In CRC cells, PTP4A3 can down-regulate PTEN resulting in an increase in AKT phosphorylation[116]. In addition, it was recently shown that gastric carcinoma samples with high PTP4A3 expression have an increased phospho-PTEN:PTEN ratio[109]. In a gastric cancer cell line, PTEN

expression and the phospho-AKT:AKT ratio depend on the presence of PTP4A3 catalytic activity[109]. In ovarian cancer cells, PTP4A3-mediated hyper-phosphorylation of AKT is autophagy dependent, and cells deficient in necessary components of autophagosome nucleation, PIK3C3, BECN1, or ATG6, do not experience enhanced proliferation or AKT activation upon PTP4A3 overexpression[135].

While the studies discussed above implicate PTP4A3 in proliferation, it has also been suggested that the primary effect of PTP4A3 is not on cell growth but instead resisting cell death. There are numerous reports of PTP4A3 overexpression resulting in anti-apoptotic effects in malignant cells[110,117,118,120,136,137]. One of the first mechanisms suggested for the PTP4A3-induced resistance of apoptosis is through Crk-associated substrate (p130Cas), and independent of p53 activity, by (1) downregulation of phosphorylated and total p130Cas and (2) increased levels of the 31kDa cleaved p130Cas fragment, which can be translocated to the nucleus and act as a transcriptional repressor leading to anoikis[138,139]. This p53-independence was disputed by another group who showed that ectopic overexpression of PTP4A3 reduced the total p53 protein in HCT116 CRC cells through the activation of AKT and ensuing increase in E3 ubiquitin ligase MDM2 phosphorylation which then targets p53 for degradation[140].

PTP4A3-mediated cellular resistance to apoptosis are likely to be caused by alterations in the signaling pathways discussed above, such as hyper-activation of AKT and Src. It has also been proposed that PTP4A3 promotes anti-apoptotic, pro-survival, and pro-invasive signaling through stimulation of nuclear factor-κB (NF-κB) pathway activation. Lian and colleagues demonstrated in CRC and gastric cancer cells that PTP4A3 interacts directly with Repressor/activator protein 1 (RAP1), which regulates the

recruitment of IκB kinases to p65 and increases phosphorylation of the p65 subunit of

NF-κB (Figure 1-4)[141]. NF-κB activation was also shown to be important for the

relationship between CRC cells and tumor-associated macrophages co-cultured *in vitro*

through the PTP4A3-induced expression of calcium channel KCNN4, driven by NF-κB

binding to the KCNN4 promoter, in both cell types, which facilitates tumor-associated

macrophage-stimulated CRC cell invasion by an interleukin-6/8 dependent

mechanism[142]. NF-κB in triple negative breast cancer transcriptionally regulates PTP4A3

expression, presenting another positive feedback loop regulating PTP4A3 expression in

cells[100]. NF-κB pathway activation is heavily linked to tumor associated inflammation

and thought to enhance tumorigenesis by triggering the accumulation of immune cells,

which compromise tissue homeostasis, implicating PTP4A3 in creating an environment

that promotes tumor formation.

PTP4A3 expression has been implicated in the signal transduction pathways

guiding cell migration and motility. For example, matrix metalloproteinase (MMP)

family proteins are responsible for the localized degradation and turnover of the extra

cellular matrix (ECM), a required proteolytic event for migration and invasion. PTP4A3

overexpression has been shown to modulate multiple MMPs (Figure 1-4). PTP4A3-

induces increased MMP14 accumulation at the cell membrane leading to increased

melanoma invasion[143]. Ectopic overexpression of PTP4A3 in LoVo CRC cells increased

MMP2 activity resulting in increased migration[144]. In DLD-1 CRC cells PTP4A3-

mediated MMP7 expression drives increased cell migration and invasion, but increased

PTP4A3 expression also increased MMP2, MMP13, and MMP14 expression[145]. Further

evidence of PTP4A3 regulation of MMP2 is seen in gastric carcinoma, wherein the

protein expression of MMP2 and MMP9 are increased upon ectopic overexpression of

PTP4A3 resulting in increased migration and invasion[109]. More recently, PTP4A3 ectopic

over expression in breast cancer cell line MCF-7 was observed to increase the mRNA

expression of MMP-9[146]. Collectively, these results suggest a prominent role for PTP4A3

in mediating this key family of ECM-interacting proteins.

In addition to MMPs, PTP4A3 expression and activity have been suggested to

impact integrin signaling, which functions to both bind and respond to the ECM

surrounding the cell. Integrin α1 interacts *in vitro* with PTP4A3, which was first

demonstrated in a yeast two-hybrid screen[147]. Subsequently, it was reported that in CRC

cells PTP4A3 also interacts with integrin β1, which heterodimerizes with integrin α1[144].

Integrin β1 is another of PTP4A3's proposed direct substrates based on a reduction of

integrin β1 Tyr783 phosphorylation (as seen in Figure 1-4 in which the red line

originating from PTP4A3 represents inhibition of phosphorylation) after transfection of

CRC cells with wildtype, but not catalytically inactive, PTP4A3[148]. Moreover, Tyr783

dephosphorylation increases integrin β1 binding to Src kinases, thereby increasing

integrin dimerization and reducing the coupling of integrins to actin[148]. In uveal

melanoma cells, PTP4A3 can interact with integrin β1 and impair its clustering in focal

adhesions on a collagen I matrix through the regulation of focal adhesion kinase (FAK)

phosphorylation at Tyr397[91]. Interestingly, the binding of PTP4A3 to integrin β1 is

enhanced by the silencing of integrin α1[148]. PTP4A3 knockdown in ovarian cancer

increased the level of integrin α2, but not integrin β1, at the cell surface due to an

increase in the transcriptional regulator c-Fos[88]. Along with transcriptional regulation of

integrins, PTP4A3 can increase the recycling of integrin α5 through PTP4A3 associating with ADP-ribosylation factor 1 in endocytic vesicles[59].

One of the first potential PTP4A3 substrates discussed in the literature is the cytoskeletal linker protein Ezrin[149]. The initial study used overexpression of PTP4A3 in CRC cells in combination with *in vitro* phosphatase assays to show Ezrin dephosphorylation at Thr567, and dephosphorylation at this site was later observed with 2D difference gel electrophoresis combined with diamond Pro-Q staining[129,149]. Ezrin is heavily implicated in tumor metastasis. It is a key component of the Ezrin-Radixin-Moesin complex, which connects the plasma membrane to the actin cytoskeleton and requires phosphatidylinositol(4,5)bisphosphate (PI(4,5)P_2), another proposed PTP4A3 substrate based on *in vitro* lipid phosphatase assays, to be activated at the plasma membrane[150,151]. Phosphorylation of Thr567 on Ezrin is necessary for proper cycling of Ezrin between active and inactive states required for the regulation of cytoskeletal dynamics. Ezrin cross-links membrane proteins to actin filaments via a cytoplasmic protein, Na^+/H^+ exchanger regulating factor 1, which acts as a scaffold. This provides another connection between PTP4A3 and Ezrin function, as it has been observed in melanoma cells that PTP4A3 increases Na^+/H^+ exchanger regulating factor 1 serine dephosphorylation causing an increased concentration of the Ezrin-complex scaffold protein in the cytoplasm[69].

PTP4A3 has also been proposed to directly dephosphorylate Ser73 and Ser431 on the intermediate filament protein Cytokeratin 8 (KRT8) based on results with SW480 CRC cells over expressing wildtype and catalytically inactive PTP4A3[152,153]. A direct interaction can be observed between PTP4A3 and KRT8 using a pull-down assay and

enhanced KRT8 phosphorylation upon treatment of cells with a PTP4A3 inhibitor[153]. It was later shown that the dephosphorylation and subsequent downregulation of KRT8 causes reduced cell migration[152]. Cytokeratins direct E-cadherin to the plasma membrane, a process important for the epithelial-mesenchymal transition[154]. The phosphorylation status of cytokeratins controls the assembly and disassembly of the insoluble and soluble pools of intermediate filaments within the cytoskeletal framework, thus providing yet another link of PTP4A3 to the cytoskeleton.

While interactions with molecules, such as Ezrin and KRT8, provide evidence for the influence of PTP4A3 the architecture of the plasma membrane, recent studies also show that PTP4A family proteins bind to magnesium transporters of the cyclin M family (CNNM) embedded directly in the plasma membrane. The binding of PTP4A proteins to these CNNM transporters regulates intracellular magnesium homeostasis by increasing intracellular magnesium levels (Figure 1-4) through a mechanism independent of its direct phosphatase activity[53,74,155-157]. These intracellular magnesium levels are typically tightly regulated and disruption of magnesium homeostasis has been shown to enhance tumor progression and dysregulate energy metabolism[158-160]. PTP4A3 binding to the intracellular Bateman domain of CNNM3 and CNNM4 has been demonstrated, and requires the PTP4A3 active site for this association[53,155,156]. There is, however, some disagreement as to whether the PTP4A-CNNM relationship regulates magnesium efflux[53,156-158] or influx[74,155] from the cell, although there appears to be general agreement that the PTP4A-CNNM complex can increase intracellular magnesium levels.

The metabolic reprogramming of cells is another hallmark of cancer that appears to be impacted by PTP4A3. PTP4A3 expression drives IL-8 secretion in CRC cells

leading to increased glucose consumption and lactate production[161], which is a hallmark

of cancer cells[162]. Additionally, there is strong evidence supporting PTP4A3 hyper-

activation of the mammalian target of rapamycin (mTOR) in cancer cells, which

regulates cell growth and response to growth factors and nutrients[77,130,163]. PTP4A3

increases mTOR activity indirectly through activation of Akt as well as through an Akt-

independent mechanism that activates the kinase via localization to the lysosome by

increasing mTOR affinity for RagGTPase heterodimers and Rheb-mediated activation[163].

While it is clear that altered PTP4A3 expression has a profound effect in malignant cell

types, there is evidence suggesting that it may also be modulating signaling pathways in

surrounding stromal cells that the tumor requires for survival and invasion.

1.2.3   *PTP4A3 in the endothelium*

The invasive potential of multiple cancer types is governed by interactions with

stromal cells, which regulate processes, such as tumor cell migration and gene

expression, through the release of both stimulatory and inhibitory factors. The tumor

microenvironment includes cancer-associated fibroblasts, immune cells, vascular and

lymphatic networks, as well as the extracellular matrix, which an expanding tumor

requires during tumorigenesis. PTP4A3 also participates in tumor stromal cell function

and is highly expressed in the tumor-associated endothelium[14,44], which has a central role

in the formation of metastases and angiogenesis[98]. PTP4A3 mRNA is observed in the

vasculature of invasive breast carcinomas but not in endothelium of normal breast

tissue[164]. The altered microenvironment in tumors, including high concentrations of the

potent vasodilator vascular endothelial growth factor (VEGF), creates a dysfunctional

endothelium, which loses critical barrier properties and results in leaky blood vessels in

and around the tumor. These leaky blood vessels no longer effectively block the

movement of cells in or out of the blood. For a tumor cell to metastasize it must detach

from the primary tumor and enter circulation; therefore, the disruption of endothelial

barrier function, which can be induced by high concentrations of VEGF, is essential for

extravasation. To a large extent, endothelial barrier integrity is regulated by the small

GTPase RhoA, a known PTP4A3 signaling effector. Angiogenesis, one of the hallmarks

of cancer, is dependent on an intricate network of growth factors and signaling pathways

to accomplish the complex process of forming new blood vessel[162]. High PTP4A3 protein

levels are observed in fetal heart tissue and developing blood vessels but not in their

mature counterparts, suggesting a general role for PTP4A3 in circulatory system

development. PTP4A3 has been shown to increase the concentration of VEGF in lung

cancer cells[98]. The proangiogenic growth factor VEGF functions by binding to receptor

tyrosine kinase VEGFR2 in endothelial cells and can induce proliferation, migration, and

sprouting of endothelial cells necessary for the creation of new vasculature. VEGF

binding to its cognate VEGFR2 receptor activates several signal transduction pathways

including the known PTP4A3 effectors Src and ERK1/2 kinase associated proteins.

The ability of PTP4A3 to increase expression of VEGF in tumor cells reported by

Ming *et al.*[98] presents a mechanistic rationale for the results seen by Guo *et al.*, wherein

the co-culture of PTP4A3 expressing cells, and those lacking transient PTP4A3

overexpression, are able to redirect the migration of human umbilical vascular endothelial

cells (HUVEC) towards them. VEGF promotes PTP4A3 transcription in endothelial cells

through Myocyte Enhancer Factor 2C (MEF2C)[13]. In this same study it was demonstrated that when PTP4A3 is depleted or pharmacologically inhibited HUVEC tube formation is hindered. This provides a positive feedback relationship in which tumor cells secrete excess VEGF, which stimulates PTP4A3 transcription in endothelial cells and leads to further VEGF expression in tumor cells. A correlation between PTP4A3 expression and tumor vascularity has been reported in human patient tumor samples. For example, PTP4A3 mRNA levels in patient hepatocellular carcinoma samples correlates with increased microvessel density[86]. Therefore, PTP4A3 phosphatase expression increases in both tumor cells and tumor-associated endothelial cells, implying a potential role in mediating the relationship between these two cell types. Collectively, these preclinical and clinical findings suggest that along with promoting oncogenic signaling in cancer cells, PTP4A3 may be fundamentally involved in both tumor angiogenesis and the control of nearby vasculature leading to tumor cell extravasation.

1.3   Therapeutic strategies for treating cancer.

1.3.1 Targeting tumor vasculature in CRC

Within a solid tumor, the tumor and endothelial cells promote the growth and function of each other through a tightly controlled system[165]. Tumor cells release proangiogenic factors, most notably VEGF, that stimulate endothelial growth, migration, and the subsequent formation of new blood vessels in a process known as tumor angiogenesis[165-167]. The new vasculature is necessary to provide the tumor with the nutrients and oxygen required for growth and metastasis[162,168]. The humanized antibody

bevacizumab (Avastin), which prevents VEGFR signal transduction by blocking receptor binding through attachment to the VEGF-A ligand[169] became the first US Food and Drug Administration-approved antiangiogenic agent for CRC[170]. Several other antiangiogenic agents, including those targeting the tyrosine kinase activity of the receptors that propagate VEGF signaling as opposed to the VEGF-ligand binding, have subsequently been approved for CRC therapy[171]. Antiangiogenic therapies result in a principally cytostatic effect and not cytotoxic effect. This means that, while they can halt tumor progression and metastasis, the primary effect of antiangiogenic therapies does not directly result in tumor cell death.

1.3.2 *PTPs in colorectal cancer and therapeutic targeting.*

Currently there are 27 small molecules targeting tyrosine kinases approved by the US Food and Drug Administration for the treatment of some form of cancer, and numerous others are in clinical trials[172]. In contrast, there are currently no approved drugs targeting phosphatases, and only three clinical trials investigating phosphatase targeted therapeutics for the treatment of cancer (Table 1-1). The oncogenic role of kinases in cancer has been well documented and as a result, it was predicted that PTPs would function antithetically and act as tumor suppressors. The first comprehensive mutational analysis of PTPs in CRC was performed by Wang and colleagues in 2004, in which the coding exons of all members of the PTP superfamily in 18 CRC samples were analyzed[173]. In this study they found 83 somatic mutations in 6 PTPs, affecting over 25% of CRCs and demonstrated *in vitro* that some of the mutations observed result in the

inhibition of the protein's phosphatase activity[173]. These data support the proposed tumor

suppressive function of PTPs, as transfection of wildtype PTPRT, the most frequently

mutated PTP from the study, reduced proliferation in malignant cells bearing the PTPRT

phosphatase inhibitory missense mutation[173]. It is now recognized that PTPs, like kinases,

can also function in an oncogenic capacity[22]. The overexpression of PTPs, such as SHP2

and PTP1B, has been directly linked to tumor formation, growth and metastasis in

multiple cancer types[22]. Moreover, in a study looking for differential expression of PTPs

in triple negative breast cancer as compared to estrogen receptor positive breast cancer

samples, 19 PTPs were significantly upregulated[21].

Table 1-1 PTP targets with active clinical trials.

PTP	Inhibitor	Mechanism of action	Disease	Phase
PTP1B	MSI-1436C	-Reversible, noncompetitive steroidal inhibition -Targets the intrinsically disordered C-terminus and traps the protein in an inactive state	Metastatic breast cancer	Phase 1
SHP2	TNO155	-Allosteric inhibition -Stabilizes the auto-inhibited conformation of Shp2	Solid tumors	Phase 1
PTP4A3	PRL3-ZUMAB	-Monoclonal PTP4A3-humanized antibody that binds intracellular PTP4A3	Solid tumors	Phase 1

In CRC, increased PTP1B expression and phosphatase activity creates a more

invasive phenotype in cellular assays and correlates with reduced patient survival[38].

Currently, the PTP1B inhibitor MSC-1436C is in a phase I clinical trial for the treatment

of metastatic breast cancer (Table 1-1). MSC-1436 is thought to function through the

binding to the disordered C-terminus of PTP1B as well as to a site adjacent to the active

site, locking the protein in the closed conformation, resulting in the inhibition of HER2

signaling[36]. Notably, PTP1B has been shown to function as both a tumor suppressor and

an oncoprotein, depending upon the cellular context[174]. In CRC, it has been suggested

that PTP1B's oncogenic function can be attributed to the propagation of active Src

signaling through dephosphorylation of inactivating Tyr residues on c-Src kinase[175].

Therefore, the PTP1B phosphatase inhibitor MSC-1436 may be useful for the treatment

of CRC as well.

SHP2 is a type I cytoplasmic non-receptor PTP that can dephosphorylate RAS,

and possibly other substrates upstream of RAS, leading to alterations in numerous

oncogenic signaling pathways such as RAS-ERK, PI3K-AKT, and JAK-STAT[176]. SHP2

contributes to KRAS-driven intestinal oncogenesis, yet prevents colitis-associated cancer

development in mice, demonstrating that SHP2's oncogenic function is context

dependent[177]. SHP2 also participates in the T-cell programmed cell death/checkpoint

pathway (PD-1) and contributes to immune evasion[176,178]. Currently, phase 1 clinical trial

recruitment has begun for TNO155, which is related to a novel allosteric inhibitor

SHP099, which binds concurrently to the interface of the N-terminal SH2, C-terminal

SH2, and catalytic domains to lock SHP2 in an auto inhibitory conformation[177,179]. In

preclinical trials oral administration of SHP099 reduces the growth of subcutaneously

implanted human squamous cell carcinoma xenografts by inhibiting the proliferation of

receptor tyrosine kinase driven cancers through the suppression of RAS-ERK

signaling[179]. These results demonstrate the therapeutic potential of using small molecules

to specifically target PTPs.

Since the first antibody was approved by the US Food and Drug Administration in

1997 for cancer, there has been a substantial growth in the number of approved

antibodies for human use. Recently, a humanized monoclonal antibody targeting

PTP4A3, PRL3-ZUMAB, has been developed. PRL3-ZUMAB was highly efficacious as

a monotherapy when compared to 5-fluorouracil alone in a nude mouse model of gastric

cancer[112]. These results are rather surprising as PTP4A3 is thought to be an intracellular enzyme but Thura and colleagues[112] observed that PTP4A3 is externalized and can bind the PRL3-ZUMAB antibody with the potential to recruit immunocytes and attack the tumor by a secondary method[112]. Currently, there is a phase 1 clinical trial being conducted with PRL3-ZUMAB for use against advanced solid tumors. Collectively, these three PTP inhibitors in clinical trials provide proof-of-concept and the inspiration for continuing efforts to target oncogenic PTPs.
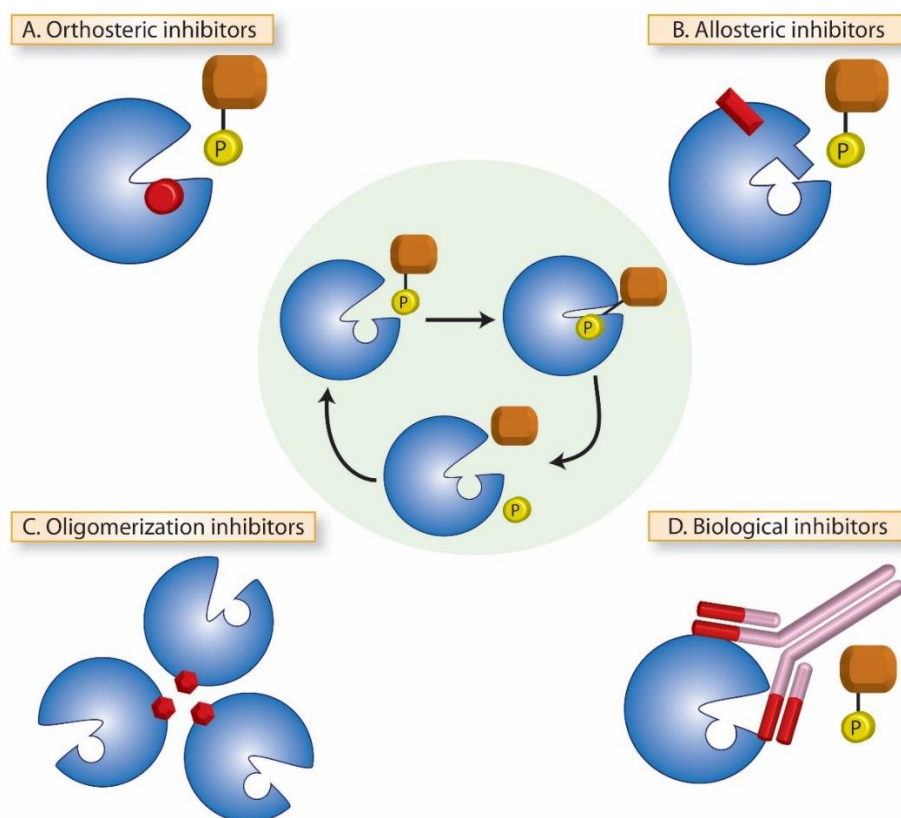
Figure 1-5 Mechanistic approaches for the inhibition of PTPs.

The central panel schematically illustrates the fundamental biochemical
dephosphorylation process of a phosphatase (blue) binding a phosphorylated substrate
(orange) via a concave catalytic site in a PTP, changing conformation, and cleaving the
phosphate moiety (yellow) resulting in the dephosphorylated substrate and the return of
the PTP to the open conformation. **A)** A competitive or orthosteric inhibitor (red disc)
blocks the direct binding of a phosphorylated substrate. **B)** An allosteric inhibitor (red
rectangle) binding to a noncatalytic site preventing catalysis often by inducing or
preventing a substrate-induced conformational change. **C)** An oligomerization inhibitor
(red hexagon) binds to a domain critical for high order structure formation and thereby
prevents catalysis. **D)** An antibody (pink and red rods) binds to the PTP in a manner that
blocks substrate binding. Figure adapted from Lazo *et al.*[180].

1.3.3 **Pharmacological inhibition of PTP4A3**

The previous section provides a compelling rationale for seeking strategies to inhibit PTP4A3 in cancer. Different approaches for targeting PTP4A3 pharmacologically are outlined in Figure 1-5. The use of biologics to target PTP4A3 (Figure 1-5D) is discussed in the previous section with regard to the antibody PRL3-ZUMAB. Therefore, this section will focus on the other inhibitors currently available. The lack of validated PTP4A3 substrates has hindered the identification and development of new small molecule inhibitors. Congruently, the shallow wide active site presents an added difficulty in developing a small molecule with any degree of specificity. Nevertheless, several small molecule PTP4A3 inhibitors have been described and some possess cellular activity that could reduce oncogenic phenotypes (Table 1-2).

Table 1-2 Small molecule inhibitors of PTP4A3 with cellular activity

Compound	*In vitro* IC$_{50}$ (µM)	Cellular and *in vivo* actions	Ref.
Pentamidine	0.30	Inhibits growth of cancer cell lines expressing endogenous PTP4As. Inhibits ectopic intracellular PTP4A phosphatase activity.	[94]
Emodin	3.5	Inhibits migration and invasion of DLD-1 cells and rescues Ezrin phosphorylation. Inhibits SGC-7901 cell proliferation and induce apoptosis while downregulating PTP4A3 mRNA.	[136,181]
BR-1	0.9	Inhibits the migration and invasion of DLD-1 cells and endothelial cells. Inhibits proliferation of H460 cells. Rescues the phosphorylation of Ezrin in treated DLD-1 cells. Increases antitumor activity of cisplatin with H450 tumor cells.	[75,182-184]
CG-707	0.8	Inhibits the migration and invasion of DLD-1 cells and endothelial cells. Inhibits proliferation of H460 cells. Rescues the phosphorylation of Ezrin in treated DLD-1 cells.	[182]
Thienopyridone	0.13	Inhibits RKO and HT29 colony formation. Suppresses human endothelial cell migration, but not proliferation.	[138]
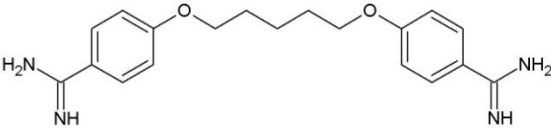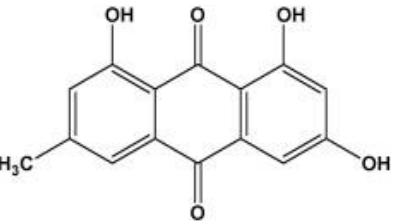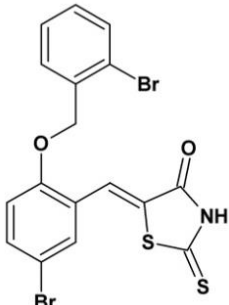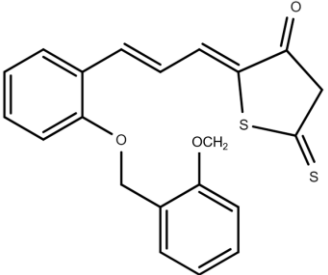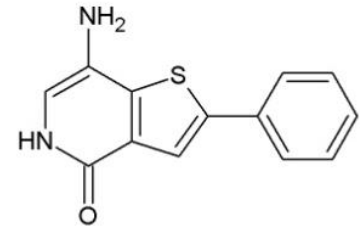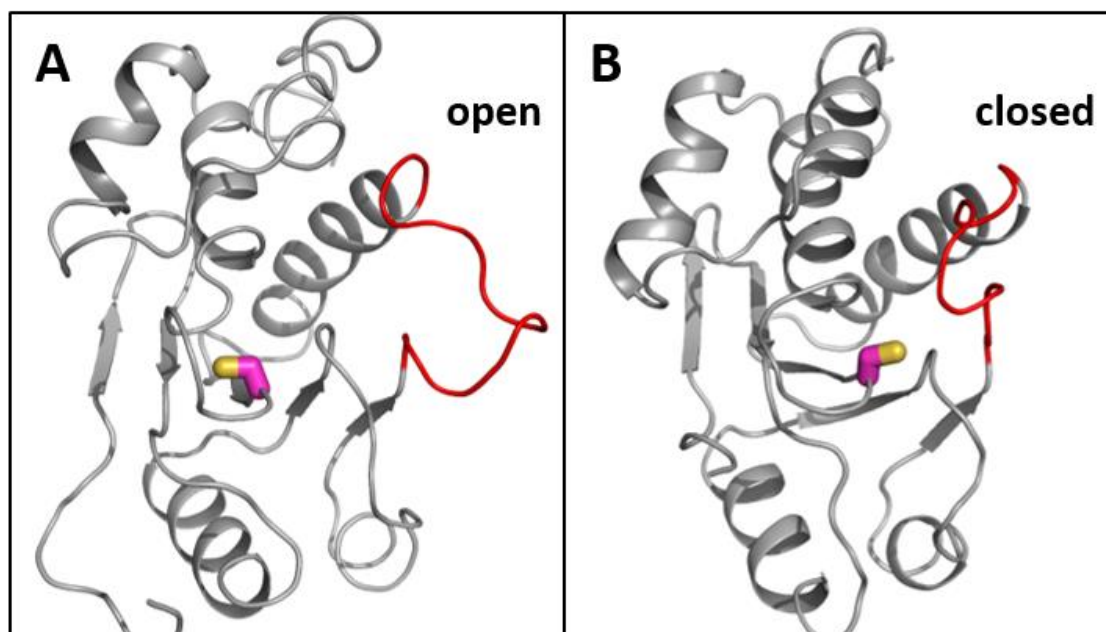
Figure 1-6 Model of open and closed conformation of PTP4A3.

Panels **A** and **B** provide snapshots of the opened (PDB entry code 1V3A) and closed

conformations of the PTP4A3 WPD loop (highlighted in red). The catalytic cysteine 104

is rendered in stick with magenta carbons. The (**A**) open conformation precludes

substrate binding. Image adapted from Lazo *et al.*[180].

One of the first reported PTP4A3 inhibitors was the antiprotozoal pentamidine[94].

Pentamidine was shown to inhibit PTP4A-1,-2, and-3 in an *in vitro* phosphatase assay

and to inhibit the growth of cancer cell lines expressing endogenous PTP4A

phosphatases[94]. Pentamidine, however, binds DNA and RNA polynucleotides, is not

specific to PTP4A3, and the *in vitro* phosphatase inhibitory activity has not been readily

reproducible. The bioflavonoids ginkgetin and sciadopitysin inhibit PTP4A3 *in vitro* with

IC_{50} values of 26 and 46 µM, respectively[185]. However, these compounds are known to

have additional pharmacological properties and no cellular activity has ever been

demonstrated. Emodin is an anthraquinone derivative that can inhibit PTP4A3 at 3.5 µM

in vitro[181]. Emodin has been shown to possess cell-based activity with respect to

PTP4A3-dependent reduction in migration, increased Ezrin phosphorylation in DLD-1

cells and in the inhibition of proliferation and induction of apoptosis in gastric cancer

cells[136,181]. PTP4A3 is susceptible to oxidation and subsequent disulfide bond formation

between Cys49 and Cys104 (Figure 1-2), which is inhibitory to its phosphatase

activity[54,57]. With this in mind, it is likely that Emodin, a quinone with high redox

potential, derives its inhibitory activity from PTP4A3's redox sensitivity. Emodin,

however, is an extremely promiscuous inhibitor and inhibits a wide range of other kinases

and phosphatases.

The most widely used PTP4A3 inhibitor, BR-1 (5-[[5-bromo-2-[(2-

bromophenyl)methoxy] phenyl] methylene]-2-thioxo-4-thiazolidinone), was initially

reported as having an *in vitro* IC_{50} of 0.9 µM[183]; although this has not been universally

reproduced[186]. BR-1 and its structural analog CG-707 have both been shown to block

migration and invasion and increase the phosphorylation of the proposed PTP4A3

substrates Ezrin and KRT8[182]. Importantly, BR-1 has been shown to inhibit the

tumorigenicity of H450 lung cancer cells and enhance *in vitro* cytotoxicity of clinical

anticancer agents[183]. In addition, BR-1 enhanced the antitumor activity of cisplatin in a

mouse xenograft model with H460 cells[184]. BR-1, however, has a high potential for

redox-activity and metal chelation due to its rhodanine-based structure, and is therefore

likely to have numerous off target effects. In contrast, the thienopyridone, 7-amino-2-

phenyl-5*H*-thienopyridin-4-one (Table 1-2), is a reasonably potent PTP4A inhibitor (*in

vitro* IC$_{50}$=~200 nM), first identified in a high throughput screening assay using a large

pharmaceutical chemical library[138]. Thienopyridone inhibits all three PTP4A3 family

members but not 11 other PTPs, and it prevents anchorage-independent cell growth of

RKO and HT-29 colorectal cancer cells in soft agar[138]. Furthermore, treatment with the

compound resulted in a concentration-dependent reduction in total p130Cas and an

increase in the amount of a cleaved 31kDa fragment of p130Cas resulting in increased

apopotosis[138]. Thienopyridone has been reported to inhibit PTP4A3 in a noncompetitive

manner, suggesting it might bind to an allosteric site to inhibit the phosphatase activity[186].

The noncompetitive inhibition of PTP4A3 phosphatase activity by thienopyridone

is of particular interest in light of the recent successes of allosteric inhibitors targeting

PTP1B and SHP2[36,179]. Efforts to design active site-directed orthosteric inhibitors

resulted in compounds that sacrificed potency, selectivity, or cellular activity, while

targeting of an allosteric site produced PTP1B and SHP2 inhibitors that are now in

clinical trials (discussed in section 1.3.2). Given these successes and the shallow DUSP-

like architecture of PTP4A3's catalytic P-loop, allosteric inhibitors are an attractive

approach to small molecule inhibition of PTP4A3 phosphatase activity. Among the

structural features of PTP4A3, reviewed in section 1.2.2, PTP4A3's large WPD loop, which regulates substrate access to the catalytic cysteine via 'opened' and 'closed' orientations, respectively (Figure 1-6), provides a potential noncompetitive site to target. The WPD-loop stabilizes the conformation of the closed, inactive state of the enzyme (Figure 1-6B) and could provide a site for allosteric inhibition.

Targeting the PTP4A family oligomerization (Figure 1-5C), which is important for cellular activity[12], has inspired an innovative approach in which the PTP4A1 trimerization is disrupted, and its catalytic activity is not directly impacted[56,187]. An extensive virtual screening campaign followed by enzymatic studies produced a small molecule, Compound 43 (Figure 1-7A), which blocks PTP4A1 trimerization and inhibits the biological function of the PTP[56]. Based on a recent X-ray co-crystal structure of Compound 43 in complex with a single PTP4A1 subunit[56], a conceptual image has been generated to illustrate how the compound would function as an oligomerization inhibitor, preventing the protein-protein interactions necessary for trimer formation (Figure 1-7B). Because the trimerization interface of PTP4A1 is shared by PTP4A2 and PTP4A3, this small molecule also inhibits all three PTP4A family members. Upon treatment of MeWo melanoma cells, Compound 43 reduces proliferation and migration and is able to suppress tumor growth in a melanoma xenograft model[56]. Collectively, these results demonstrate the potential to design small molecule inhibitors targeting not only the phosphatase active site, but other unique functional domains to ablate the oncogenic functions of the PTP4A family.

A.

CH₃

CH₃

Compound 43

B.
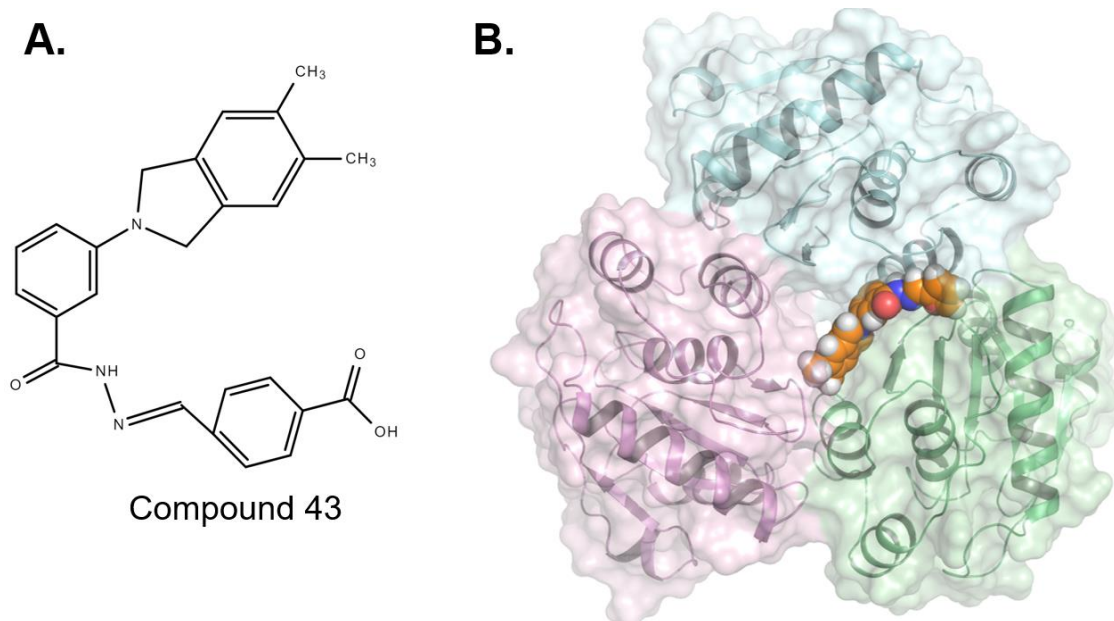
Figure 1-7 Conceptual image of Compound 43 interface with PTP4A1

oligomerization.

A) Chemical structure of PTP4A oligomerization inhibitor, Compound 43. **B)** Based on

the co-crystal structure of Compound 43 bound to a single PTP4A1 subunit (PDB entry

code 5BX1), a conceptual image of how the compound would interfere with trimerization

was generated. PDB entry code 1ZCK (which was solved as a trimer of PTP4A1

subunits) was used as the template. Each PTP4A1 subunit is depicted with a differently

colored surface. The small molecule inhibitor is shown in CPK (orange carbons). The

model illustrates how small molecule inhibitor binding would interfere with the ability of

the enzyme subunits to oligomerize. Conceptual image adapted from Lazo *et al.*[180].

1.4   Statement of hypothesis and aims

PTP4A3 may be a nodal participant in oncogenesis. The phosphatase activity of the protein seems necessary for this functionality. Nonetheless, additional studies are necessary to fully credential PTP4A3 as a valid clinical cancer target and to avoid some pitfalls common to preclinical cancer target investigations[188]. The central hypothesis (Figure 1-8) being tested is that PTP4A3 phosphatase activity contributes to tumor progression in CRC. A sophisticated cellular model system and a novel potent and selective small molecule phosphatase inhibitor were developed to probe PTP4A3's function. Using these tools, two aims were established to address the central hypothesis: (1) determine the impact of PTP4A3 phosphatase activity on migration and invasion in both tumor cells and endothelial cells; and (2) determine how alterations in PTP4A3 expression promote oncogenic phenotypes in malignant cells. The combined genetic and pharmacological approaches used to address these objectives strengthen the conclusions derived from the experiments. Accordingly, this thesis provides evidence for the importance of PTP4A3 phosphatase activity for tumor propagation in CRC and its value as a therapeutic target.
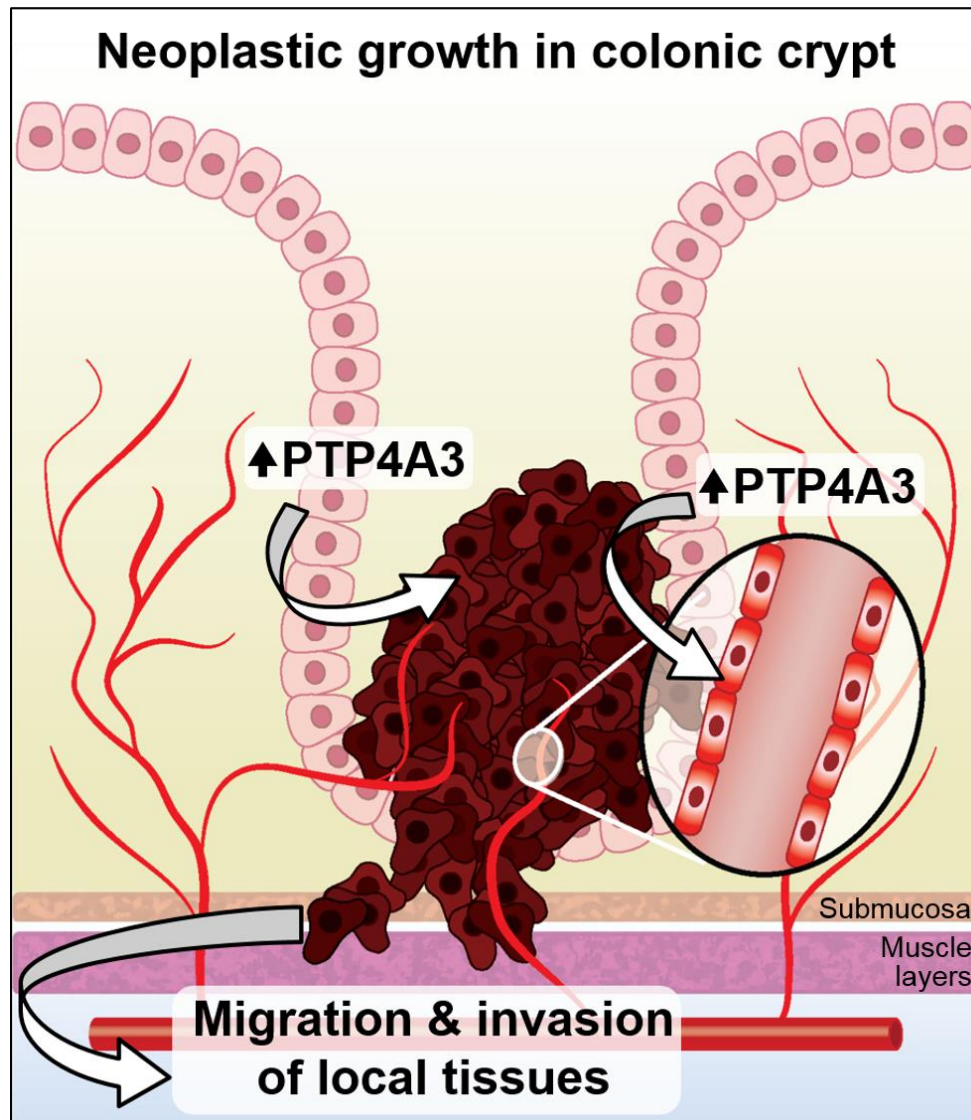
Figure 1-8 Visual representation of hypothesis: PTP4A3 promotes tumor growth and progression in colorectal cancer.

Increased PTP4A3 in malignant cells (dark red cells within colonic crypt) in combination with increased PTP4A3 in endothelial cells (bright red cells depicted in inset magnification of blood vessel) contribute to the ability of the tumor cells to migrate and invade local tissues. Light pink cells represent nonmalignant colonic epithelial cells.

CHAPTER 2:   MATERIALS AND METHODS

2.1   Cell culture

Murine, rat, and human cells were used to conduct the work presented. This included the use of cell lines commercially available, freshly isolated cell preparations, and newly generated cell lines.

2.1.1 Murine colorectal tumor cell culture

Mouse CRC cells were derived from our previously described primary colon tumor epithelial cells, which were obtained from *Ptp4a3*^{fl/fl} mice treated with AOM and DSS[45]. The mouse CRC cells were initially plated on a confluent feeder layer of lethally irradiated (80 Gy) LA7 rat mammary tumor cells (American Type Culture Collection CRL-2283) at ~80,000 cells/cm^2 and in DMEM/F12 medium with 0.5% FBS, 25 mg/mL gentamycin (Sigma-Aldrich, MO) and 1% insulin-transferrin/selenium (Mediatech, VA). When cells reached ~70% confluence, the *Ptp4a3*^{fl/fl} cells were detached from the feeder layer by incubation with Earl's Balanced salt solution/1mM EGTA/1% HEPES followed by 0.25% trypsin/ 0.1% EDTA as previously described[45]. A mouse CRC feeder layer-independent cell population was generated by serially decreasing the feeder layer at the time of passaging (~once per week with a 20% reduction in number of cells in feeder layer) and increasing the FBS concentration (15% increase in concentration at time of passage). After 7 passages, cells were successfully maintained in DMEM/F12 medium

with 7.5% FBS, 25 mg/mL gentamycin and 1% insulin-transferrin/selenium. The
C57BL/6J origin of the resulting cell population and the lack of contamination by
residual rat feeder layer cells was confirmed with short tandem repeat profiling
(CellCheck, IDEXX BioResearch, Columbia, MO). The feeder layer-independent cell
population was divided into two pools and infected with an adenovirus expressing either
Cre recombinase accompanied by a green fluorescent protein (GFP) marker or GFP
alone. Four days after infection, GFP-expressing cells were isolated by fluorescence
activated cell sorting (FACS). The resulting cell populations were expanded and either
used immediately or frozen in liquid nitrogen for future use. The sorted GFP-infected
population is referred to as PTP4A3$^{fl/fl}$, while the sorted Cre/GFP infected population is
referred to as PTP4A3$^{-/-}$. Cells were discarded after 20 passages. PTP4A3 mRNA levels
were determined by qRT-PCR and protein levels by Western blotting as described below.

2.1.2 Human colorectal tumor cell culture

HCT116 and DLD-1 cells were purchased from the American Type Culture
Collection (Manassas, VA) and cultured in McCoy's 5A or RPMI medium, respectively,
with 10% FBS, penicillin (100 IU/mL), streptomycin (100 µg/mL) and glutamine (10
mM). Cells were passaged < 22 times and then discarded.

2.1.3 Endothelial cell culture

Mouse primary endothelial cells were isolated from pulmonary tissue (n=12/genotype) as previously described[75]. Cells were cultured on a collagen matrix in 2% O_2, 5% CO_2, and 93% N_2 in a hypoxic chamber using Opti-MEM (Gibco) supplemented with 10% FBS, 2 mM glutamine, 0.2% retinal derived growth factor (Vec Technologies), 10 U/mL heparin, 0.1 mM non-essential amino acid supplement (Gibco) and 55 μM β-mercaptoethanol.

Commercially available human microvascular endothelial cells (HMVECs) (Lonza) were cultured in EGM-2 (Lonza) under normoxic conditions (5% CO_2) in collagen-coated tissue culture flasks. The primary growth factor components of EGM-2, namely IGF, EGF, FGF, and VEGF, were purchased from Lonza and used at the manufacturer's recommended concentrations. The PTP4A3 inhibitor BR-1 (Santa Cruz Biotechnology) was solubilized in tissue culture grade dimethyl sulfoxide (DMSO) (Sigma) and added to HMVECs at the indicated concentrations in 6- or 12-well plates. Lysates from BR-1-treated HMVECs were collected following 24 h of treatment. Cells were discarded after 8 passages.

All experiments investigating transendothelial resistance used primary human lung microvascular endothelial cells (MVEC) (a gift from Professor John D. Catravas, Old Dominion University, Norfolk, VA) that were harvested, identified, and cultured from fresh specimens obtained from patients undergoing pneumonectomy or lobectomy, as previously described[189].

2.2   Animals

2.2.1 PTP4A3 mutant mice

The generation of *Ptp4a3* mutant mice was previously described[46] and these mice were transferred from the University of Pittsburgh. A phage-based *E.coli* recombination system was used to construct the conditional *Ptp4a3* gene-targeting vector. The location of the transcriptional start site on exon 2 was specifically targeted to disrupt proper translation of the mRNA transcript. The resulting mutation was referred to as the floxed allele and left the *Ptp4a3* genetic locus intact. The global *Ptp4a3* knockout mouse was generated by crossing the *Ptp4a3* floxed mouse with mice expressing a Cre transgene from the EIIA promotor. The strain has been donated to the Jackson Laboratory mutant strain repository (Stock #21159). Experimental mice were produced by mating heterozygous breeding pairs and genotyping was performed by PCR of genomic DNA using primers specific to the floxed region exon 6 of the *Ptp4a3* genomic locus. All animal experiments were performed in accordance with the guidelines of the University of Virginia Animal Care and Use Committee.

2.2.2 Nude mouse tumor studies

For *in vivo* colorectal tumor growth studies, female athymic nude mice, *Foxn1^{nu}*, (Envigo, Dublin, VA) received subcutaneous bilateral injections (200 μL/injection) containing 1×10^6 cells suspended in a 1:1 PBS/Matrigel (BD, Biosciences, CA) solution. Expanded cells were washed, trypsinized, resuspended and drawn into 21-gauge needles

for injection. The injections were performed by Marya Dunlap-Brown in the University of Virginia Molecular Assessments and Preclinical Studies Core Facility. The size of the mass at the site of injection was determined based on width and length measurements of the exterior (to the nearest 0.1 mm) taken by Vernier caliper twice weekly. The volumes were estimated using the formula volume= (width)^2 x (length)^2. The mice were weighed twice weekly. The study occurred over a 48 day period. Following completion of the study all tumors were excised and weighed. In accordance with University of Virginia IACUC regulations, the animals were euthanized as a group when total tumor volume was estimated to be < 1.5 cm^3. All *in vivo* procedures were performed using the University of Virginia approved IACUC protocols. Animal care was administered in accordance to guidelines established by the American Association for Accreditation of Laboratory Animal Care.

2.3   Experimental assays

2.3.1 Fluorescent cell imaging

Cells were plated in CellCarrier-96 Ultra microplates (PerkinElmer, Waltham, MA) at 30,000 cells/well and grown at 37°C in 5% CO_2. At 48 h cells were fixed in 4% paraformaldehyde for 10 min, permeabilized in 0.5% Triton X-100 for 5 min, and stained with 100 nM Acti-stain 488 phalloidin (Cytoskeleton, Denver, CO). Cells were stained for 5 min with Hoechst 33342 to visualize nuclei. The Operetta CLS (PerkinElmer) was used to obtain confocal images using a 20x-water objective.

2.3.2 Quantitative Real Time PCR (qRT-PCR)

Total RNA was purified from cells using an RNAeasy Plus RNA isolation kit per the manufacturer's protocol (Qiagen, Valencia, CA). A total of 500 ng of mRNA were converted to cDNA using the RT2 first strand synthesis kit (Qiagen). Primers were obtained from Qiagen and PTP4A3 amplification was performed at a final primer concentration of 400 nM. Real-time monitoring of the qPCR reaction was performed on a BioRad CFX Connect thermocycler with RT2 SYBR Green ROX Mastermix (Qiagen). The program was run at 95°C for 10 min, and 40 cycles at 95°C for 15 sec and 60°C for one min. PTP4A3 gene expression was normalized to human GAPDH and β-actin. Total RNA was extracted from cells using the RNeasy Mini kit (Qiagen, Hilden, Germany) according to the manufacturer's protocol. A total of 1 μg of mRNA was treated to eliminate genomic DNA and converted to cDNA using the RT^2 first strand kit (Qiagen). The validated primer pairs for amplification of target genes were purchased from Qiagen and used with SYBR Green/ROX qPCR mastermix. Quantitative PCR was performed by incubating at 9°C for 10 min, followed by 39 cycles of 95°C for 15 sec and 60°C for 1 min while monitoring reactions on a BioRad CFX Connect Real-Time PCR detection system. A melt curve analysis was included to ensure the absence of non-specific primer binding.

2.3.3 Immunoblotting

Cell lysates were generated by removing growth medium, washing cells 3x in ice cold PBS, adding lysis buffer, detaching cells from the plate with a scraper, and then

placing cells in a microcentrifuge tube on ice. Cell lysate was passed through a 26-gauge

needle (3x), followed by sonication using three 10-sec pulses, and clarified by

centrifugation for 10 min at 4 °C and 7,000xg. Tissue lysates were generated by placing

samples in ice cold lysis buffer, using a Potter-Elvehjem homogenizer, passing

homogenate through a 25-gauge needle (3x), followed by sonication using three 10-sec

pulses, and clarified by centrifugation for 10 min at 4 °C and 7,000xg. Cells and tissues

were lysed in 20 mM Tris-HCl (pH 7.5), 150 mM NaCl, 1 mM Na_2EDTA, 1 mM EGTA,

1% Triton, 2.5 mM sodium pyrophosphate, 1 mM β-glycerophosphate containing 1x

Complete Mini EDTA-free Protease Inhibitor (Roche, Basel, Switzerland) and

phosphatase inhibitor cocktail (Sigma Aldrich). Total protein in the lysate was quantified

by a BCA assay (Thermo Fisher Scientific, Waltham, MA). A total of 30 µg of protein

was separated using Novex SDS-PAGE reagents and transferred to a PVDF membrane.

Membranes were blocked in 5% dry milk in TBS+0.1% Tween-20 and incubated with

primary antibodies overnight followed by secondary fluorescent antibodies according to

the manufacturers' instructions. The following commercially available primary antibodies

were used: PTP4A3 (#6484), GAPDH (#2118), Ezrin (#3145), phospho-Ezrin

(Thr567)/Radixin (Thr564)/Moesin (Thr558) Antibody (#3141) (Cell Signaling

Technology, Danvers, MA). Membranes were imaged using Li-COR Odyssey imaging

system (LI-COR Biotechnology, Lincoln, NE).

2.3.4 Cell proliferation assay

Cell proliferation rates were determined with a CyQuant Direct Cell Proliferation kit (Thermo Fisher Scientific) according to manufacturer's instructions. Cells in mid-logarithmic growth phase were detached as above, centrifuged, re-suspended in complete medium with 10% FBS, and counted. Cells were re-suspended and 1.5×10^3 cells per well were added to black clear-bottom 96-well plates. CyQuant reagent was added at 24, 30, 45, 55, 71, and 77 h and incubated at 37°C for 30 min. The fluorescence was measured using a SpectraMax M5 plate reader (Molecular Devices, LLC, Sunnyvale, CA) at 480 nm excitation and 535 nm emission.

2.3.5 Colony formation assays

Colony formation on plastic was assessed using 6-well plates. Containing a total of 2 mL of growth medium. Cells were washed, detached from a 10 cm plate at ~60% confluence, and seeded into individual wells at 500 cells/well. After 12 days the medium was aspirated, cells were washed with 1x PBS, and then cells were stained with 0.02% Crystal Violet. For 10 min. Following, staining, the wells were washed with 1x PBS and colonies containing >50 cells were manually counted.

Soft agar assays were performed in 12-well plates by adding 1.25 mL complete medium containing 0.6% agar and allowing it to solidify and generate a base layer. Cells were detached with 0.25% trypsin/ 0.1% EDTA, centrifuged at 100xg for 3 min, counted, and then resuspended in complete medium containing 0.4% agar at a final concentration of 1.5×10^4 cells/1.25 mL/per well. Complete medium (300 µL) was added on top of soft

agar in each well every 4 days. After 14 days, cells were fixed using 10% ethanol and

10% acetic acid, and then stained using 0.01% Crystal Violet. Mouse CRC cell colonies

were manually counted with an Olympus IX70 microscope.

2.3.6 Spheroid growth assays

For the scaffold-free model, PTP4A3$^{fl/fl}$ and PTP4A3$^{-/-}$ cells were harvested and

plated (500 cells/100 µL) into individual wells of a 96-well round bottom plate coated in

polyHEMA to prevent cell attachment. Cells were grown in an incubator at 37°C in 5%

CO_2. After 48 h, images of spheroids were taken using an Olympus IX70 with a 10x

objective.

For human CRC viability assays, test and control compounds (15 µL) were added

into each well of a 384-well ultralow attachment spheroid microplate (Corning, Corning,

NY) with vehicle and positive controls being 0.5% and 10% DMSO, respectively. DLD-1

and HCT116 cells were seeded (100 cells/10 µL) into each well of the microtiter plate.

The microtiter plates were incubated for 48 h (37°C, 5% CO_2) and 25 µL of CellTiterGlo

3D (Promega, Fitchburg, WI) reagent was added. Plates were incubated while shaking for

30 min at room temperature. Luminescence data were captured on a SpectraMax M5

multimodal plate reader. EC_{50}s were calculated using GraphPad Prism 7.0 (La Jolla, CA).

2.3.7 Migration assays

Differences in cell migration were quantified by our previously described *in vitro*

scratch wound healing assay[75]. Cells were grown to confluence in 24-well tissue culture

plates (BD Biosciences). Each well (N=3/genotype or treatment) was scratched

longitudinally with a pipette tip and incubated for 16 h to allow gap closure. Cell

migration images were captured and the distance was determined by measuring the gap

distance between cell fronts following inward migration using ImageJ Fiji software.

For transwell migration assays, chambers were assembled using 8 μm

polyethylene terephthalate membrane transwell inserts (Costar) as upper chambers and

24-well plates as lower chambers. Cells were detached from the monolayer with 0.25%

trypsin/ 0.1% EDTA as described above, centrifuged, and re-suspended in medium

containing 0.5% FBS and placed ($2.5x10^5$ cells/well) in the upper chamber. The lower

chamber contained cell medium supplemented with 10% FBS to act as a chemo-attractant

to stimulate migration. After 20 h, cells were fixed in 100% methanol and stained with

0.2% Crystal Violet for 30 min to visualize cells. The cells that migrated to the bottom of

the membrane were counted manually with an Olympus IX70 microscope.

2.3.8 *Impedance-based adhesion assay*

Impedance based adhesion assays were performed using the xCELLigence Real-

Time Cell Analyzer Dual Plate in combination with the E-Plate 16 (ACEA, San Diego,

CA). The cell analysis instrument was placed in an incubator (37 °C in 5% CO_2) for all

experiments. The background measurements for each experiment were determined by

filling each well with 100 μL of medium, allowing plate to equilibrate for 30 min, and

calibrating the instrument immediately prior to adding cells. Cells at >60% confluence

were detached and seeded in an E-plate in a total volume of 100 μL. Cells were pretreated

with compound or vehicle control for 3 h in serum-free medium then harvested as

described above, and plated the cells with compound or vehicle to determine the effect of

small molecules. Impedance readings were taken every 10 min over the course of 25 h.

2.3.9 Immunohistochemistry

Tumors were removed, photographed, and fixed by the University of Virginia

Molecular Assessments and Preclinical Studies Core. They were rinsed in ice-cold

phosphate buffered saline (PBS) and immediately submerged in 10% neutral buffered

formalin and incubated at room temperature overnight. Fixed tissues were then embedded

in paraffin and sectioned onto glass slides. Sections were deparaffinized and rehydrated

prior to staining. Samples were permeabilized with 0.1% Triton X100 (Sigma-Aldrich,

MO) for 10 min, blocked with 5% Bovine Serum Albumin (BSA) for 30 min, and stained

with hematoxylin & eosin (H&E) or primary antibody against Mucin2 (MUC2) (Santa

Cruz, TX) in PBS containing 0.5% BSA (Fisher, PA) for one hour followed by anti-

rabbit Alexa Fluor secondary (Life Technologies, NY) for 30 min followed by

counterstain with DAPI. For fluorescent staining, slides were imaged using a Zeiss LSM

510 microscope equipped with a ×100 oil immersion plan-apochromatic lens. The images

represent a z-stack projection of 7–10 confocal sections from the basal to apical cell side.

For H&E staining, images were taken using an IX70 inverted microscope (Olympus,

PA). The H&E stained slides were analyzed by board certified pathologist Dr.

Christopher Moskaluk.

2.3.10 Gene expression array

The expression profile of 84 key genes impacting cellular adhesion was determined using a 96-well format murine extracellular matrix and adhesion molecule RT^2 Profiler PCR array (Qiagen) according to the manufacturer's instructions. For normalization, the array contains 6 housekeeping genes. Plates for qPCR were run on a BioRad CFX Connect Real-Time PCR detection system, using RT^2 SYBR Green/ROX qPCR mastermix (Qiagen). Data analysis was performed by the $\Delta\Delta C_T$ method on the Web-based software available through the manufacturer (http://pcrdataanalysis.sabiosciences.com). Three PCR microarray replicates were used per cell population.

2.3.11 In vitro biochemical analysis of JMS-053 and thienopyridone

PTP4A3 activity assays were performed in triplicate in 384-well Greiner bio-one black microtiter plates as previously described[190] with recombinant His$_6$-tagged PTP4A3 and substrate 6,8-difluoro-4-methylumbelliferyl phosphate (DiFMUP) (15 µM) incubated at 25°C for 30 min in 40 mM Tris-HCl (pH 7.0), 75 mM NaCl, 2 mM EDTA, and 4 mM DTT buffer. Bacterial recombinant PTP4A1 and PTP4A2 were purchased (R&D Systems, Minneapolis, MN) and assayed under the same conditions as PTP4A3. Reversibility assays were performed in a 100 µL final volume. PTP4A3 (1.25 µg) was pre-incubated for 30 min with 10X the IC$_{50}$ of the inhibitor and then diluted to the 1X IC$_{50}$. Reactions were initiated by the addition of 45 µL of substrate for a final DiFMUP concentration of 4 µM (K$_m$). The competitive nature of the inhibition was determined by

a previously described assay[190] with fixed concentrations of the compounds and DiFMUP

substrate concentrations that were varied from 2.5-25 μM. The data were analyzed with

GraphPad Prism version 7.00 (GraphPad Software, La Jolla CA).

2.3.12 Computational studies

Drug-like properties for the compounds were determined with Data Warrior

(http://www.openmolecules.org/datawarrior/). Chemical similarity analyses were

performed with PubChem (https://pubchem.ncbi.nlm.nih.gov) and ChemSpider

(www.chemspider.com) using a 2D Tanimoto score of ≥0.8. Modeling software Maestro

version v11 (Schrödinger, LLC, New York, NY), and Insight 2005 and Discovery Studio

v16 (both: Dassault Systèmes BIOVIA, San Diego, CA), operating on a Dell (Round

Rock, TX) Precision T7600 with Red Hat (Raleigh, NC) Enterprise Linux 6.7, were used

for all modeling studies. The three-dimensional (3D) coordinates of PTP4A3 were

extracted from PDB entry 5TSR[156]; the 3D coordinates of inhibitor JMS-053 were

obtained from the Cambridge Crystallographic Data Centre (CCDC number 1476250)[190].

The structure of PTP4A3 was energy refined in Insight 2005 using a previously reported

strategy starting with hydrogens only minimization, followed by side-chain relaxation,

and finally, all atoms optimization until the norm of the gradient was <0.001 kcal/Å[191].

The RMSD of the energy refined structure versus the starting X-ray structure was 1.29 Å,

which was well within crystallographic resolution. Maestro and Discovery Studio binding

site detectors were used to identify a location for JMS-053 binding in a cavity (volume ~

350 Å^2) surrounded by helices α3, 4, 6 and loop residues 68 – 78. This cavity was chosen

for docking studies given that its location was removed from the active site, yet in contact with the critical WPD loop. Docking of the inhibitor in this site was guided by the constant scoring of favorable and unfavorable intermolecular, atom-atom contacts using the HINT program (implemented in Discovery Studio) as described previously[191]. Briefly, a systematic optimization of the binding pose applied iterative steps and manual adjustments to the inhibitor in Cartesian space, as well as to inhibitor bond torsions, in conjunction with adjustments to amino acid side chain torsions. The Maestro refine loops algorithm was applied to loop residues 68-78, followed by all atoms minimization of the complex using conjugate gradients in Insight 2005 until the norm of the gradient was < 0.001 kcal/Å.

2.3.13 Phosphatase specificity of JMS-053

The inhibition specificity of JMS-053 was determined for 26 phosphatases by Eurofins (Dundee, Scotland, UK) with their PhosphataseProfiler[TM] platform using 10 µM DiFMUP as a substrate and fluorescent intensity at $A360_{EX}/A450_{EM}$. Inhibitory effects were calculated as the mean percent phosphatase activity remaining compared with the activity of the vehicle control. Kinase profiling of JMS-053 was performed by Luceome Biotechnologies (Tucson, AZ) using their luciferase-based KinaseSeeker[TM] platform. JMS-053 was evaluated at 1 µM in duplicate in both profiling platforms. The CDC25B assays were performed with a slight modification to our previously described methods[192] using recombinant enzyme and the substrate DiFMUP at ~3X the K_m (150 µM). PTP4A1 and PTP4A2 assays were performed in triplicate in 384-well microtiter plates using the

same conditions as for PTP4A3 as indicated above. PP2A was a gift from Dr. David

Brautigan (University of Virginia) and was assayed with the substrate DiFMUP at ~3X

K_M (150 µM) in 120 mM Tris-HCl (pH 7.0), 225 mM NaCl, 0.1% BME, and 0.1% BSA

buffer. All assays were incubated for 30 min at 25°C. Fluorescence was measured using a

SpectraMax M5 plate reader (Molecular Devices, LLC, Sunnyvale, CA) at

$A358_{EX}/A455_{EM}$. The human active site phosphatase dendrgram comprising 11 amino

acids was modeled on the published[193] dendrogram supplemented with the alignment of

other PTPs tested using ClustaW2 and the full length amino acid sequence trees were

modeled using the longest isoform[194].

2.3.14 Thermal shift biophysical binding assay

PTP4A3 melting curves were obtained at a protein concentration of 16 μM (50

mM Tris, 150 mM NaCl, and 1 mM DTT pH 7.4) with 20X SYPRO orange (Invitrogen)

and a ligand concentration of 100 μM. Fluorescence was monitored using a QuantStudio

6 Flex real-time PCR system (Applied Biosystems). Scans were measured from 25° to

65°C at a scanning rate of 1 °C/min. The data were analyzed using derivative methods to

assess the melting temperature (T_m) using Graphpad Prism as previously described[195].

2.3.15 Pharmacokinetic studies

Pharmacokinetic studies were conducted by Sai Life Sciences Ltd (Hinjewadi,

India) using 20% 1-methyl-2-pyrrolididone, 25% Kolliphor HS 15, and 55% 1X

phosphate buffered saline as the vehicle and a single IP dose of 10 mg/kg JMS-053.

Blood samples were collected under light isoflurane anesthesia from retro orbital plexus pre-dose and at eight time points, the last being at 24 h. Three mice were used for each time point. Sample were processed for analysis by protein precipitation using acetonitrile and analyzed by liquid chromatography/mass spectroscopy/mass spectroscopy.

2.3.16 Measurement of endothelial barrier function

The transendothelial electrical resistance (TEER) study of endothelial barrier function were performed at Old Dominion University in the laboratory of Dr. John Catravas. The barrier function of endothelial cell monolayers grown on electrode arrays was estimated by our previously described[196,197] electric cell-substrate impedance sensing (ECIS) method using an ECIS model 1600R from Applied BioPhysics (Troy, NY). Experiments were conducted on cells seeded at a density of 6 x 10^4 cells/well in 8W10E+ arrays that achieved at least 800Ω baseline steady-state resistance and capacitance between 22-29 nanofarads at a frequency of 4000Hz. Each 0.6 mL well of the 8 well arrays had 40 small gold film surface active electrodes (2 mm^2 area) and a large counter electrode. A uniform confluent endothelial monolayer reduced the amount of current flowing across the gold electrodes to the counter electrode, and thus increased the resistance. The TEER measured dynamically across the monolayer reflected the combined resistance between the ventral surface of the cell and the electrode, reflective of focal adhesion, as well as the resistance between cells. Intercellular gaps increase current flow and reduce resistance. Thus, a change in TEER represented a change in cell-cell adhesion and/or cell-matrix adhesion. All experiments used primary human lung

microvascular endothelial cells (MVEC) that were harvested, identified, and cultured in-house from fresh specimens obtained from patients undergoing pneumonectomy or lobectomy, as previously described[189] and in accordance with our Institutional Review Board criteria. MVEC were exposed to 100 ng/mL VEGF, 0.5 endotoxin units (EU) lipopolysaccharide (LPS), or vehicle control. In some studies cells were pre-treated and then continuously treated with 5 µM of JMS-053, JMS-038, or Compound 43. In other studies, cells were treated 3 h after exposure to VEGF or LPS. Experiments were performed in quadruplicate and data were expressed as mean values ± SE. One-way or two-way ANOVA with Bonferroni post-hoc test was performed to determine statistically significant differences among groups ($P<0.05$).

2.3.17 RhoGTPase activity assay

RhoA activation in HeyA8 cells was detected by the luminescence formatted RhoA G-LISA Activation Assay (Cytoskeleton Inc., Denver, CO), according to manufacturer's instructions. Following a 24 h serum starvation in RPMI supplemented with 0.1% fatty-acid free bovine serum albumin, HeyA8 cells at ~60% confluence were pretreated in serum-free medium for 30 min with compounds in a final DMSO concentration of 0.5%, as was the vehicle control. HeyA8 cells were then stimulated for 30 min with RPMI containing 10% FBS and the compounds in a final DMSO concentration of 0.5% and harvested on ice. Total protein was determined using Precision Red Advanced protein assay reagent (Cytoskeleton Inc.). Fifteen µg of cell lysate protein per Rho-GTP affinity well were incubated at 4°C for 30 min on an orbital shaker to

facilitate binding. As a positive control, 1 ng of purified recombinant RhoA was bound to the affinity well. The provided primary and secondary antibodies were used at a 1:250 and 1:500 dilution, respectively. Luminescence data were captured on a SpectraMax M5 multimode plate reader set to 50 msec integration time following 2 min incubation with luminescence detection reagent.

Human MVEC were pretreated with vehicle (DMSO) or JMS-053 (5 µM) prior to vehicle or LPS treatment (0.5 EU/mL) for 1 or 24 h. MVEC RhoA activation was detected using the bead pull-down format RhoA Activation Assay Biochem Kit (Cytoskeleton Inc.). Cells were lysed in CelLyticM Lysis Reagent and total protein in the lysate was determined with a Pierce BCA protein assay (ThermoFisher Scientific, Waltham, MA). Five hundred µg of total cell lysate protein were incubated at 4°C with 80 µg Rhotekin-RBD protein beads for 1 h rotating. After precipitation, the complexes were washed four times with wash buffer, eluted in 2X SDS-PAGE sample buffer, immunoblotted, and probed with RhoA antibody. GTP-bound RhoA detection was performed using a monoclonal rabbit RhoA antibody (Cell Signaling, no. 2117)[196]. Proteins were visualized using a LICOR Odyssey CLx imaging system (Lincoln, NE). Aliquots were taken from supernatants prior to precipitation and were used to quantify total RhoA. Rac1 activity was determined using the Rac Activation Assay Biochem Kit (Cytoskeleton Inc., BK-035) per the manufacturer's instructions. Secondary mouse and rabbit antibodies were purchased from LICOR. ImageJ software was used to perform densitometry of immunoblots. All data were expressed as mean values ± SE. Student's *t*-test, one-way, or two-way ANOVA with Bonferroni post hoc test was used to determine statistically significant differences among groups ($P<0.05$).

2.3.18 VEGF-mediated vascular permeability (Miles) assay

Adult male mice (n=6-8 per genotype, 8-12 weeks) under normal diet and

environmental conditions were injected intravenously (IV) with Evans blue dye (100 µL

of a 1% solution in 0.9% NaCl). After 20 min, 400 ng of recombinant murine VEGF

(Peprotech) dissolved in 20 µL of PBS and 0.1% BSA or 20 µL of vehicle alone was

injected intradermal into the shaved right or left flank of the mouse, respectively. After

20 min, the animals were euthanized and perfused with 10 mL saline via the left

ventricle. The area of skin containing the injection site was removed using a 5 mm biopsy

punch (Miltex). Evans blue dye was extracted from the skin by incubation with 200

µL formamide for 24 h at 57°C and the absorbance of the extracted dye was measured at

620 nm in triplicate in a 96-well plate.

2.4   Pharmacological reagents

Thienopyridone, Compound 43, JMS-053, JMS-038 and thienopyridone inactive

analogs were synthesized as previously described[56,190]. DiFMUP was purchased from

ThermoFisher Scientific. DMSO was obtained from VWR (Radnor, PA).

2.5   Clinical gene analysis

PTP4A3 mRNA expression data were obtained using cBioPortal and the Cancer

Cell Line Encyclopedia (Agilent microarray), which contained 967 cell lines, or the

TCGA Provisional colorectal adenocarcinoma database (RNA Seq V2), which contained

379 tumor samples. Data analyses were conducted 12/2017. In the Cancer Cell Line

Encyclopedia, 70 (7%) of the tumor cell lines had elevated PTP4A3 levels (z-score

threshold of 2.0). In the Cancer Genome Atlas (TCGA) (Nature, 2012) colorectal

database 52 patient tumor samples (14%) with highly elevated PTP4A3 mRNA (z-score

threshold of 2.0). Gene expression pattern visualization by heatmap used the SVG data

file downloaded from cBioPortal imported into Graphpad Prism 7.0. The data were sorted

based on degree of altered expression in each gene and 30% of the total samples were

depicted. Overall survival was calculated using a Kaplan-Meier program in cBioPortal

from patients with tumors that over-expressed *Ptp4a3* or *Mmp1* or under-expressed

Emilin 1. Fbln 1, Vcan, Itgb 2, Itgb 3 or Thbs3.

2.6   Statistics

Statistical analyses were performed with GraphPad Prism 7.0. Data were

presented as average (mean) ± SD or SEM. Normality was assessed using the Shapiro-

Wilk normality test. Normally distributed groups were compared using student's t-test for

comparisons involving two groups or one-way or two-way ANOVA for comparisons

involving >two groups. $P<0.05$ was considered statistically significant. Each experiment

represents at least three biological replicates and three technical replicates.

CHAPTER 3: DEVELOPMENT AND CHARACTERIZATION OF A GENETIC MODEL TO PROBE PTP4A3 EXPRESSION IN COLORECTAL CANCER CELLS

3.1   Introduction

Our group recently developed and characterized the first global *Ptp4a3* gene deletion mouse model enabling a more comprehensive analysis of the pathological role of PTP4A3 in CRC[46]. The *Ptp4a3*^{-/-} mice are viable and do not display any gross histological irregularities in tissues or organs, which suggests that PTP4A3 targeted therapy may have minimal adverse effects. The widely accepted AOM-DSS treatment was used to model colitis-induced CRC in these mice. The AOM-DSS model of colorectal tumorigenesis simulates sporadic tumor formation in the colon through dysregulation of β- catenin/APC and TGF-β signaling pathways, as well as K-Ras activation[198,199]. The study revealed that the global loss of PTP4A3 results in fewer tumors[46]. Furthermore, when primary CRC cells are isolated from the tumors of *Ptp4a3*^{fl/fl} and *Ptp4a3*^{-/-} mice and cultured on a lethally irradiated rat cell feeder layer, the *Ptp4a3*^{-/-} cells produce fewer *in vitro* colonies by limited dilution analysis[45]. In addition, upon subcutaneous injection into nude mice, 5 of the 6 *Ptp4a3*^{fl/fl} tumor cell injections resulted in tumor formation while none of the 6 *Ptp4a3*^{-/-} tumor cell injections resulted in tumor formation[45]. While these feeder-layer dependent cells provide valuable insights and encouraging preliminary data, they were isolated from mice treated with the mutagen AOM and may harbor other PTP4A3-independent genetic differences. Moreover, the isolated cells require the presence of a monolayer of lethally irradiated rat mammary

carcinoma cells to survive, which complicates any analyses and limits the overall

usefulness of the cells. Therefore, in the current study, I have generated a feeder layer-

independent paired CRC tumor cell lines to probe further the role of PTP4A3 in CRC.

3.2   Results

3.2.1 Generation of isogenic PTP4A3$^{fl/fl}$ and PTP4A3$^{-/-}$ murine CRC cell lines.

Ptp4a3 wildtype and null cells derived from primary colon tumor epithelial cells

of *Ptp4a3*$^{fl/fl}$ and *Ptp4a3*$^{-/-}$ mice treated with AOM and DSS have been described

previously[45,46]. I developed feeder-layer independent cells that could be used to

specifically remove the *Ptp4a3* gene and yield a unique paired CRC tumor cell model.

Our overall experimental scheme is illustrated in Figure 3-1. Over the course of 17

passages, the *Ptp4a3*$^{fl/fl}$ cells were liberated from the feeder-layer and proliferated in the

presence of medium with 7.5% FBS. The resulting cells were infected with an adenovirus

expressing either Cre recombinase accompanied by a GFP marker or GFP alone. Four

days after infection, GFP-positive cells were isolated by FACS and the sorted populations

were plated on plastic and cultured. There was no obvious difference in the nuclear to

cytoplasmic area ratio between the two cell populations (Figure 3-2A). Relative to

Ptp4a3 gene expression in the normal colon of a *Ptp4a3*$^{fl/fl}$ mouse, whole tumor lysate

showed an ~8-fold increase in *Ptp4a3* mRNA while the original *Ptp4a3*$^{fl/fl}$ cells and the

GFP-expressing *Ptp4a3*$^{fl/fl}$ cells, hereafter referred to as PTP4A3$^{fl/fl}$ cells, demonstrated

an ~12-fold increase in expression (Figure 3-2B). Notably, infection with the adenovirus

expressing GFP did not significantly alter *Ptp4a3* mRNA levels compared to the

uninfected cells. The *Ptp4a3*^{-/-} cells showed no detectable mRNA and the Cre/GFP

infected cells, hereafter referred to as PTP4A3^{-/-} cells, had almost a complete loss of

Ptp4a3 mRNA (Figure 3-2B). In agreement with the PTP4A3 mRNA expression data,

the PTP4A3^{-/-} cells lacked detectable PTP4A3 protein as determined by Western blotting

(Figure 3-2C). In addition, the loss of PTP4A3 protein did not result in a significant

compensatory change in the mRNA levels of the other two members of the PTP4A

family, *Ptp4a1* and *Ptp4a2* (Figure 3-2D). There were, however, no significant

differences in the levels of total Ezrin or phosphorylated Ezrin as measured by Western

blotting (Figure 3-3). It is important to note, however, that the antibody used to identify

Thr567 phosphorylated Ezrin, also detects phosphorylated Radixin and Moesin.

Therefore, it is possible that a difference in Ezrin Thr567 phosphorylation may be

obscured by phosphorylation of phosphorylation of Radixin and Moesin.
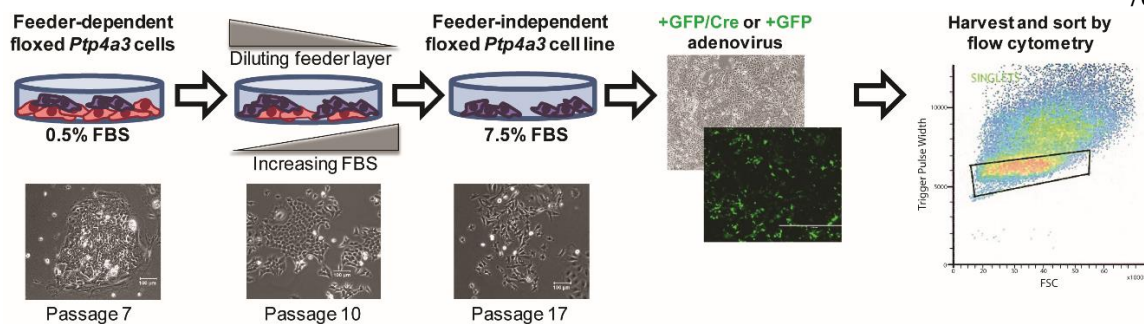
Figure 3-1 Experimental workflow of the development of isogenic PTP4A3$^{fl/fl}$ and PTP4A3$^{-/-}$ murine CRC cell lines.

Cells isolated from the chemically induced colorectal tumors of *Ptp4a3*$^{fl/fl}$ mice were made feeder layer-independent by serially decreasing the irradiated LA7 rat mammary feeder layer cells while increasing exposure to FBS to a final concentration of 7.5% by passage 17. The resulting cells were infected with either a GFP/Cre or a GFP adenovirus. Four days after infection, GFP positive cells were isolated by FACS and used to generate the PTP4A3$^{fl/fl}$ and PTP4A3$^{-/-}$ cells.
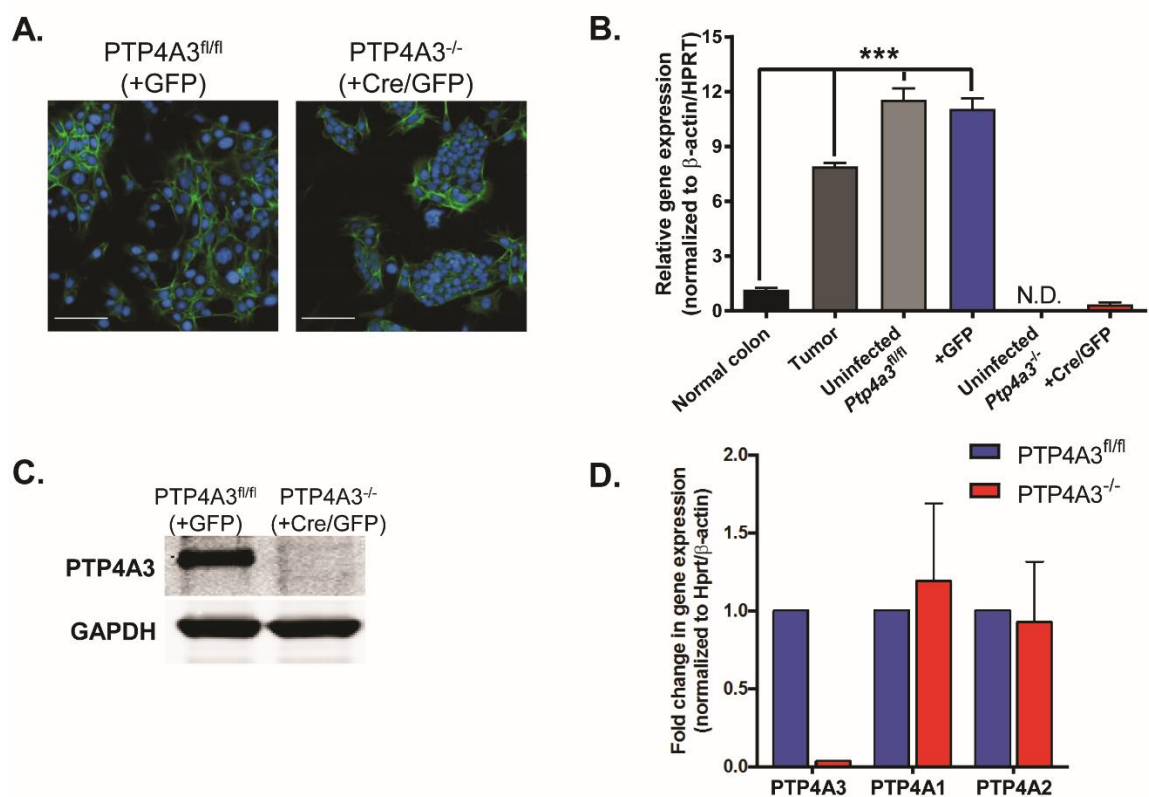
Figure 3-2 Validation of PTP4A3$^{fl/fl}$ and PTP4A3$^{-/-}$ murine colorectal tumor cell lines.

A) Fluorescence confocal 20x images of PTP4A3$^{fl/fl}$ and PTP4A3$^{-/-}$ cells using Acti-stain 488 phalloidin to visualize the cytoskeleton (green) and Hoechst to visualize the nuclei (blue). Scale bars=100 µm. **B)** qRT-PCR analysis of *Ptp4a3* gene expression in normal mouse colon, murine tumor, uninfected *Ptp4a3*$^{fl/fl}$ and *Ptp4a3*$^{-/-}$ cells, and Cre/GFP and GFP infected *Ptp4a3*$^{fl/fl}$ cells. Expression levels are relative to normal colon tissue. ***=P<0.0001, N=4, error bars=SEM. N.D.=Not determined. P-value determined by 1-way ANOVA. **C)** PTP4A3 protein as determined by Western blotting. GAPDH was used as the loading control. N=4. **D)** qPCR analysis of *Ptp4a1*, *Ptp4a2,* and *Ptp4a3* gene expression in PTP4A3$^{fl/fl}$ and PTP4A3$^{-/-}$ cells. N=4, error bars= SEM.
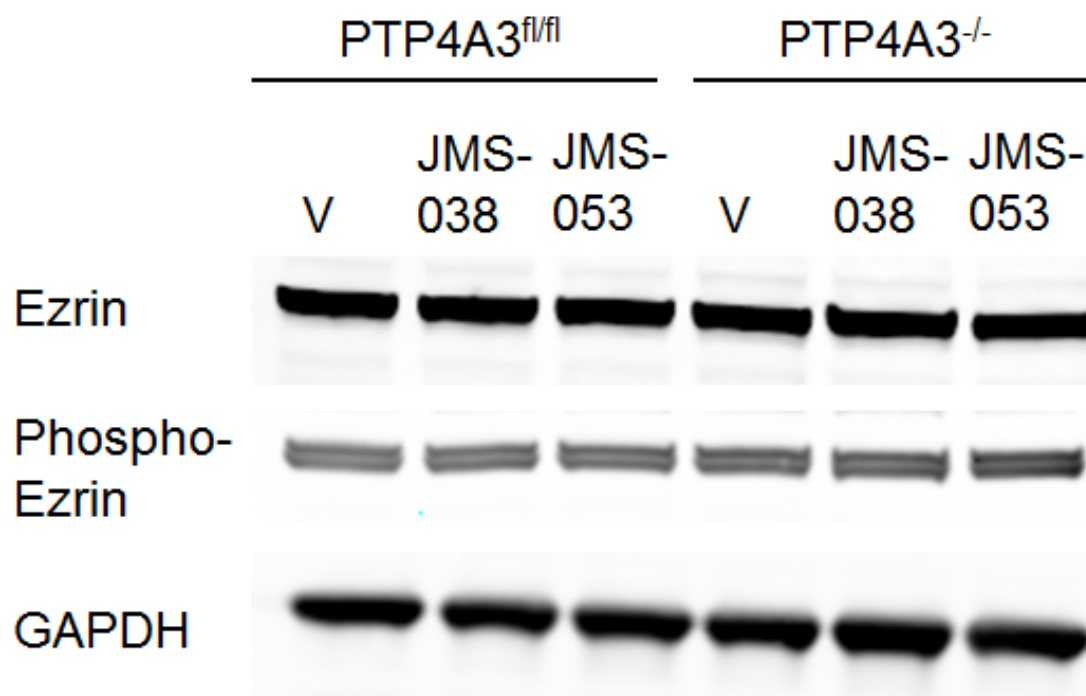
Figure 3-3 PTP4A3 loss or inhibition does not affect the levels of total Ezrin protein or phospho-Ezrin.

Murine CRC cells treated with 2.5 µM JMS-053, the control compound JMS-038, or DMSO vehicle (V) for 24 h. Levels of total Ezrin and phospho-Ezrin as determined by Western blotting. GAPDH was used as the loading control. The use of the JMS-038 and JMS-053 compounds will be discussed in CHAPTER 4: .

3.2.2 PTP4A3 deletion or inhibition reduces CRC colony formation, spheroid formation, migration, and adhesion.

When PTP4A3^{fl/fl} and PTP4A3^{-/-} cells were grown on a two-dimensional (2D) plastic monolayer, no significant difference in the growth rate was detected (Figure 3-4A), consistent with previously published observations of an unchanged proliferation rate of *Ptp4a3* wildtype cancer cells after siRNA suppression of PTP4A3[138]. Despite the similar growth rate in 2D, when the cells were investigated in a clonogenic assay the PTP4A3^{-/-} cells produced fewer colonies than the PTP4A3^{fl/fl} cells indicating a reduced capacity to produce progeny (*i.e.* a reduced reproductive viability) when seeded on plastic (Figure 3-4B). There was an even more striking contrast in the colony forming ability of the two cell populations observed when they were suspended in soft agar (Figure 3-4C). Anchorage-independent colony formation and cell growth on a semisolid medium, such as soft agar, has been a fundamental method to define *in vitro* transformation because it is associated with tumor cell aggressiveness *in vivo*, tumorigenesis, and metastatic potential[200]. It is notable, therefore, that the soft agar colony forming efficiency of PTP4A3^{fl/fl} cells was 15-fold greater than their PTP4A3^{-/-} counterpart (Figure 3-4C). This is consistent with, but more pronounced than, the decreases previously reported with siRNA for PTP4A3[138].

Three-dimensional (3D) culture conditions are generally regarded as superior to 2D tumor cell models, because 3D cell cultures possess several features of tumors, such as cell-cell interaction, hypoxia, drug penetration, response and resistance, and production/deposition of ECM[201]. These factors can shift growth dependence away

from the phenotype of unrestrained proliferation, which is dominant in standard 2D cultures. Therefore, scaffold-free conditions were used to examine the growth of the paired CRC lines. Homotypic cell interactions in a scaffold-free environment were assessed by plating between 500-5000 cells in polyHEMA coated round bottom plates to examine the morphology of the spheroid 48 h later. PTP4A3$^{fl/fl}$ cells formed well-defined spheroids, whereas PTP4A3$^{-/-}$ cells failed to form organized spheroids at all cell concentrations (Figure 3-5).

Overexpression of PTP4A3 has been previously shown to increase cell migration[11,134] while reduction by siRNA[93] or complete gene deletion[75] decreases cell migration. Consistent with these observation, PTP4A3$^{-/-}$ cells displayed a ~40% reduction in transwell migration (Figure 3-6A), and more than a 50% decrease in migration as measured by a scratch wound assay (Figure 3-6B). The altered homotypic interactions and reduced migratory ability suggested a change in the adhesive properties of the cells in the absence of PTP4A3. The ability of circulating tumor cells to attach to a secondary site is a fundamental step during invasion and metastasis[202]. Therefore, I examined differences in cellular adhesion based upon impairment of the impedance of electrical current across the cell culture surface, reported as cell index. PTP4A3$^{-/-}$ cells exhibited reduced cell index compared to the PTP4A3$^{fl/fl}$ cells (Figure 3-6C).
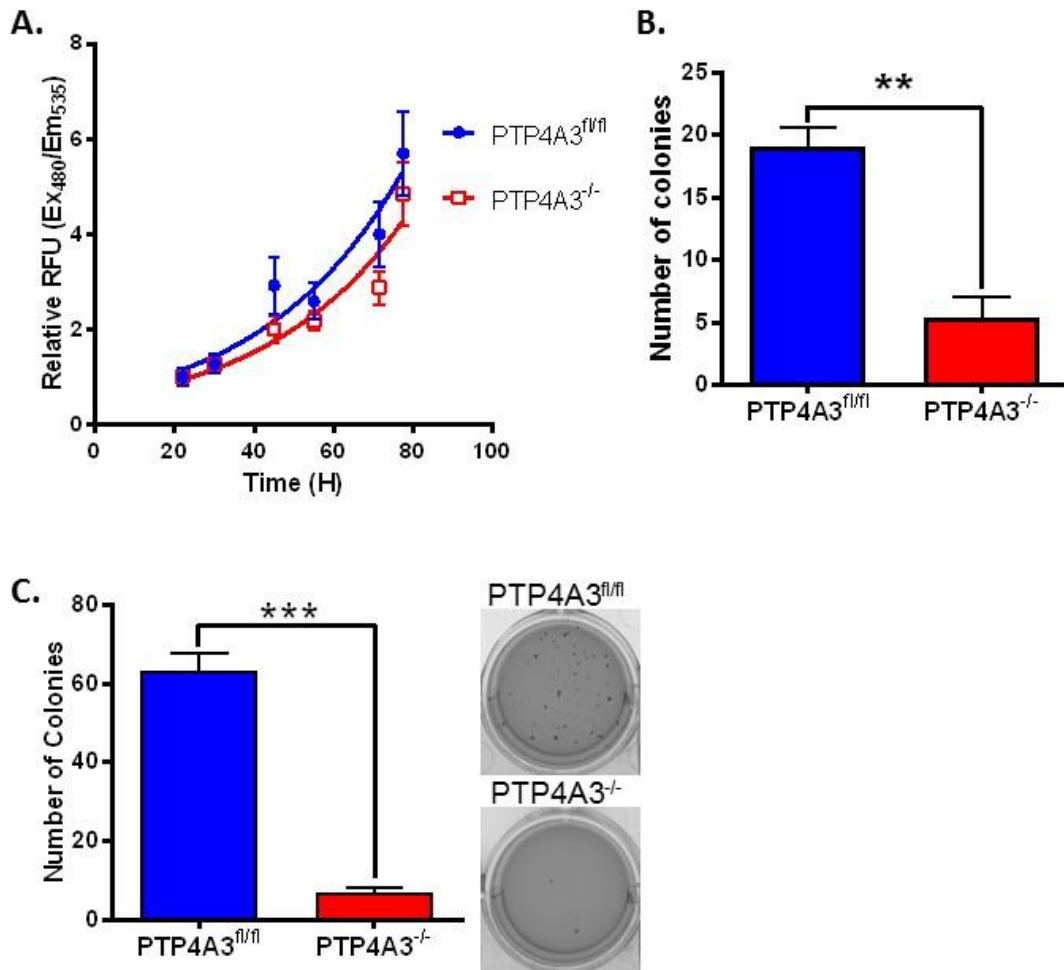
Figure 3-4 Loss of PTP4A3 did not alter 2D growth but significantly reduced colony formation.

A) Growth rate of PTP4A3$^{fl/fl}$ and PTP4A3$^{-/-}$ cells grown as monolayer on plastic. N=6, error bars=SEM. **B)** Number of colonies containing >50 cells counted after plating 500 cells/well in a 6-well dish. Cells were allowed 12 days to grow and stained with crystal violet for visualization. **C)** PTP4A3$^{-/-}$ cells displayed a marked decrease in colony formation when grown in soft agar compared to PTP4A3$^{fl/fl}$ cells. Representative images of cells stained with crystal violet seen below graph. N=3, error bars=SEM, **=P<0.005, ***=P<0.001.
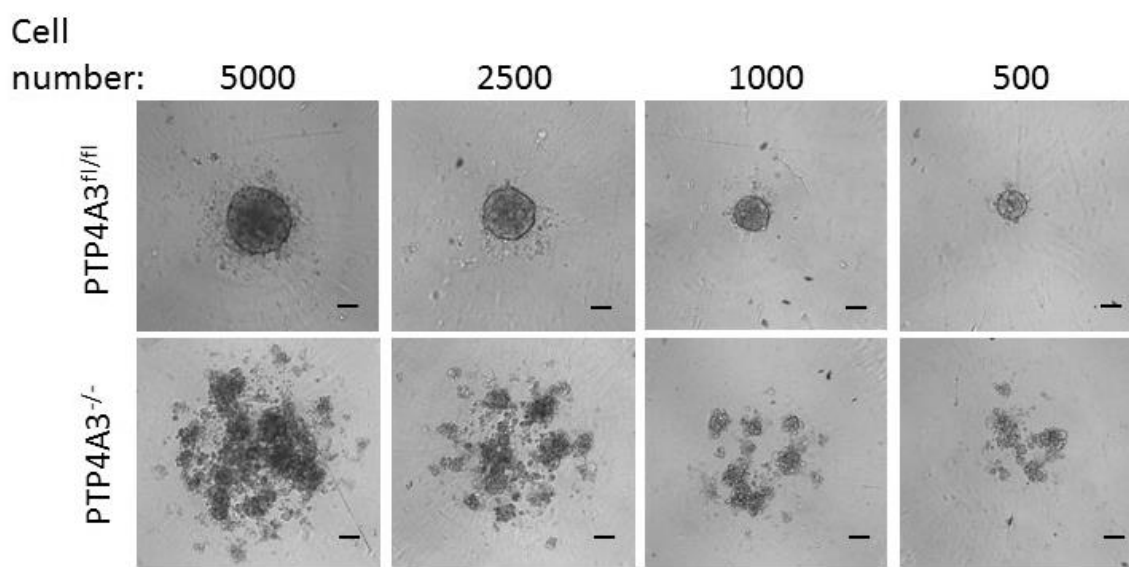
Figure 3-5 Loss of PTP4A3 impaired tumor cell spheroid formation.

PTP4A3$^{-/-}$ cells were unable to form spheroids when cultured in cell repellent plates. The indicated number of PTP4A3$^{fl/fl}$ and PTP4A3$^{-/-}$ cells were plated and images of spheroids were obtained 48 h later using a 10x objective. Scale bars=50 µm.
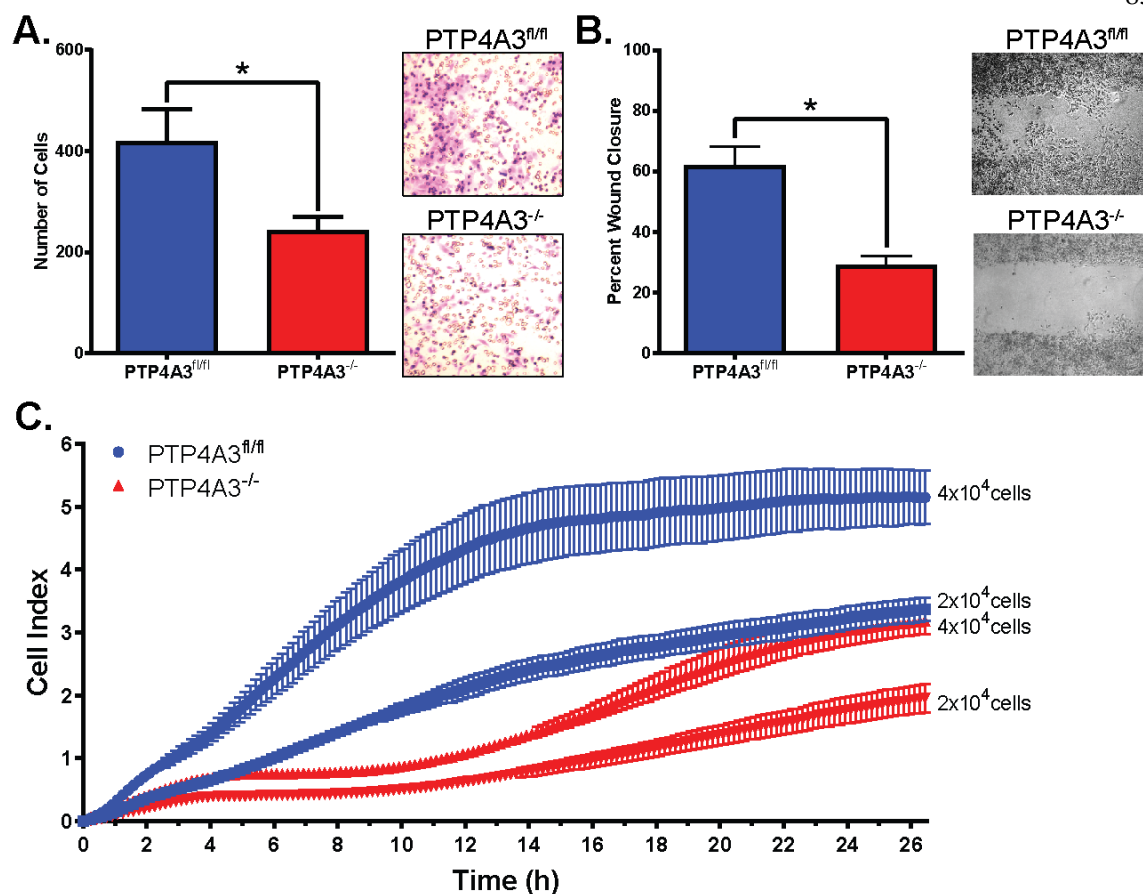
Figure 3-6 Loss of PTP4A3 causes reduced migration and adhesion in tumor cells.

A) Loss of *Ptp4a3* decreased cell migration as measured by a transwell assay. N=4, error bars= SEM. *=P<0.05. **B**) Loss of PTP4A3 decreased cell migration as measured by a scratch wound healing assay. N=3, error bars=SEM. * =P<0.001. **C**) Real-time monitoring of cell impedance using xCELLigence biosensor, which detects cell attachment, spreading, and number based on changes in impedance, reported as Cell Index. N=4, error bars=SEM.

3.2.3 PTP4A3 regulates the expression of key ECM and adhesion genes.

Cell migration, colony formation, spheroid formation, and adhesion all require

highly coordinated interactions with the ECM[203]. Therefore, I next examined the changes

in the expression of genes encoding key adhesion and ECM proteins caused by the

absence of PTP4A3. Of the 84 genes examined by a commercially available PCR array,

eight were significantly overexpressed in the PTP4A3^{-/-} cells compared to PTP4A3^{fl/fl}

cells: *Emilin 1*, *fibulin 1* (*Fbln1*), *tissue inhibitor of metalloproteinase 1* (*Timp1*),

versican (*Vcan*), *thrombospondin 1* (*Thbs1*), *integrin subunit β2* (*Itgb2*), *integrin subunit*

β3 (*Itgb3*), *hemolytic complement* (*Hc*), and *matrix metallopeptidase 3* (*Mmp3*) (Figure

3-7A). *Matrix metalloproteinase 1* (*Mmp1*) was significantly suppressed. All of these

changes were confirmed by qRT-PCR, with *Emilin 1* being the most highly

overexpressed (Figure 3-7B). I next examined the expression of these adhesion and ECM

genes in the 967 human cell lines in the Cancer Cell Encyclopedia and the TCGA

colorectal adenocarcinoma database (cBioPortal). In both the Cancer Cell Encyclopedia

(Figure 3-8A) and the TCGA datasets (Figure 3-8B) high expression of PTP4A3 mRNA

is generally accompanied by low expression of the adhesion and ECM interacting genes

identified as upregulated in the PTP4A3^{-/-} cells, as illustrated in the heatmap by the

isolation of the PTP4A3-high (red) subset in the top row. Notably, in the TGCA patient

samples (Figure 3-8B), not only were PTP4A3-high expressors isolated, but also high

expression of the ECM and adhesion genes of interest appeared to co-occur, as illustrated

by the clustering of high expressers (red) in individual samples. Of the 379 cases with

RNA-Seq data, 52 (14%) had increased expression of *Ptp4a3*, while 97 (26%) had altered

expression of *Ptp4a3* and/or one of the other genes identified in our ECM PCR array

panel. Moreover, a significantly reduced overall survival was observed in patients with

tumor samples having altered expression of *Ptp4a3* or any of the identified ECM and

adhesion genes (Figure 3-8).
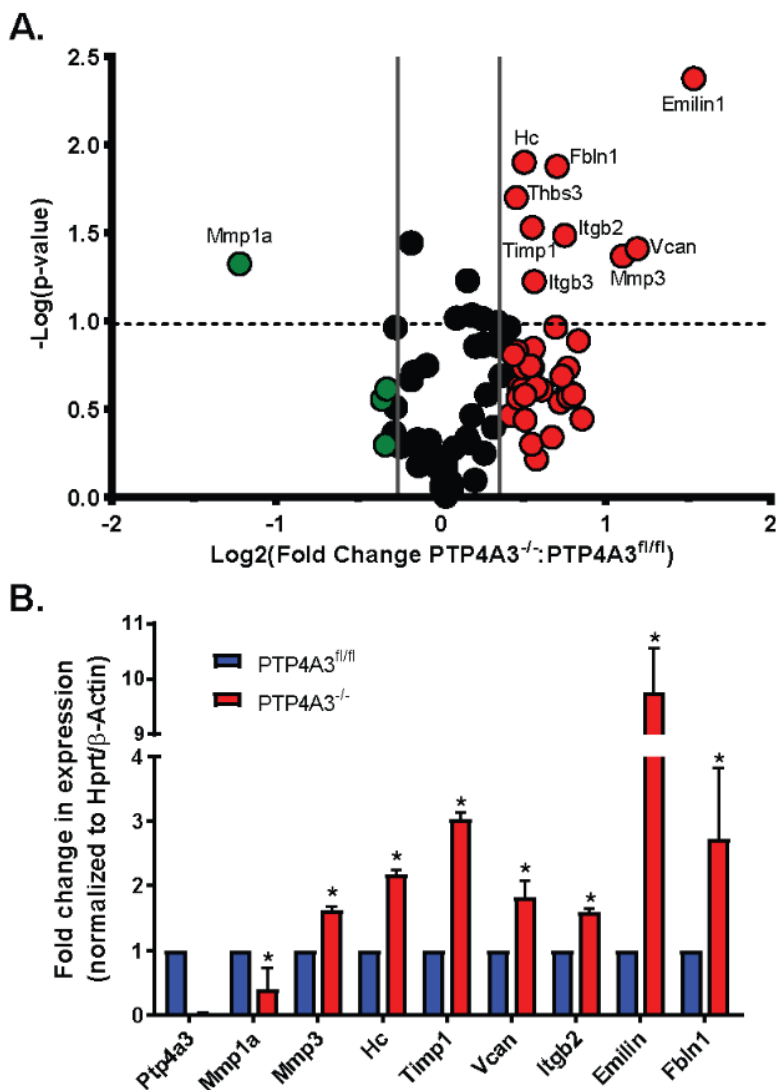
Figure 3-7 Loss of PTP4A3 alters the gene expression of ECM and adhesion genes.

A) Volcano plot of differences in mRNA gene expression. Changes in relative gene expression from Qiagen Extracellular Matrix and Adhesion PCR Array of PTP4A3^{-/-} versus PTP4A3^{fl/fl} cells are shown. Genes with ≥1.5-fold overexpression are noted in red and genes with ≥1.5-fold underexpression are noted in green. The dashed line=P<0.05. N=3. **B)** Confirmation by qRT-PCR of gene expression changes in PTP4A3^{-/-} cells identified in RT-PCR array. mRNA levels relative to *Hprt* and *Gapdh*. N=4, error bars=SEM. *=P<0.05. N=3.
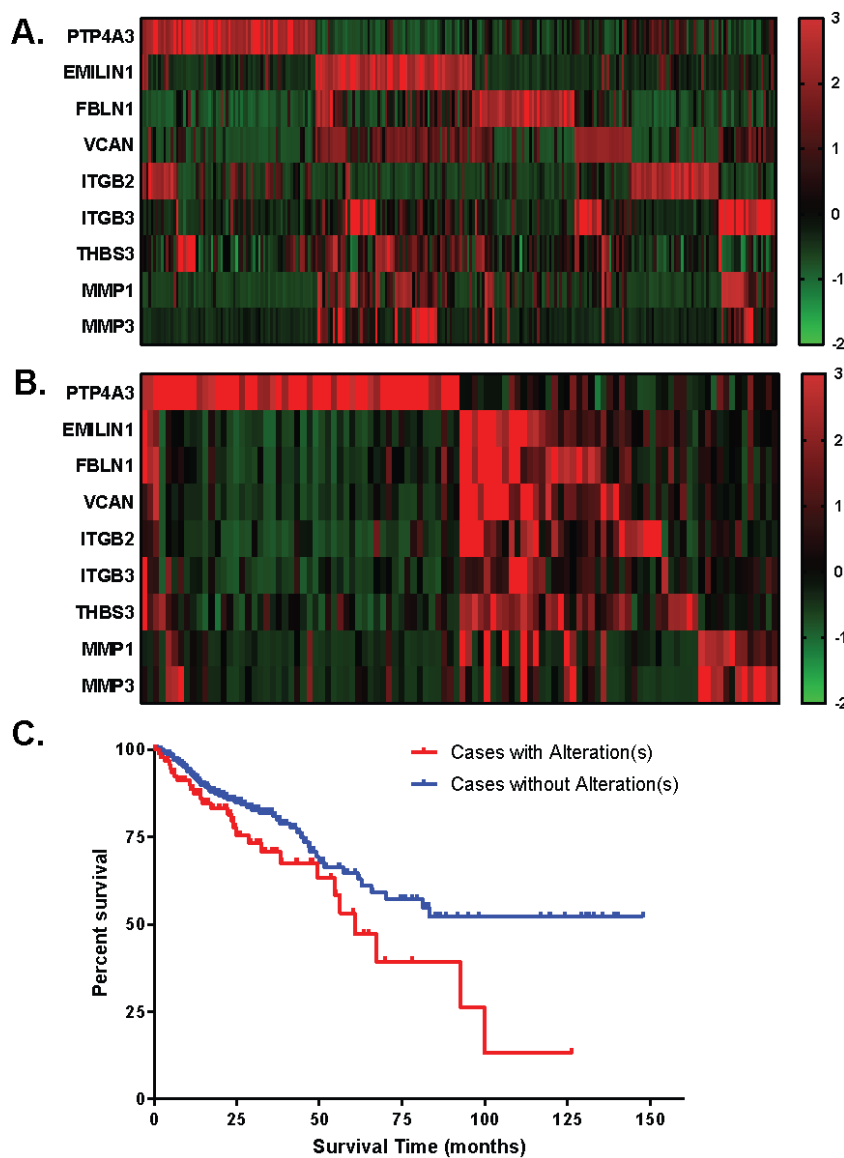
Figure 3-8 Changes in *PTP4A3* and ECM and adhesion genes in cancer cells and CRC patient samples.

A-B) Cancer Cell Line Encyclopedia (**A**) and TCGA Provisional CRC sample (**B**) heat map of the expression levels of *Ptp4a3* and genes previously identified with the PCR array. Red indicates overexpression and green underexpression. Each bar represents an individual patient sample. **C**) Kaplan-Meier plot of overall survival of patients who had altered gene expression of *Ptp4a3* or the identified adhesion and ECM genes. P=0.032.

3.2.4 PTP4A3$^{fl/fl}$ and PTP4A3$^{-/-}$ cell in vivo tumorigenicity.

Based on the phenotypic data, gene expression data, and the correlation of changes in the genes identified with patient tumor data, I predicted that PTP4A3$^{-/-}$ cells would have a reduced tumorigenicity *in vivo* compared to PTP4A3$^{fl/fl}$ cells. The ability of the feeder-layer independent cells to form tumors facilities the investigation of the importance of total PTP4A3 protein as well as PTP4A3 phosphatase activity in the tumor cells. Consistent with the formation of tumors by the parental *Ptp4a3$^{fl/fl}$* feeder-layer dependent cells, the PTP3A3$^{fl/fl}$ cells successfully established tumors upon subcutaneous injection into athymic nude mice. A histological analysis of H&E stained (1) primary colonic tumors[46], (2) tumors formed by feeder-layer dependent cells in nude mice[45], and (3) tumors formed by feeder-layer independent PTP4A3$^{fl/fl}$ cells in nude mice confirmed that all three tumors accurately reflect the pathological features of murine colonic adenocarcinoma (Figure 3-9). MUC2 is a mucin family protein that marks mature goblet cells in the intestine. MUC2 expression was undetectable in both the feeder-layer dependent[45] and feeder layer-independent cells in culture but clearly visible by immunofluorescent staining of the feeder-independent PTP4A3$^{fl/fl}$ cell-derived tumors (Figure 3-9). The MUC2 positive staining in the tumors derived from PTP4A3$^{fl/fl}$ cells indicates that, despite growing as a monolayer in culture, the cells still maintained colonic tumor cell-intrinsic multipotency.

Mirroring the initial studies of the non-paired cell lines, PTP4A3$^{fl/fl}$ and PTP4A3$^{-/-}$ cells were subcutaneously injected into the right and left flank, respectively, of athymic nude mice. In contrast to what was observed previously with the non-paired, feeder layer-dependent cells[45], both the PTP4A3$^{fl/fl}$ and PTP4A3$^{-/-}$ feeder-layer independent cells

formed tumors upon injection into athymic nude mice (Figure 3-10A). The change in the

estimated tumor volume (mm^3) over time of masses formed by PTP4A3$^{fl/fl}$ and PTP4A3$^{-/-}$

cells was determined based on bi-weekly longitudinal caliper measurements and can be

seen in Figure 3-10B and C, respectively. There was a large variance in the estimated

tumor volume but there appeared to be a trend toward a smaller volume at day 47 in the

PTP4A3$^{-/-}$ tumors. There was no significant difference in the size of the tumors formed,

although the tumors generated by the PTP4A3$^{-/-}$ cells trended towards a lower mean total

tumor weight at the completion of the study (Figure 3-10D). At the time of sacrificing the

mice, there were no obvious metastatic lesions as determined by necropsy.
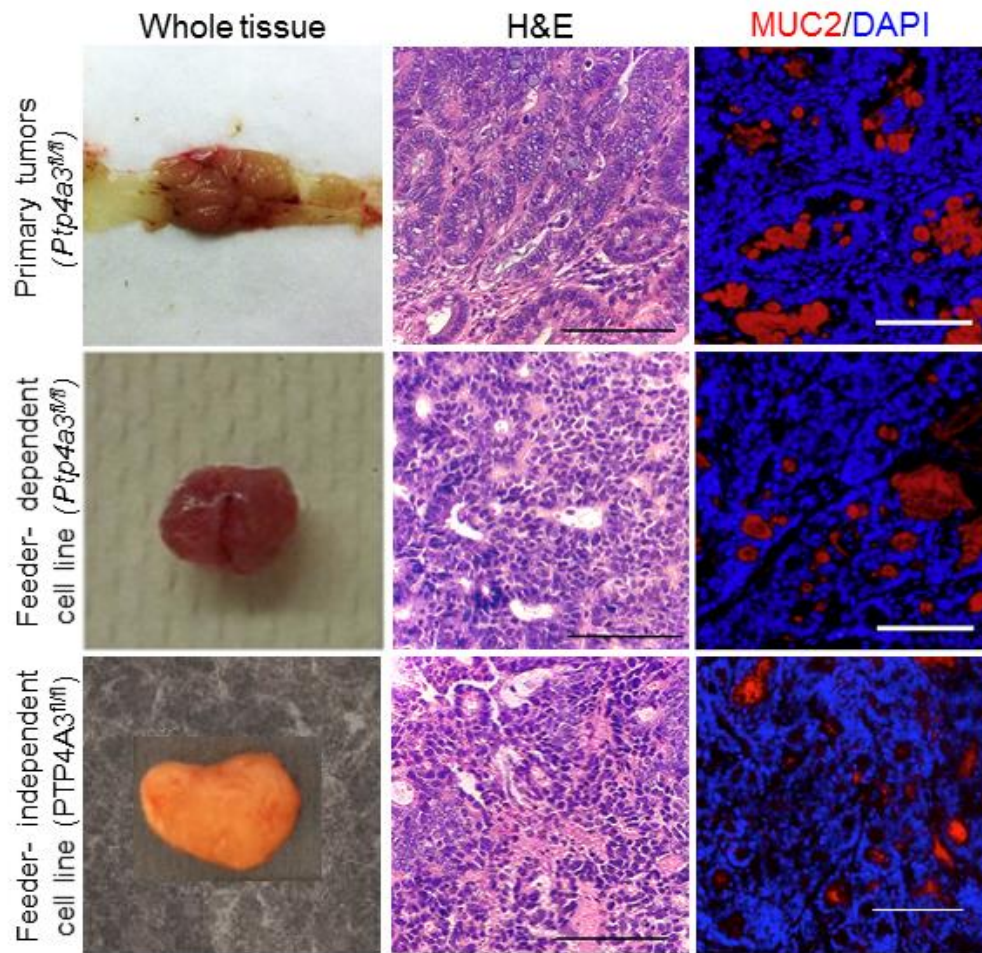
Figure 3-9 Cultured PTP4A3$^{fl/fl}$ cells maintain tumorigenicity and multipotency indicative of a colonic tumor.

Comparison of primary *Ptp4a3$^{fl/fl}$* tumors[45,46] to tumors formed in nude mice following subcutaneous injection of 1x10^6 feeder layer-dependent *Ptp4a3$^{fl/fl}$* cells[45] or 2x10^6 feeder layer-independent PTP4A3$^{fl/fl}$ cells revealed similar composition and tissue structure in sections stained with H&E and immunostained for MUC2 (red) and nuclei (DAPI, blue). Scale bar= 100 μm. MUC2 staining of primary tumor and feeder dependent cell line performed by Dr. Julie Cramer at University of Pittsburgh and reported in Cramer *et al.*[45].
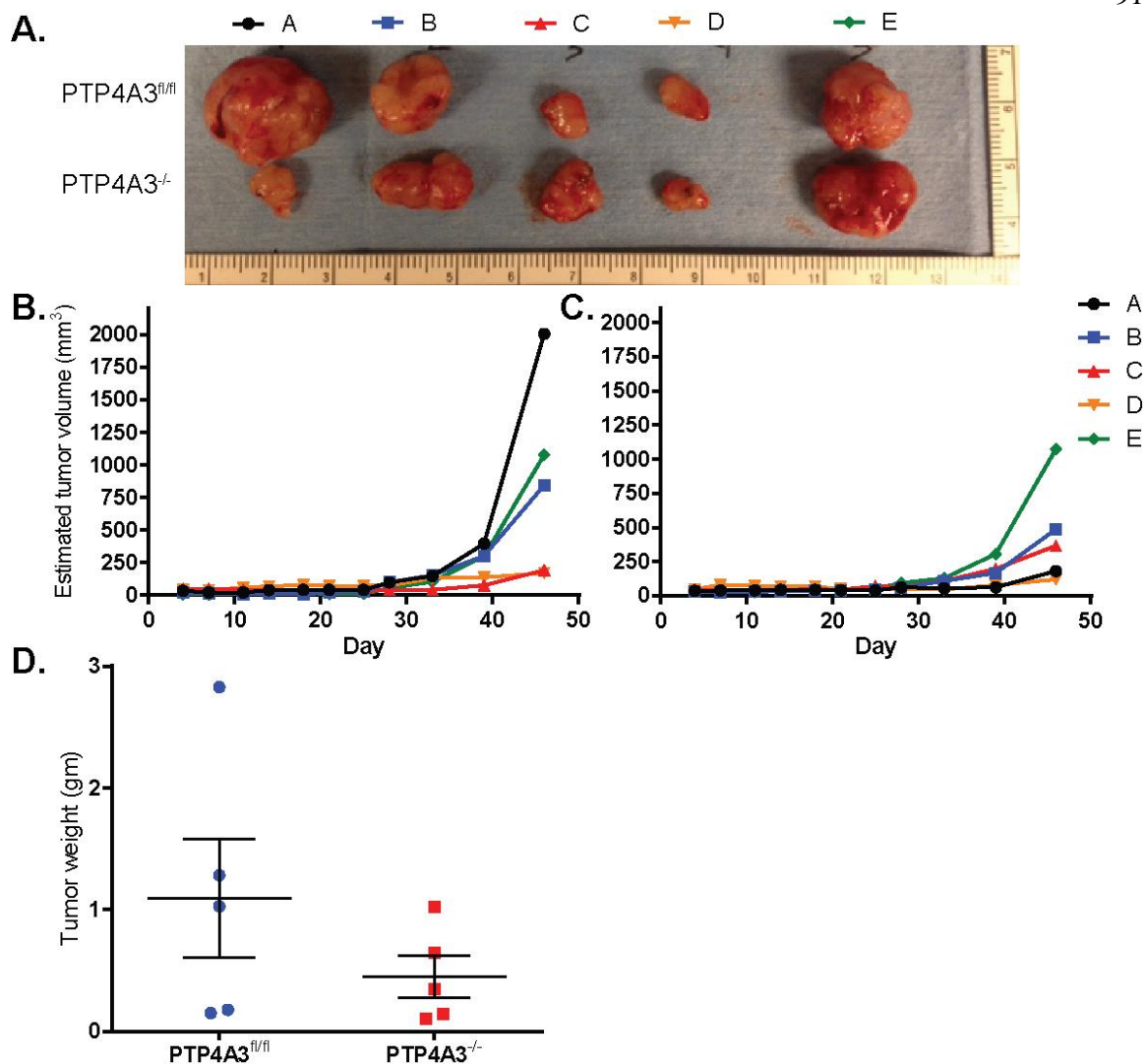
Figure 3-10 Tumor formation in nude mice bilaterally injected with PTP4A3^{fl/fl} and PTP4A3^{-/-} cells lines.

A) Photograph of PTP4A3^{fl/fl} and PTP4A3^{-/-} paired tumors excised from mice following 46 day study. **B**) PTP4A3^{fl/fl} and **C**) PTP4A3^{-/-} estimated tumor volume over time as determined by longitudinal measurements by digital caliper of mass at site of injection where the depth was assumed to be equivalent to the shortest of the perpendicular axes. **D**) Graph of final tumor weights at the end of 47-day study. Scale bar=SEM, N=5, P=0.27 as determined by paired two-tailed t-test.

3.3   Summary

PTP4A3 phosphatase appears to have a complex role in cancer biology and its direct substrates have not been established. Consequently, new cellular models provide valuable reagents to clarify PTP4A3's functionality. The pair of PTP4A3 replete and PTP4A3 deplete colon cancer cells, which are independent of any companion mixed species feeder layer, afford a powerful and stable tool for investigating the phosphatase. Coupling the PTP4A3 replete cell line with its PTP4A3$^{-/-}$ cell line partner provides a controlled experimental system to further delineate the functionality of PTP4A3 phosphatase and its role in cellular function and signaling. The model system presented demonstrated that loss of PTP4A3 total protein in CRC tumor cells did not affect 2D proliferation of cells grown in a monolayer on plastic, however, the PTP4A3 deficient cells were significantly less able to form colonies both on plastic and when suspended in soft agar. When prohibited from adhering to plastic, PTP4A3$^{fl/fl}$ cells were capable of forming cohesive spheroids while their PTP4A3$^{-/-}$ obverse was unable to construct these spherical assemblies. Furthermore, the genetic loss of PTP4A3 reduced the murine CRC cell migration and adhesion. These collective phenotypes provoked the investigation of how the loss of PTP4A3 altered the expression of ECM and adhesion genes and revealed previously unknown effects of PTP4A3 on its molecular regulators. The most provocative change is *Emilin 1*, a reported tumor suppressor, which binds specifically to elastin and is a key component of the ECM in tumor tissue[204,205]. PTP4A3 mRNA and protein overexpression in metastatic CRC have been noted by others[9,44]. There is an increase in PTP4A3 mRNA expression in 14% of the CRC tumors sequenced in the

TCGA database. Moreover, the relationship between PTP4A3 loss and significantly altered ECM and adhesion gene expression appeared to translate into expression correlation in other cancer cell lines and patient CRC tumor samples. In addition, changes in PTP4A3 mRNA and/or mRNA from these identified effectors correlated with a significant reduction in overall patient survival. I found both the PTP4A3$^{fl/fl}$ and PTP4A3$^{-/-}$ cells formed tumors upon injection into nude mice. Although there was a trend in the reduction of tumors produced by cells lacking PTP4A3, the difference in tumor weight was not statistically significant different and further investigation is warranted, given the caveats of the experimental design described above. Regardless of the results, the ability of the paired CRC cell lines to form tumors facilitates the study of the on-target effects of inhibitors that disrupt PTP4A3 phosphatase activity *in vivo*.

CHAPTER 4:   DEVELOPMENT AND CHARACTERIZATION OF A POTENT NONCOMPETITIVE SMALL MOLECULE INHIBITOR TO TARGET PTP4A4 PHOSPHATASE ACTIVITY

4.1   Introduction

While genetic approaches have enormous power, pharmacological tools often provide compelling orthogonal methods for discerning the biochemical functions of enzymes. The interrogation of PTP4A3's biochemical function and therapeutic authentication would be greatly abetted by potent, reversible, and selective small molecule inhibitors. The problems with the currently available small molecule inhibitors discussed above (Section 1.3.3), including lack of selectivity, redox potential and ready availability, compelled our endeavor to generate an improved PTP4A3 phosphatase inhibitor. Using the structure of the sub-micromolar PTP4A3 inhibitor thienopyridone[138] as a starting point, initial evaluation of the structure-activity relationship (SAR) with regard to the inhibitory activity of the thienopyridone scaffold was performed. Upon identifying a thienopyridone analog with enhanced potency, the mode of inhibition, biochemical properties, and specificity were determined. This compound, along with an inactive analog, has now been employed to demonstrate the role of PTP4A3 phosphatase activity in the oncogenic phenotypes provoked by the physiologically relevant levels PTPA3 overexpression observed in the murine CRC cells. The combined use of the newly developed cell pair and a small molecule inhibitor can be used to investigate how the phosphatase activity of PTP4A3 controls cellular interactions, which could be

relevant to PTP4A3's involvement in the malignant cell phenotype and in tumor

progression.

4.2   Results

4.2.1 Thienopyridone photooxygenation product JMS-053 is a potent PTP4A3 phosphatase inhibitor.

To facilitate the study of thienopyridone compound analogs, our collaborators at

the University of Pittsburgh established a scalable thienopyridone synthesis route[190]. I

then determined the IC_{50} of newly synthesized thienopyridone to be ~132 nM using an *in*

vitro PTP4A3 phosphatase assay and DiFMUP as an artificial substrate (Table 4-1,

Figure 4-1B). This value was consistent with previous reports[138]. I was also able to begin

to generate a structure-activity relationship for the thienopyridone chemotype. With the

same *in vitro* phosphatase assay, the presence of the 7-amino substitution was determined

to be essential based on the total lack of inhibitory activity of JMS-095 (Table 4-1). The

7-iminothieno[3,2-*c*]pyridine-4,6(5*H*,7*H*)-dione, referred to as JMS-053, was produced

using photooxygenation conditions to selectively introduce oxygen atoms onto

thienopyridone[190]. The addition of this oxygen atom is highlighted in red in Table 4-1.

The structural assignment of JMS-053 was confirmed by X-ray crystallography of JMS-

053 crystals generated by the evaporation of the acetonitrile solution (Figure 4-1A). JMS-

053 provides a dramatic increase in the potency as compared to the parent thienopyridone

(JMS-050) and has an IC_{50} of ~18 nM (Figure 4-1B), and, thus, is the most potent

PTP4A3 inhibitor reported. JMS-053 is novel as no structurally similar compounds were found in either the PubChem or ChemSpider databases using a 2D Tanimoto score of ≥0.8. Similar to the thienopyridone parent compound, JMS-053 also inhibits PTP4A1 and PTP4A2, although at a slightly reduced potency compared to PTP4A3 (Figure 4-1C). Because both PTP4A1 and PTP4A2 also have oncogenic properties and are overexpressed in cancer, a pan-PTP4A family inhibition profile may be a valuable attribute for a small molecule inhibitor[12,89].

Given the success of modifying the thienopyridone scaffold, the SAR was expanded by investigating pyrimidinediones. The pyrimidinedione scaffold is characterized by a pyrimidine ring substituted with two carbonyl groups, presenting an amalgam of the previously described BR-1 structure (Table 1-2) and thienopyridone. JMS-038 (Table 4-1) contains a pyrimidinedione group and therefore the carbonyl groups present on JMS-053, yet it has not inhibitory activity towards PTP4A3. By replicating the thione functionality, the scaffold of BR-1 is more closely paralleled in JMS-072 and JMS-088 (Table 4-1). Neither of these compounds, however, displayed inhibitory activity toward PTP4A3 in the DiFMUP phosphatase assay. The failure of JMS-038, JMS-072, and JMS-088 to inhibit PTP4A3 emphasizes the importance of the 7-nitrogen substitution in JMS-053.

Table 4-1 *In vitro* evaluation of PTP4A3 phosphatase activity inhibition

Compound	Structure	IC$_{50}$ (µM)
Thienopyridone (JMS-050)		0.132
JMS-095		>80
JMS-053		0.018
JMS-038		>240
JMS-072		>100
JMS-088		>100
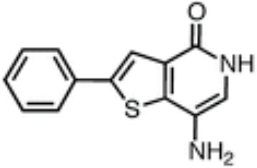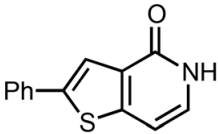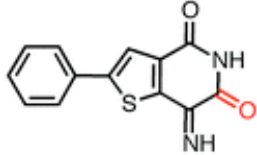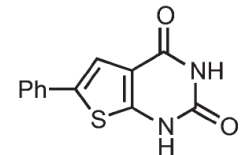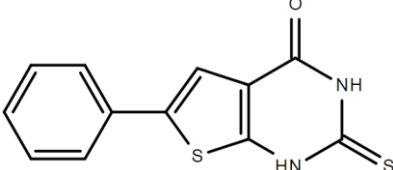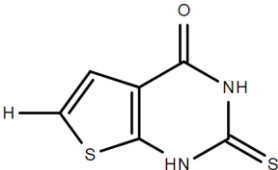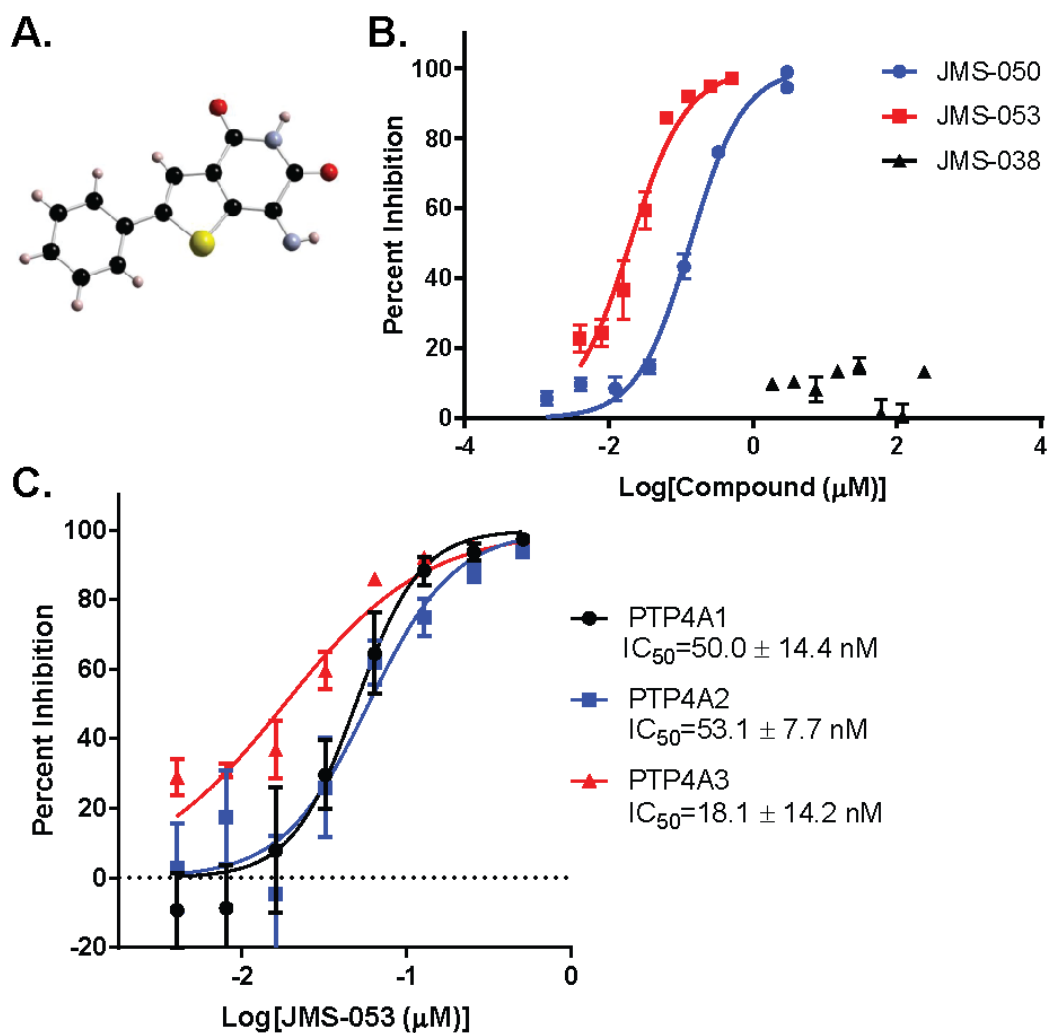
Figure 4-1 The X-ray crystallography confirmed amino-thienopyridone potently inhibits PTP4A family phosphatase activity.

A) Structure of crystalline JMS-053 as determined by X-ray crystallography. Black balls represent carbons, pink represent hydrogen, yellow represent sulfur, gray represent nitrogen, and red represent oxygen. **B)** Representative IC_{50} curves for PTP4A3 inhibition with the parent thienopyridone (JMS-050) (●), JMS-053 (■), and a control compound (JMS-038) (▲). Error bars=SEM, N=5. **C)** Representative IC_{50} curves using recombinant PTP4A1/2/3 as determined by DiFMUP phosphatase assay. Error bars=SEM, N=3.

4.2.2 JSM-053 is a reversible noncompetitive PTP4A3 phosphatase inhibitor.

JMS-053 is a low-nanomolar small molecule inhibitor that introduces a powerful

tool for the interrogation of PTP4A3's role in CRC. Moreover, the close structural analog

JMS-038 was inactive at concentrations as high as 100 µM, and therefore serves as a

useful negative control compound (Figure 4-1B). Both the parent thienopyridone, JMS-

050, and JMS-053 bind reversibly to PTP4A3, as indicated by relief of total inhibition

seen upon dilution of the compound to IC_{50} concentrations (Figure 4-2A). Reversible

inhibition further distinguishes JMS-053 from many other PTP inhibitors, which

frequently are irreversible, because they form covalent adducts or generate species that

oxidize the catalytic Cys[12]. Thienopyridone and JMS-053 behaved as a noncompetitive

inhibitor of DiFMUP substrate dephosphorylation (Figure 4-2B-C). In addition to the

enhanced potency, JMS-053 also has significantly improved *in silico* drug-like properties

compared to thienopyridone (Table 4-2). Profiling JMS-053 against a panel of 25 other

phosphatases (Figure 4-3A-C, Table 4-3) and 50 kinases (Table 4-4) shows this

chemotype is highly specific for the PTP4A family despite its rather small mass. The

PTPs surveyed were broadly representative of the major human superfamily members,

including three receptor-like PTPs, ten cytosolic PTPs, and five closely related dual-

specificity phosphatases. This specificity was irrespective of whether one compared the

amino acids in the catalytic domain (Figure 4-3A) or the full-length protein (Figure 4-3B-

C). JMS-053 also inhibited the two homologous PTP4A family members, PTP4A1 and

PTP4A2, with IC_{50} values of 50 ± 14 and 53 ± 8 nM, respectively (Figure 4-1C).

Comparatively minimal inhibition was detected with the other phosphatases or kinases

using a 1 µM screening concentration, with the exception of CDC25B and p38α, which

were inhibited by ~50%. Overall, JMS-053 shows at least a 20-fold selectivity for the

PTP4A enzymes.

Based on kinetic studies and the nature of the relationship of IC_{50} and K_i in non-

competitive inhibitors, the K_i of JMS-053 for PTP4A3 was calculated to be 18 nM. Initial

attempts to co-crystalize JMS-053 with PTP4A3 have been unsuccessful. Therefore,

PTP4A3 thermal denaturation profiling was conducted using SYPRO orange dye, an

environmentally sensitive fluorophore that exhibits increased fluorescence on binding to

hydrophobic protein segments. A T_m of 50.5 ± 0.6ºC ($n = 3$) was obtained for the apo

protein lacking the ligand, while adding JMS-053 (100 µM) produced a ΔT_m of 3.0ºC or a

destabilizing effect against PTP4A3 indicative of ligand binding[206] (Figure 4-4A). This

ΔT_m exceeded the 1.7ºC shift seen with a similar concentration of the much less potent

thienopyridone. The negative control JMS-038 (100 µM) showed no effect on PTP4A3

stability. The recently available X-ray structure of PTP4A3 in a complex with CNNM3

(PDB 5TSR) was used to identify possible PTP4A3 binding modes for JMS-053[156].

Based on computational docking studies with an energy refined structure, a putative

binding site in the closed conformation was identified that was in agreement with a

noncompetitive mechanism (Figure 4-2C and Figure 4-4B). The theoretical allosteric site

is removed from the active site, and is flanked by the α3, α4, and α6 helices, and the

WPD loop. As the highly flexible WPD loop clamps down on the active site, the imine

moiety of the inhibitor could engage in a hydrogen bond with Asp72. As a result, this

acidic residue would no longer be available to support enzymatic activity through

interactions with catalytically important P-loop residues Cys104 and Arg110[207].

Moreover, a tight, well desolvated inhibitor binding mode is predicted to hold the WPD

loop in the closed conformation (Figure 1-6B). This would be facilitated by: 1) hydrogen bonds between the compound's pyridinedione oxygens and the side chain amine and hydroxyl groups of residues Lys144 and Tyr148, respectively, 2) π-stacking between the thienopyridinedione and the Tyr148 side chain aromatic ring, and 3) favorable π-π and hydrophobic contacts between the inhibitor's phenyl substituent and the aromatic side chains of residues Phe70 and Trp84, as well as the alkyl side chains of residues Pro76, Val80, Val81, Leu85, Leu114, and Leu117, respectively. The proposed JMS-053 binding mode (Figure 4-4B) suggests that the thienopyridone structure is less active than JMS-053, because the former cannot engage in a hydrogen bond with Lys144, while JMS-038 is void of activity, because it lacks the ability to orient in the proposed binding site such that a hydrogen bond with Asp72 is established. All of the proposed JMS-053 amino acid contact sites, with the exception of Val80, are conserved in the three PTP4A family members, which is consistent its inhibitory profile.
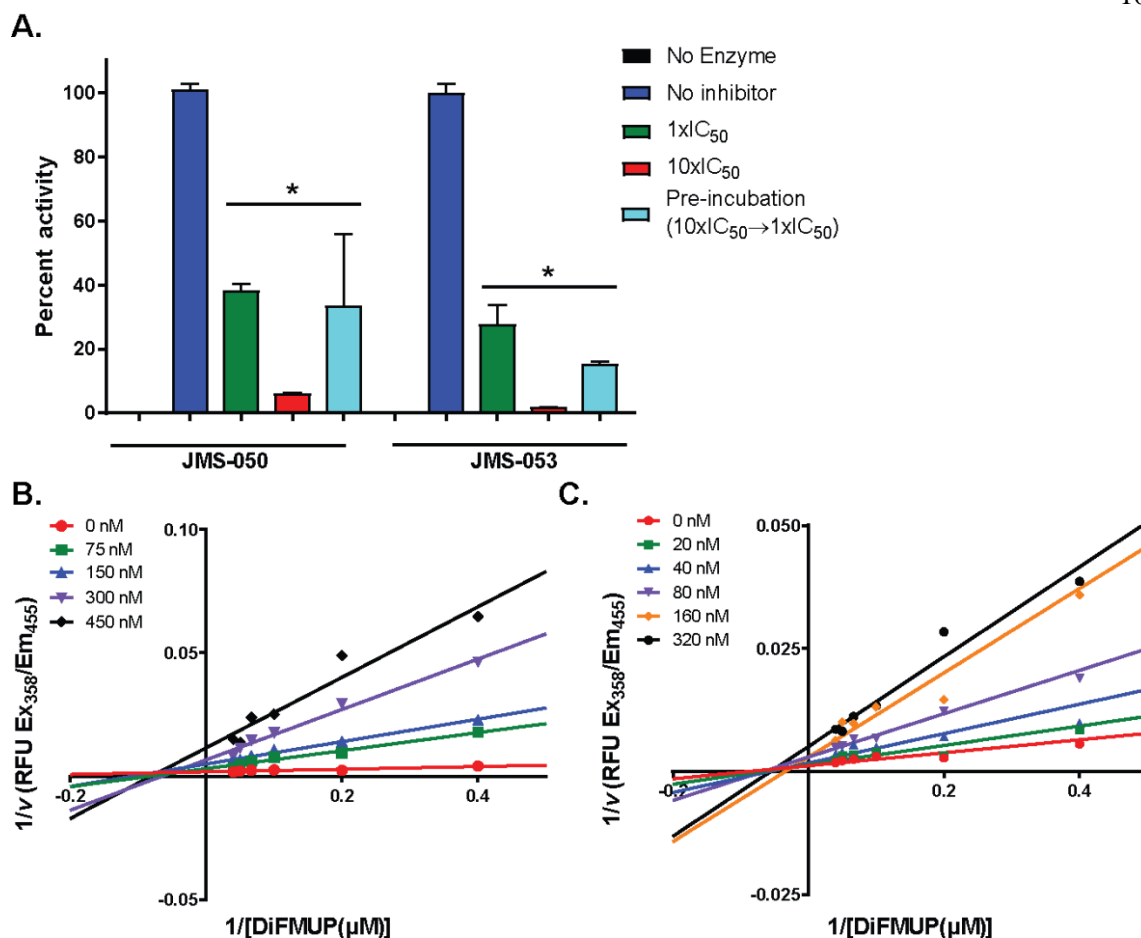
Figure 4-2 JMS-053 mechanism of PTP4A3 phosphatase inhibition.

A) Reversible PTP4A3 inhibition by JMS-053. Full length PTP4A3 was treated with vehicle (0.5% DMSO) or with a concentration of JMS-050 (thienopyridone) or JMS-053 equal to the IC_{50} or 10-fold higher, i.e. 132 or 1320 nM and 18 or 180 nM, respectively. Pre-incubated samples were exposed to the compound for 30 min and then diluted to 132 or 18 nM, (IC_{50}). Phosphatase activity is expressed as a percent maximal activity. Error bars=SD, N=12, *=P<0.01 verses no inhibitor control. **B** and **C)** Lineweaver Burk plots indicated noncompetitive inhibition by both thienopyridone (**B**) and JMS-053 (**C**). Bars=SEM, N=8.

Table 4-2 Drug-like properties of parent thienopyridone compound and JMS-053.

Properties	Thienopyridone (JMS-050)	JMS-053
H Donor	2	2
H Acceptor	3	4
Total Surface Area	177.9	182.0
Relative Polar Surface Area	0.338	0.402
Polar Surface Area	83.36	98.26
cLogP	2.125	1.545
cLogS	-4.283	-3.43
Druglikeness	3.683	4.393

Figure 4-3 PTP dendrograms.

A) PTP dendrogram of the 11 amino acids in the active site as described by Almo *et al.*[193], depicting in red the PTPs tested for *in vitro* inhibition by JMS-053. JMS-053

inhibitory activity was tested on those phosphatases indicated in red. The blue branches

indicate tyrosine phosphatases and the orange branches are the dual specificity

phosphatases. **B**) Dendrogram represents the alignments of the longest isoform of the full

length PTP as described by St-Denis *et al.*[194]. Marked in red are the PTPs that were

assayed in this project. **C**) Dendrogram represents the alignments of the longest isoform

of the full length dual specificity phosphatase with assayed phosphatases indicated in red.

Table 4-3 Phosphatase specificity profiling of JMS-053.

JMS-053 (1 µM) was profiled *in vitro* against 26 phosphatases. Assays performed by a

commercial vendor unless otherwise marked with an asterisk. N=2.

Phosphatase	% Activity (Mean ± SD)
PTPRC (CD45)	88 ± 3
DUSP22	91 ± 6
PTPN7 (HePTP)	97 ± 3
ACP1 (LMPTP-A)	95 ± 4
LMPTP-B	99 ± 0
DUSP10 (MKP5)	87 ± 0
PTPN4 (PTP-MEG1)	100 ± 1
CDC25B*	52 ± 6
PTPN9 (PTP-MEG2)	88 ± 5
PTPN1 (PTP-1B)	90 ± 5
PTPN22	94 ± 2
PTPRB (PTPβ)	95 ± 5
PTPRM (RPTPµ)	80 ± 1
PTPN6 (SHP-1)	97 ± 11
PTPN11 (SHP-2)	100 ± 9
PTPN2 (TCPTP)	95 ± 3
DUSP13 (TMDP)	95 ± 1
DUSP3 (VHR)	87 ± 11
PTP4A1*	1 ± 0
PTP4A2*	0 ± 0
PTP4A3*	0 ± 0
PP1α	75 ± 0
PP2A*	99 ± 0
PP5	96 ± 2
YopH (Yersinia)	86 ± 4
Lambda PP (Phage)	72 ± 3

Table 4-4 Kinase specificity profiling of JMS-053.

JMS-053 (1 µM) was profiled *in vitro* against 50 kinases. Assays performed by a

commercial vendor. N=2.

Kinase	Family	Activity Ave ± SD		Kinase	Family	Activity Ave ± SD
AAK1	Other	82 ± 1		MARK2	CAMK	86 ± 3
ABL1	TK	95 ± 3		MLK2	TKL	101 ± 3
ACVR2A	TKL	93 ± 2		MLK3	TKL	101 ± 3
AKT1	AGC	87 ± 0		MSK2	AGC	94 ± 2
AKT2	AGC	87 ± 5		MST2	STE	99 ± 5
AKT3	AGC	91 ± 3		MUSK	TK	98 ± 5
AMPKa1	CAMK	98 ± 1		p38a	CMGC	50 ± 3
AURKA	Other	104 ± 1		PDGFRB	TK	87 ± 0
AURKB	Other	90 ± 2		PDPK1	AGC	92 ± 2
AURKC	Other	90 ± 0		PIM1	CAMK	86 ± 1
CAMK1D	CAMK	90 ± 2		PKA	AGC	87 ± 1
CAMK2D	CAMK	100 ± 4		PKCe	AGC	86 ± 1
CDK5	CMGC	84 ± 2		PKG1	AGC	98 ± 2
CLK2	CMGC	76 ± 2		PLK4	Other	90 ± 3
DAPK3	CAMK	86 ± 1		PRKX	AGC	94 ± 1
DDR1	TK	88 ± 3		PYK2	TK	91 ± 1
EPHA5	TK	96 ± 1		RSK2	AGC	100 ± 2
EPHB2	TK	98 ± 8		SLK	STE	85 ± 0
FLT1	TK	90 ± 2		SNF1LK	CAMK	100 ± 2
FLT3	TK	108 ± 2		SNF1LK2	CAMK	92 ± 1
HCK	TK	93 ± 1		SRC	TK	83 ± 6
IGF1R	TK	87 ± 0		TNK1	TK	84 ± 1
ITK	TK	87 ± 2		VEGFR2	TK	90 ± 0
KIT-KD	TK	94 ± 1		YANK2	AGC	88 ± 3
MARK1	CAMK	87 ± 3		YSK1	STE	100 ± 2
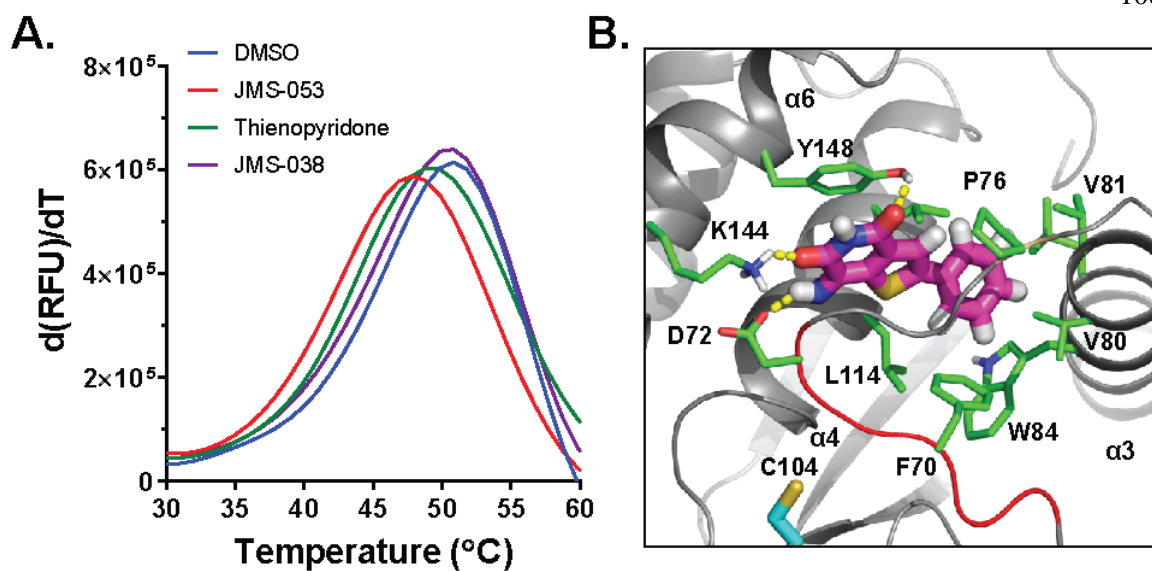
Figure 4-4 Proposed binding of JMS-053 to PTP4A3.

A) Thermal shift assay for PTP4A3 protein (T_m = 50.5ºC) showing destabilization by 100 µM JMS-053 (T_m = 47.5ºC) and by 100 µM thienopyridone (T_m = 48.8ºC). JMS-038 (100 µM) produced no significant thermal shift. **B)** Hydrogen bonds are shown with yellow dashes, and WPD loop residues W68PFDD72 are indicated by red cartoon. For reference, active site residue C104 is shown with cyan carbons.

4.2.3 JMS-053 replicates the effects of Ptp4a3 gene deletion and can inhibit the viability of human CRC cells.

The small molecule thienopyridone was previously described to inhibit anchorage-independent cell growth of RKO and HT-29 CRC cells grown in soft agar with an $EC_{50} \approx 7.5$ µM[138,186]. Treatment of the murine colorectal tumor cells with our newly synthesized thienopyridone produced a similar EC_{50} in cells with functional PTP4A3, PTP4A3^{fl/fl}, while no further reduction in colony formation was seen in cells lacking the phosphatase, PTP4A3^{-/-} (Figure 4-5A). JMS-053 was 10x more potent than thienopyridone and inhibited anchorage-independent growth in PTP4A3^{fl/fl} cells in a concentration-dependent manner with an $EC_{50} \approx 0.35$ µM (Figure 4-5B). Importantly, treatment of PTP4A3^{-/-} cells acted as a control to demonstrate that the JMS-053 inhibition of colony formation was PTP4A3-dependent, and upon treatment with JMS-053 did not result in further reduction in colony formation. Moreover, there was no statistically significant difference in the number of soft agar colonies between the PTP4A3^{fl/fl} and PTP4A3^{-/-} cells upon treatment with 5 µM JMS-053 (Figure 4-5B).

The reduced migratory ability of PTP4A3^{-/-} cells was also replicated by JMS-053 treatment (Figure 4-6A). In a scratch wound healing assay, the PTP4A3^{fl/fl} cells were unaffected by the inactive congener JMS-038 (5 µM), but wound closure decreased with increasing JMS-053 concentrations resulting in an EC_{50} of ~337 nM. Treatment with ≤15 µM JMS-053 had no significant effect on PTP4A3^{-/-} cell wound closure. Likewise, treatment of PTP4A3^{fl/fl} cells with 1 or 5 µM JMS-053 replicated the reduction in cellular impedance seen in PTP4A3^{-/-} cells (Figure 4-6B). Significantly, JMS-053 replicated more

than just the phenotypic differences observed in the absence of PTP4A3. Upon treatment

of PTP4A3$^{fl/fl}$ cells with JMS-053 for 48 h, the increase in *Emilin 1* mRNA expression

seen in PTP4A3$^{-/-}$ cells was reproduced (Figure 4-7). There was no significant impact of

the JMS-053 treatment on the PTP4A3$^{-/-}$ cells (Figure 4-7). It is notable that inhibition of

PTP4A3 phosphatase activity by JMS-053 in PTP4A3$^{fl/fl}$ cells, as well as control

compound JMS-038, had no effect on Ezrin Thr567 phosphorylation, which is similar to

the previously mentioned lack of a change in Ezrin Thr567 phosphorylation status in the

untreated PTP4A3$^{-/-}$ cells compared to untreated PTP4A3$^{fl/fl}$ cells.

Importantly, JMS-053 inhibited the growth of human CRC cells. This is in

contrast to the lack of any inhibitory activity seen with JMS-053 treatment of non-

malignant IMR-90 cells[208]. A 48 h exposure to JMS-053 inhibited human HCT116 and

DLD-1 CRC spheroid cell growth with an EC$_{50}$ of 2.6±0.4 and 2.9±0.7 μM, respectively

(Figure 4-8A-B), which demonstrated the growth inhibition was not unique to the mouse

CRC cells. No growth inhibition or cytotoxicity was seen with the control compound,

JMS-038 (Figure 4-8A-B). HCT116 colony formation in soft agar was inhibited with an

EC$_{50}$ of 1.1±0.1 μM (Figure 4-8C-D). No inhibition of HCT116 colony formation was

observed with concentrations of JMS-038 as high as 5 μM.
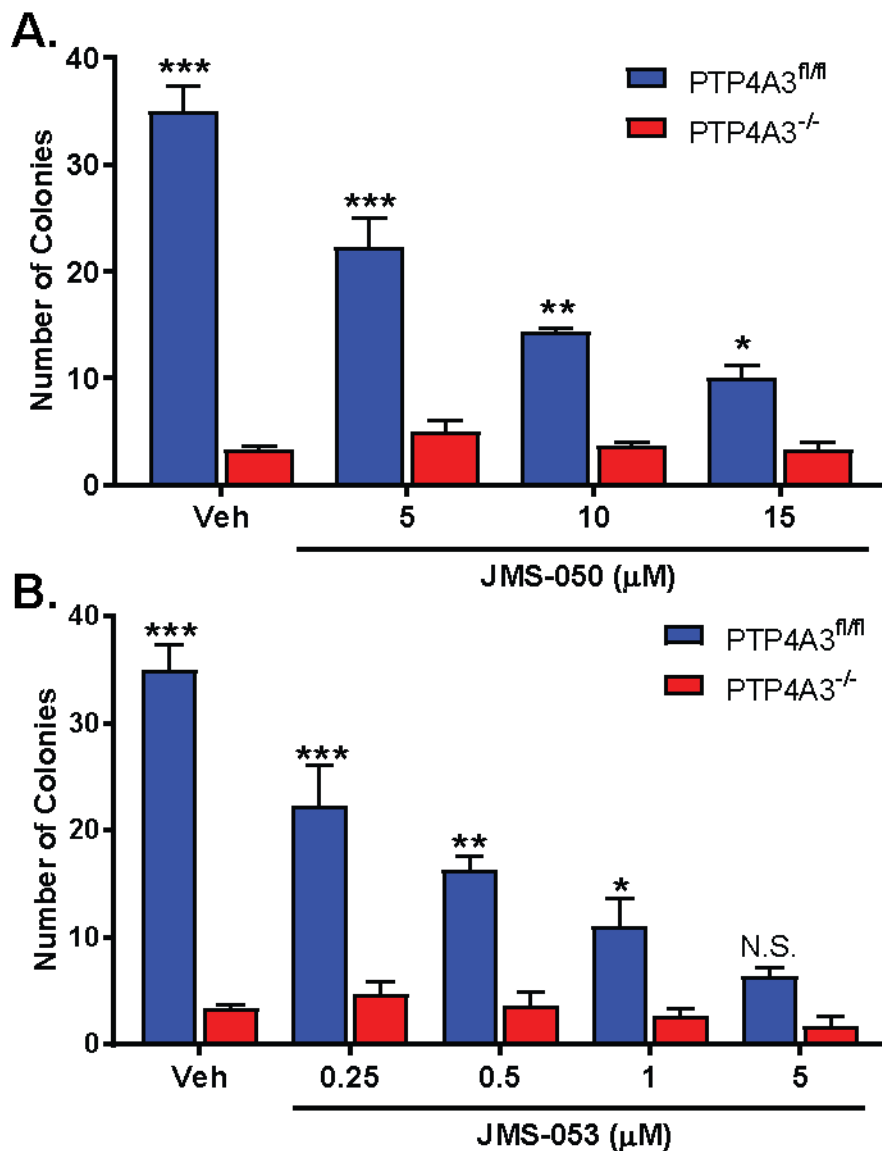
Figure 4-5 Treatment of murine colorectal cells with JMS-053 inhibits colony formation with an increased potency compared to thienopyridone (JMS-050).

A) and **B)** Concentration-dependent reduction in anchorage-independent colony formation of PTP4A3$^{fl/fl}$, but not PTP4A3$^{-/-}$ cells, after exposure to thienopyridone (JMS-050) and JMS-053, respectively. N=3, error bars=SEM, *=P<0.02, **=P<0.0005, ***=P<0.0001. P-value determined by 2-way ANOVA. N.S.=Not significant.

A.

B.
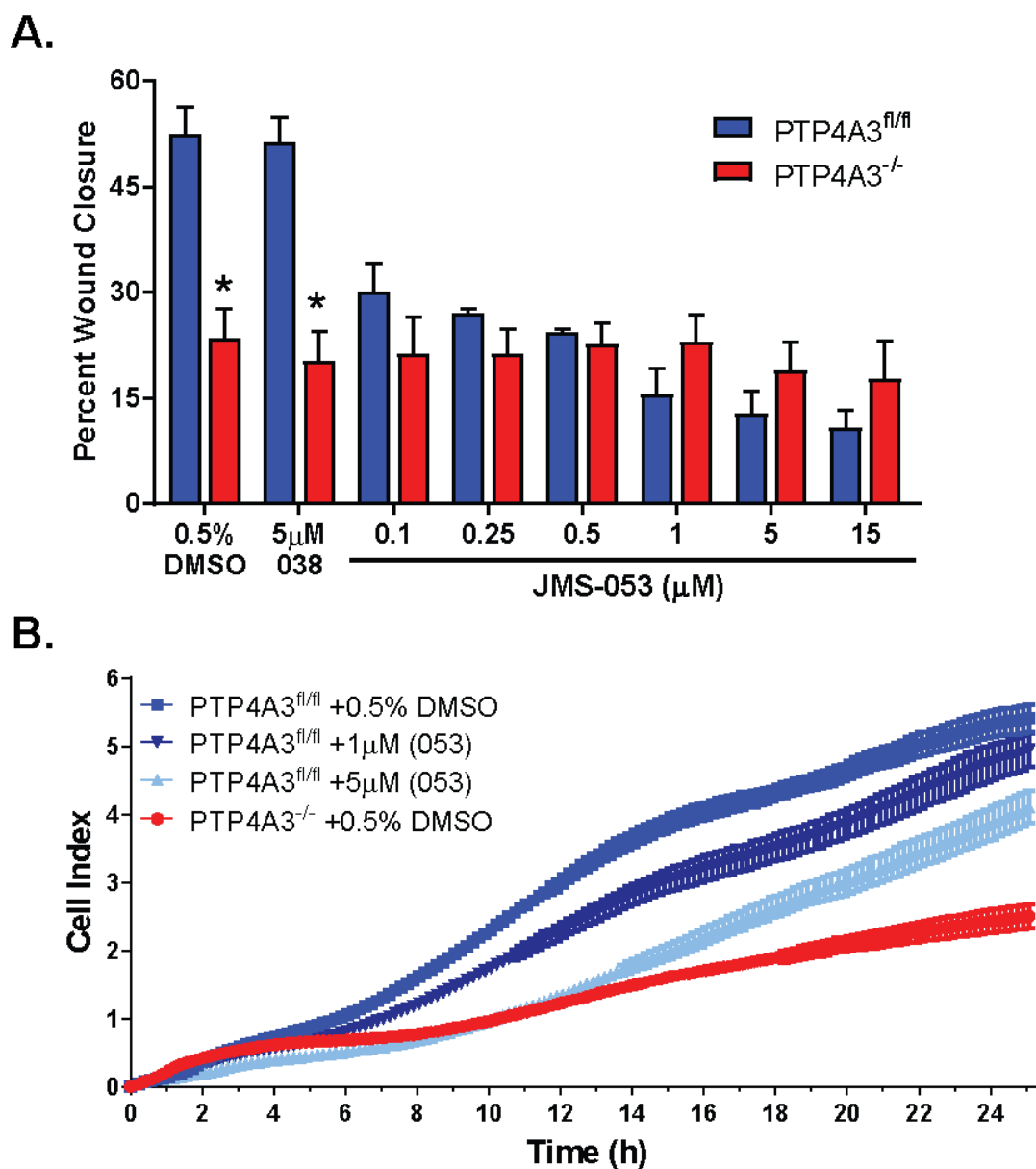
Figure 4-6 JMS-053 treatment inhibits PTP4A3$^{fl/fl}$ cell migration and adhesion.

A) Concentration response of PTP4A3$^{fl/fl}$ cells upon JMS-053 treatment in scratch wound healing assay. N=3, error bars=SEM. *P>0.001. P-value determined by 2-way ANOVA.
B) Real-time monitoring of cell impedance using xCELLigence biosensor, which detects cell attachment, spreading, and number based on changes in impedance, reported as Cell Index. N=4, error bars=SEM.
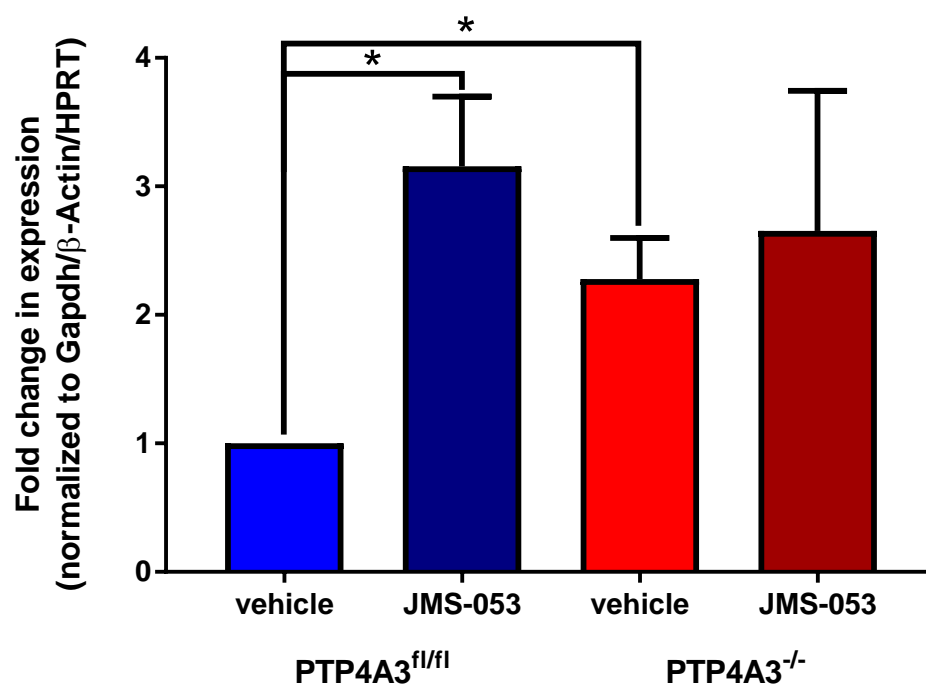
Figure 4-7 Treatment with JMS-053 increases *Emilin* expression in PTP4A3^{fl/fl} cells.

Emilin 1 mRNA expression following 48 h treatment of murine tumor cells with JMS-053 mimics the effect of genetic loss of PTP4A3. mRNA levels relative to *β-actin*, *Hprt* and *Gapdh*. N=4, error bars=SEM. *=P>0.05.
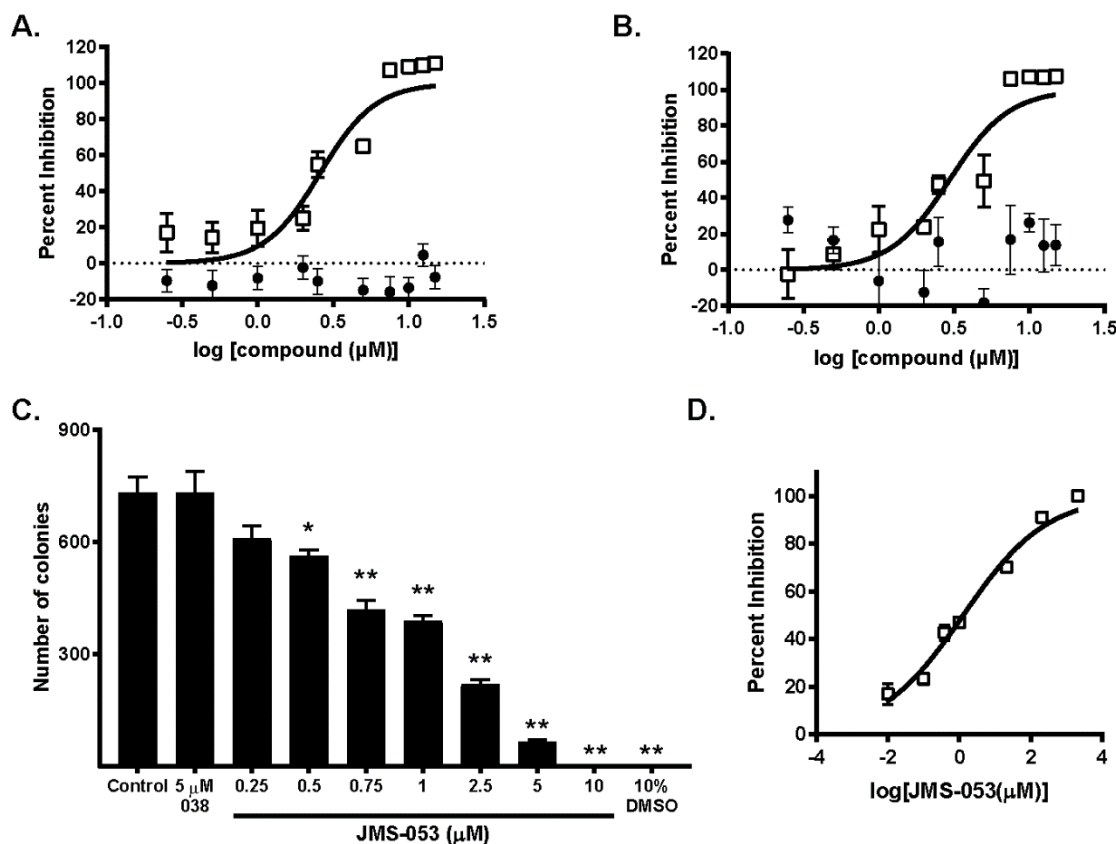
Figure 4-8 Pharmacological inhibition of PTP4A3 with JMS-053 in human CRC cell lines reduces spheroid viability and colony formation.

A-B. (□)=JMS-053; (●)=JMS-038. JMS-053 inhibited DLD-1 **(A)** and HCT116 **(B)** colon cancer cell viability when cells were cultured as spheroids with an EC_{50} of 2.6 ± 0.4 µM and 2.9 ± 0.7 µM, respectively. **C-D.** JMS-053 inhibited HCT116 colony formation with an EC_{50} of 1.1 ± 0.1 µM. C. Total number of colonies counted in each treatment group. N=3, error bars=SEM. *=$P<0.05$, **=$P<0.0001$. **D.** EC_{50} curve plotting the data shown in panel C. N=3, error bars=SEM.

4.3   Summary

The absence of a widely available potent, selective, reversible, cell-active

PTP4A3 inhibitor left the interrogation of PTP4A3's biological function and,

consequentially, its contribution to CRC pathogenesis incomplete. Pharmacological tools

provide a valuable method to dissect the role of individual functional motifs in enzymes

and statistically independent validation of genetic studies. Herein, the discovery and

development of the thienopyridone analog JMS-053, the most potent PTP4A3 inhibitor to

date (*in vitro* $IC_{50}\approx18$ nM)[190,208], is described. JMS-053 is a PTP4A-family selective

reversible inhibitor, which has been computationally predicted to bind to PTP4A3 at a

site proximal to the WPD-loop. If correct, this interaction would be predicted to inhibit

phosphatase activity by locking the enzyme in the closed conformation (Figure 1-6). As a

pan-PTP4A inhibitor, JMS-053 is a useful chemical probe for the PTP4A subfamily and

can be used to determine functional roles of the individual PTP4A family members[138,190].

For example, the results presented herein suggest PTP4A3, and not PTP4A1 or PTP4A2,

is the major family member determinant of colony formation (as determined by the soft-

agar colony formation assay), migration (as determined by the scratch wound healing

assay) and adhesion in the PTP4A3$^{fl/fl}$ CRC cells, based on the observation that treatment

of PTP4A3$^{-/-}$ cells with JMS-053 produced no further changes in these processes. Thus,

JMS-053, coupled with our loss-of-function CRC cell line pair, provides us with

complementary orthogonal methods to interrogate and confirm PTP4A3 phosphatase

functionality.

CHAPTER 5:   INVESTIGATION OF PTP4A3 EXPRESSION IN ENDOTHELIAL CELLS

5.1   Introduction

Given the broad spectrum of the reported effects of PTP4A3 on signaling and the findings presented in CHAPTER 3: 4, it is likely that PTP4A3 function is tightly regulated by cell type-specific cues from the extracellular environment. While the induction of *Ptp4a3* gene expression in HUVECs in response to VEGF treatment has been reported[13], the distal effects of PTP4A3 in the endothelium have not yet been fully explored. The potential role of PTP4A3 in vascular function during angiogenesis and metastases (reviewed in section 1.2.3), drove the investigation of PTP4A3's actions as a mediator of endothelial cell behavior and response to VEGF signaling stimulation. In the initial study of CRC tumor formation in the *Ptp4a3*^{fl/fl} and *Ptp4a3*^{-/-} mice, the tumors formed in mice lacking PTP4A3 displayed a significant reduction in microvessel density as determined by CD31 immunocytochemistry[46,75]. Moreover, in an *ex vivo* tissue explant assay, skeletal muscle tissue from *Ptp4a3*^{-/-} mice implanted in a collagen matrix exhibited reduced outgrowth of vascular cells, indicating a contribution of PTP4A3 to the invasive potential of vascular cells[75]. In an effort to more specifically investigate the impact of PTP4A3 in endothelial cells, a combination of isolated murine *Ptp4a3*^{fl/fl} and *Ptp4a3*^{-/-} endothelial cells and human endothelial cells treated with pharmacological PTP4A3 inhibitors were employed. Using these tools, I was able to not only monitor phenotypic changes, but also investigate the impact of PTP4A3 phosphatase activity on the signal transduction pathways controlling these responses in these non-malignant endothelial

cells. Moreover, the use of *Ptp4a3^{fl/fl}* and *Ptp4a3^{-/-}* mice allowed me to assess the implications of the results acquired in cell culture in the context of the whole mouse. In aggregate, this enabled me to test the hypothesis that PTP4A3 phosphatase activity promotes endothelial cell behaviors that are beneficial to tumor formation and progression.

5.2   Results

5.2.1 Knockout of PTP4A3 decreased endothelial cell migration and response to VEGF exposure in vitro.

The literature discussing PTP4A3 expression in the endothelium and the reduced microvessel density observed in the *Ptp4a3^{-/-}* murine tumors[75] led to the investigation of the function of PTP4A3 in the vasculature using cultured primary pulmonary endothelium from adult *Ptp4a3^{fl/fl}* and *Ptp4a3^{-/-}* mice. Cells were isolated, cultured, and the purity of the endothelial population was assessed as described previously[209]. Cell migration was measured *in vitro* by a wound healing assay in which endothelial cells were incubated for 16 h, a duration below the doubling time of cells to exclude wound healing by means of increased cell number, to permit gap closure via migration. This revealed that endothelial cells isolated from *Ptp4a3^{-/-}* mice migrated significantly less than their *Ptp4a3^{fl/fl}* counterpart, exhibiting a 50% reduction in gap closure (Figure 5-1A). This supports the participation of PTP4A3 in endothelial cell migration, a necessary component for angiogenesis.

The activation state of several known angiogenesis-associated pathways following

VEGF treatment was analyzed to investigate the molecular effects of eliminating

PTP4A3 in endothelial cells. Endothelial cells from wildtype and *Ptp4a3*-null pulmonary

tissue were cultured and incubated in serum-free medium for 4 h. VEGF was added to the

culture medium (50 ng/mL) and protein samples were collected at various time points for

up to 8 h. Two known VEGF-dependent mediators of the angiogenic phenotype, Src and

ERK1/2, have also been associated with PTP4A3 signaling[11,98]. Activation of both

proteins was examined in VEGF treated wildtype and *Ptp4a3*-null endothelial cells by

Western blotting methods (Figure 5-1B). As expected, mature VEGFR2 protein levels

decreased in both genotypes following VEGF treatment, presumably due to

internalization of the receptor upon activation. Significant differences in basal Src protein

phosphorylation (Y416) prior to VEGF treatment were not observed (Figure 5-1B).

Unlike basal Src (Y416) phosphorylation, however, a significant increase in phospho-Src

(Y416) was observed in wildtype cells as early as 15 min following VEGF treatment, and

persisted up to 8 h (Figure 5-1B-C). Comparatively, *Ptp4a3*^{-/-} endothelial cells did not

exhibit an increase in Src phosphorylation at any time point following VEGF exposure

(Figure 5-1B-C). An increase in phosphorylation of ERK1/2 protein was observed in both

genotypes following treatment with VEGF (Figure 5-1B). Levels of total Src and ERK1/2

protein were unchanged throughout this time course. A modest increase in the

phosphorylation of FAK (Y576/577) and paxillin (Y118) was also observed upon the

treatment of wildtype endothelial cells with VEGF (Figure 5-1D). This was not observed

with the *Ptp4a3*^{-/-} endothelial cells (Figure 5-1D). Thus, PTP4A3 appeared to be

necessary for VEGF-induced activation of Src, but not necessary for ERK1/2 activation

in endothelial cells.
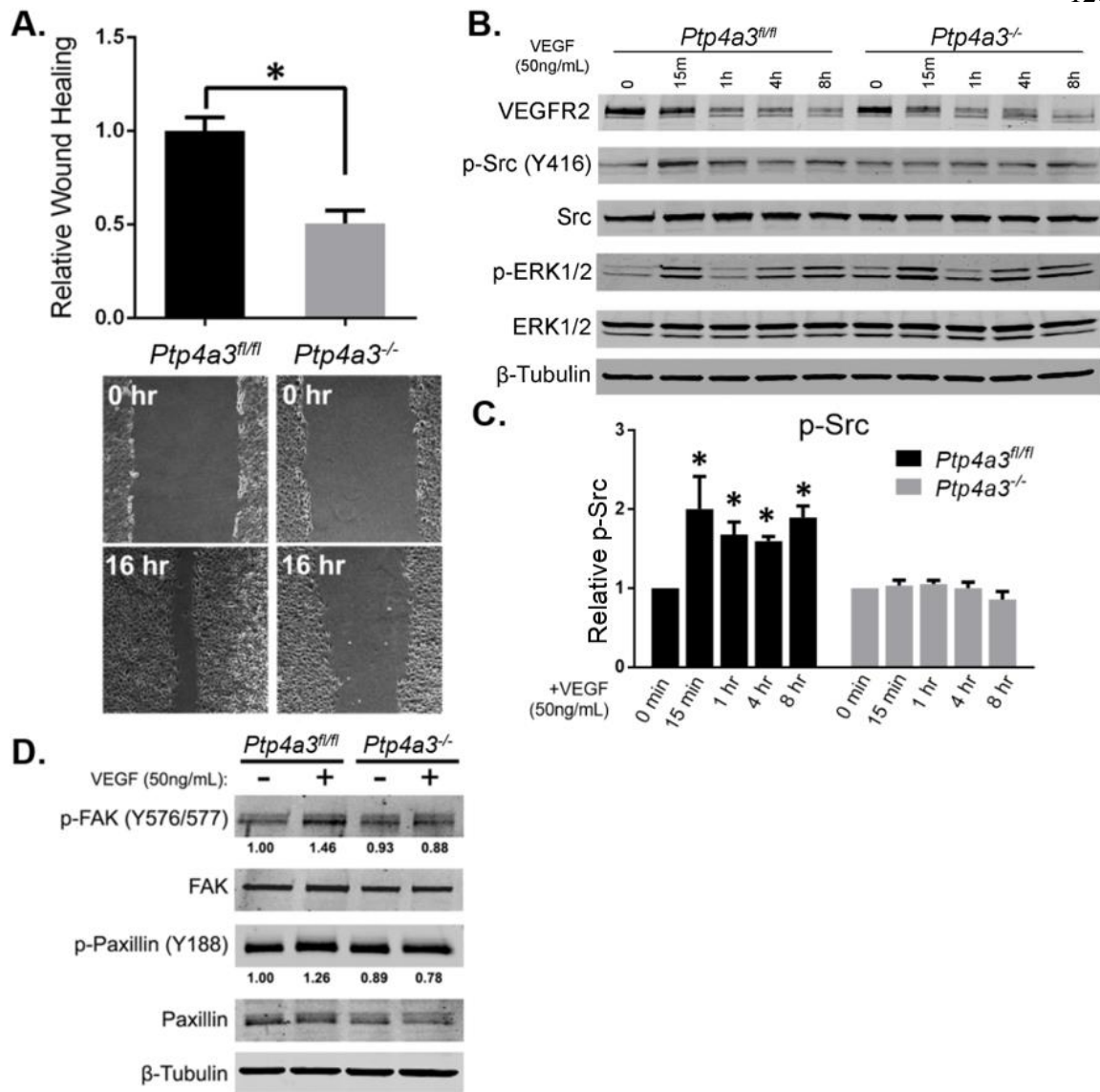
Figure 5-1 Loss of PTP4A3 decreases endothelial cell migration and response to VEGF exposure.

A) Relative wound healing was determined by measuring the gap closure between cell fronts following the 16 h migration period. *Ptp4a3*-null cells migrated 50% less compared to wildtype endothelial cells (*=P<0.001). Error bars=SEM. Representative images of the initial wound and gap closure at 16 h are below the corresponding quantification. **B-D**). Wildtype and *Ptp4a3*-null endothelial cells were grown in culture

and treated with VEGF (50 ng/mL) for up to 8 h. Protein lysates were collected at

indicated time points and Western blot analysis was performed. **B**) Western blot analysis

of levels of VEGFR2, Src, phospho-Src (p-Src), ERK, and phospho-ERK (p-ERK)

relative to β-Tubulin. **C**) Quantification of p-Src (Y416) relative to total Src visualized in

panel **B.** Error bars=SEM, N=3, *=P<0.05 as determined by two-way ANOVA. **D**).

Wildtype and *Ptp4a3*-null endothelial cells were grown in culture and treated with VEGF

(50 ng/mL) for 8 h. Protein lysates were collected as in panel A and Western blot analysis

was performed to assay activation of the downstream Src targets FAK and paxillin.

5.2.2 Pharmacological inhibition of PTP4A3 reduces human microvacsular endothelial cell (HMVEC) migration and Src activation in a VEGF-dependent manner.

As a complement to the genetic studies in murine cells, the role of PTP4A3 in HMVEC migration was examined using a pharmacological tool to block PTP4A3 phosphatase activity. At the time of the studies presented in Figure 5-2 the synthesis of thienopyridone was not complete and JMS-053 had yet to be discovered. Therefore, the commercially available PTP4A3 inhibitor BR-1, discussed in section 1.3.3, was employed to investigate the contribution of PTP4A3 phosphatase activity. The essential role of VEGF in HMVEC migration was demonstrated by addition/removal studies of the complete growth medium, which contained IGF-1, EGF, FGF and VEGF (Figure 5-2A-B). Using the *in vitro* wound healing assay, there was almost complete closure of the HMVEC wound within 16 h in the presence of complete growth factors (Figure 5-2C). Removal of VEGF from the complete growth factor mixture resulted in an almost complete loss of migration while removal of FGF had a minimal effect (Figure 5-2A). Exclusion of either EGF or IGF-1 produced an intermediate reduction in migration. Unlike IGF-1, VEGF alone was competent in reproducing most of the migration seen with the complete growth factor mixture, indicating its central role in the process of endothelial migration. The PTP4A3 inhibitor BR-1 produced a concentration-dependent decrease in endothelial cell motility when examined in a wound healing assay but had no effect on the basal migration in the absence of growth factors or with complete growth factors lacking only VEGF (Figure 5-2B-D). Moreover, 10 µM BR-1 significantly

reduced migration stimulated by VEGF alone (Figure 5-2B). Lysates were obtained from

BR-1 treated HMVECs cultured in the presence of growth factors and assayed for Src

protein by Western blotting methods (Figure 5-2E). The level of Src phosphorylation

(Y416) was significantly decreased relative to total Src protein, which showed no

significant change (Figure 5-2F). These results demonstrated that inhibition of PTP4A3

phosphatase activity could replicate the loss of PTP4A3 protein and reduced both Src

activation and endothelial cell migration in response to VEGF stimulation.
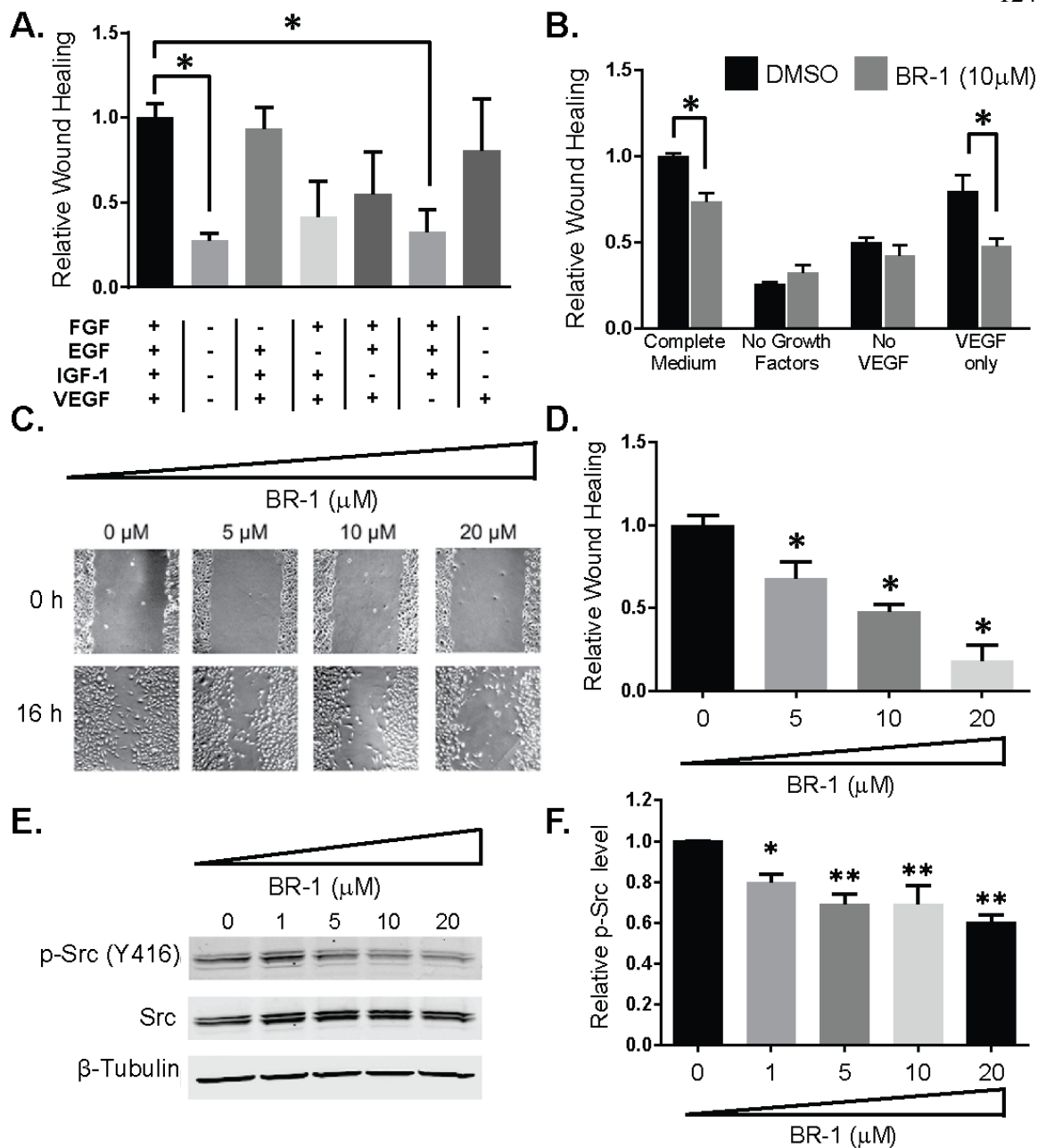
Figure 5-2 Pharmacological inhibition of PTP4A3 altered human microvascular endothelial cell migration and Src activation through a VEGF-dependent mechanism.

A) Growth factors stimulated migration of HMVECs. Confluent endothelial cells were scratched longitudinally and wound healing was measured 16 h after exposure to various

growth factors. Data analyzed by one-way ANOVA. *=P<0.05, N=3, error bars=SEM. **B)**

Effect of PTP4A3 inhibitor BR-1 on wound closure in the presence of complete growth

factors, growth factors lacking VEGF, or VEGF alone. Data analyzed by two-way

ANOVA. *=P<0.05, N=3, error bars=SEM. **C)** and **D)** BR-1 concentration-dependent

inhibition of HMVEC wound closure in complete growth medium. Representative

images of HMVECs treated with BR-1 or a DMSO vehicle control and incubated for 16

hours. Native HMVECs exhibited a significant decrease in migration when treated with

BR-1 relative to DMSO vehicle control. Data analyzed by one-way ANOVA. *=P< 0.02.

Error bars=SEM. **E)** Lysates from HMVECs treated with the PTP4A3 inhibitor BR-1

were collected and assayed by immunoblot for Src phosphorylation (Y416). **F)**

Quantification of p-Src relative to total Src protein level revealed a decrease in active Src

following PTP4A3 inhibition, which was also determined to be concentration dependent.

Data analyzed by one-way ANOVA. *=P<0.05, **=P<0.007, N=3, error bars=SEM.

5.2.3 PTP4A3 inhibition normalizes trans-endothelial electrical resistance after VEGF or LPS challenge.

In addition to stimulating endothelial cell migration, hyper-activation of VEGF signaling, and more specifically an increase in Src activation, have other effects including disruption of the integrity of the endothelial barrier and vascular permeability[210,211]. Therefore, I investigated the impact of PTP4A3 phosphatase inhibition by JMS-053 on the integrity of isolated primary human microvascular MVEC barrier function. Barrier function was measured by differences in TEER, a method that quantifies changes in macromolecular permeability and allows for continuous, quantifiable, real-time monitoring of barrier function[196,197]. Exposure of MVECs to VEGF (100 ng/mL) induced a profound disruption or "leakiness" of the endothelial barrier function that persisted for at least 22 h (Figure 5-3A). The precipitous decrease in endothelial barrier integrity after VEGF treatment was normalized when MVECs were pretreated for 2 h with 5 µM JMS-053 and then continuously exposed to the compound (Figure 5-3A). Post-treatment with JMS-053 at 3 h after VEGF exposure normalized endothelial barrier function, indicating the lack of a requirement for pretreatment (Figure 5-3A). JMS-038 was used as a vehicle control as MVECs showed no pronounced change in TEER over a 24 h incubation period. Restoration of MVEC barrier dysfunction was independent of the agonist. LPS is a well-known exogenous disruptor of endothelial barrier function, which is mediated by RhoA activation[212]. The loss of MVEC barrier is frequently mediated by changes in the actin cytoskeleton where cortically distributed actin is re-arranged to form stress fibers via activation of RhoA and a decrease in Rac1. Exposure to JMS-053 24 h prior to LPS

treatment prevented LPS-induced disruption of the endothelial barrier function (Figure

5-3B). There was no observed mitigation of LPS-induced vascular permeability with

JMS-053 treatment 3 h after LPS exposure. Protection and mitigation of VEGF-induced

increased endothelial permeability was also observed with the recently described PTP4A

trimerization inhibitor Compound 43[56] (discussed in section 1.3.3) (Figure 5-3C), which

is structurally and mechanistically quite distinct from JMS-053. This provided strong

orthogonal support for a role of the PTP4A family in the regulation of endothelial

permeability. JMS-053 treatment blocked both the LPS-mediated RhoA activation and

the LPS-mediated reduction in Rac1 activation (Figure 5-3D-E). Collectively, these data

suggest PTP4A phosphatases have a regulatory role in endothelial barrier function

through the RhoA-Rac1 axis.
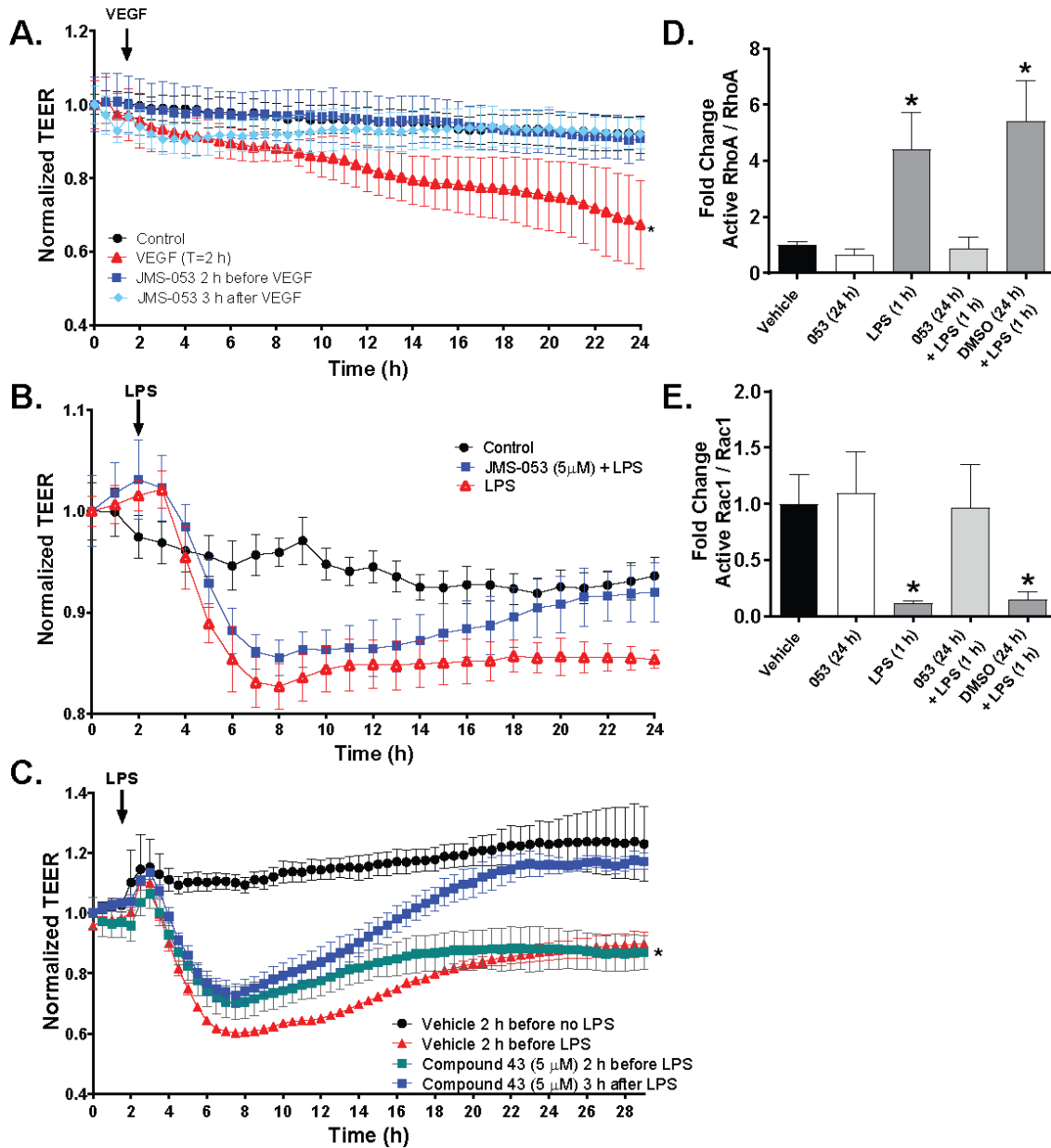
Figure 5-3 Pharmacological inhibition of PTP4A3 normalizes VEGF- and LPS-induced decreases in TEER.

A-C) Confluent MVEC cell TEER was monitored over time using electric cell-substrate impedance sensing. **A)** Cells were treated with VEGF alone (▲), JMS-053 (5 μM) for 2 h before (■) or 3 h after VEGF (100 ng/mL) (◆) exposure (indicated by the black arrow).

TEER was monitored for 24 h. Resistance was normalized to time 0. Error bars=SEM,

N=3, *=P<0.05 versus vehicle control (●). **B)** Cells were pretreated with (■) or without

(▲) JMS-053 (5 μM) and 24 h later challenged with LPS (0.5 EU/mL) (LPS treatment

indicated by the black arrow). Vehicle alone treated cells are indicated with the ● symbol.

Resistance was normalized to time 0. Error bars=SEM, N=3, *=P<0.01 versus control.

C) MVEC cells were pretreated with 5 μM Compound 43 (■) or vehicle control (▲) 2 h

before 0.5 EU LPS (LPS treatment indicated by the black arrow) followed by continuous

exposure to either Compound 43 or vehicle control or they were treated 3 h after LPS

with 5 μM Compound 43 (■). Vehicle alone treated cells are indicated with the ● symbol.

Error bars=SEM, N=4. *=P<0.01 versus control. **D)** and **E)** The effect of JMS-053 on the

LPS induced RhoA activation and Rac1 deactivation by phosphorylation. Quantification

of Western blot analysis of active RhoA, RhoA, active Rac1 and Rac1 in human MVECs

pretreated for 24 h with vehicle (DMSO) or JMS-053 (5 μM) prior to treatment with

vehicle or LPS treatment (0.5 EU/mL) for 1 h. Protein levels were normalized to total

RhoA or Rac1. Signal intensity of active RhoA and Rac1 was quantified by densitometry.

Error bars=SEM. N=3 *=P< 0.05 versus vehicle as determined by two-way ANOVA.

5.2.4 PTP4A3 increases vascular permeability in response to VEGF in vivo.

The disruption of endothelial barrier function is concomitant with an increase in vascular permeability. Additionally, it is well established that tumors exhibit vascular hyper-permeability, which is induced by elevated levels of VEGF[213]. The enhanced permeability accompanies pathogenic angiogenesis and facilities the extravasation of tumor cells and movement of growth factors and other cell types. While VEGF-induced vascular permeability was initially believed to be independent of Src[214], more recent studies[210,215,216] reveal a fundamental role for Src in regulating VEGF-mediated vascular permeability. I therefore examined VEGF-induced changes in vascular permeability in *Ptp4a3*^{fl/fl}, *Ptp4a3*^{fl/-} and *Ptp4a3*^{-/-} mice using a modified Miles assay[217,218]. Wildtype, *Ptp4a3*^{fl/fl}, mice exhibited a robust response to VEGF intradermal injection compared to vehicle alone (Figure 5-4). In contrast, mice lacking PTP4A3 were almost nonresponsive to VEGF treatment (Figure 5-4). The VEGF-dependent vascular permeability of the heterozygous mice was intermediate (Figure 5-4). These *in vivo* results strongly support the conclusion that PTP4A3 has a previously unrecognized role in controlling VEGF signaling and could be significant for the angiogenic needs of a primary tumor as well as tumor metastasis via PTP4A3 function in endothelial cells.
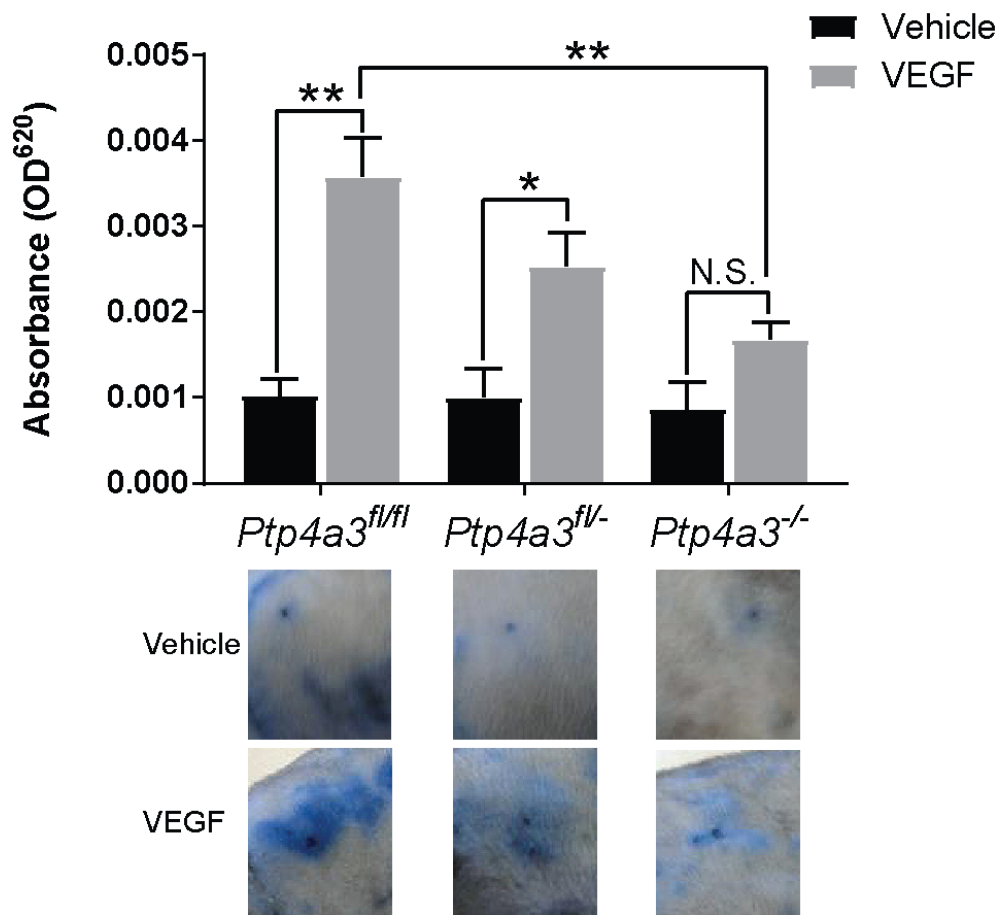
Figure 5-4 Loss of PTP4A3 reduced VEGF-mediated vascular permeability.

Adult male mice (n=6-8 per genotype) were injected iv with Evans blue dye and 20 min received intradermal injections of 400 ng of recombinant murine VEGF (gray bars) or PBS (black bars) in the flank. Total dye in 5 mm biopsy punch was extracted and dye absorbance was determined with a spectrophotometer. Representative images of site of injection and biopsy shown below quantification. Error bars=SEM; *=P<0.005, **=P≤0.001 using two-way ANOVA.

5.3   Summary

The work presented herein gives insight into a previously unrecognized function of PTP4A3 in controlling endothelial cell behavior in response to VEGF stimulation. The ability of the murine endothelial cells to migrate in an *in vitro* wound healing assay is impaired when PTP4A3 is genetically ablated. To determine the importance of PTP4A3 catalytic activity in driving this behavior, I examined the impact of phosphatase inhibition in a human endothelial cell model. Following treatment of HMVECs with increasing concentrations of the PTP4A3 inhibitor BR-1, there was a concentration-dependent decrease in cell migration, paralleling the results obtain upon total PTP4A3 loss. Inhibition or loss of PTP4A3 in murine and human endothelial cells alter prominent signaling proteins, notably Src, RhoA, and Rac1. The role of Src as a downstream effector of PTP4A3 in malignant cells was reflected in endothelial cells. In response to VEGF exposure, *Ptp4a3*-null cells lost the ability to increase Src Tyr416 phosphorylation, as well as the consequential increases in FAK Tyr576/577 and paxillin Tyr118 phosphorylation that are incited by Src activation. Importantly, there was no difference in Src Tyr416 phosphorylation in unstimulated cells, suggesting PTP4A3-induced activation of Src in endothelial cells is VEGF-dependent. Furthermore, VEGF was determined to be the primary growth factor influencing HMVEC migration and the impact of PTP4A3 inhibition by BR-1 on migration was lost in VEGF-deficient medium. In medium containing VEGF, there was a significant decrease in HMVEC p–Src Tyr416 expression following a 16 h incubation with BR-1 concentrations as low as 1 µM and as

high as 20 µM. Thus, the inhibition of PTP4A3 by BR-1 mirrors the reduction in p–Src

Tyr416 seen in the *Ptp4a3*-null cells.

The observed change in Src signaling in response to VEGF stimulation suggested

not only proangiogenic effects of PTP4A3, but also a potential effect on endothelial

barrier function[216,219]. The vascular endothelium regulates macromolecular and cellular

trafficking through the vessel walls. Many substances increase trans-endothelial

permeability including growth factors, such as VEGF, pro-inflammatory factors, such as

cytokines, and exogenous substances, such as bacterial LPS. As discussed in section

1.2.3, the disruption of endothelial barrier integrity in the vasculature presents an

opportunity for invasive cells from a primary tumor to enter circulation by migrating

directly through leaky endothelial cell junctions. Therefore, I investigated the effect of

PTP4A3 phosphatase inhibition on the TEER of a monolayer of cells as a measure of

endothelial barrier integrity. Upon exposure to PTP4A3 inhibitor JMS-053, the

compromised barrier function induced by VEGF or LPS challenge in MVECs was

restored. This coincided with JMS-053 inhibition of RhoA activation and promotion of

Rac1 activation, pharmacodynamic endpoints of undamaged membrane permeability.

Complementing the results regarding endothelial barrier function, the structurally distinct

small molecule inhibitor of PTP4A trimerization, Compound 43[56], also restored

compromised barrier function. In agreement with PTP4A3 phosphatase inhibition

improving endothelial barrier function, *Ptp4a3*^{-/-} mice displayed significantly reduced

vascular permeability in response to VEGF when compared to mice expressing functional

PTP4A3. The results presented in this report add novel *in vivo* evidence that PTP4A3 has

a vital role in controlling the migratory and invasive properties of nonmalignant cells,

specifically endothelial cells.

CHAPTER 6: DISCUSSION, SIGNIFICANCE, AND FUTURE DIRECTIONS

While there is a copious amount of evidence that PTP4A3 is overexpressed in tumors, and this overexpression correlates with poor patient prognosis and metastasis[9,72,100,106,110,220,221], the mechanism by which PTP4A3 supports a cancer phenotype has been largely obscure. The work described in this thesis, as well as the publications stemming from it[75,190,208], support the hypothesis that the phosphatase activity of PTP4A3 promotes CRC tumor progression by stimulating behaviors in both endothelial and malignant cells that are beneficial for tumor growth.

The work presented suggests PTP4A3 overexpression in tumor cells acts to enhance anchorage independent growth and migration by altering the expression of key ECM genes and, in tandem, PTP4A3 overexpression in tumor vasculature acts to enhance vascular permeability and endothelial cell migration by increasing the responsiveness of endothelial cells to VEGF. The findings demonstrate: (1) PTP4A3 loss or phosphatase inhibition reduces CRC cell colony formation, migration, and adhesion, (2) PTP4A3 loss in CRC cells increases the expression of genes controlling cell-ECM interactions, including *Emilin 1*, and inhibition of PTP4A3 phosphatase activity is sufficient to rescue *Emilin 1* expression, (3) the relationship between PTP4A3 expression and genes controlling cell-ECM interactions is supported by patient data and significant alteration in any of these genes reduces overall survival, (4) PTP4A3 loss or phosphatase inhibition in endothelial cells reduces migration and Src is a key downstream effector that is unresponsive to VEGF stimulation in the absence of PTP4A3, (5) PTP4A3 phosphatase inhibition reduces endothelial barrier function *in vitro* and (6) PTP4A3 loss reduces

vascular permeability *in vivo*. These findings are illustrated in Figure 6-1. The cumulative results of this research provide a foundation for the continued interrogation of this phosphatase and its contribution to CRC pathogenesis.
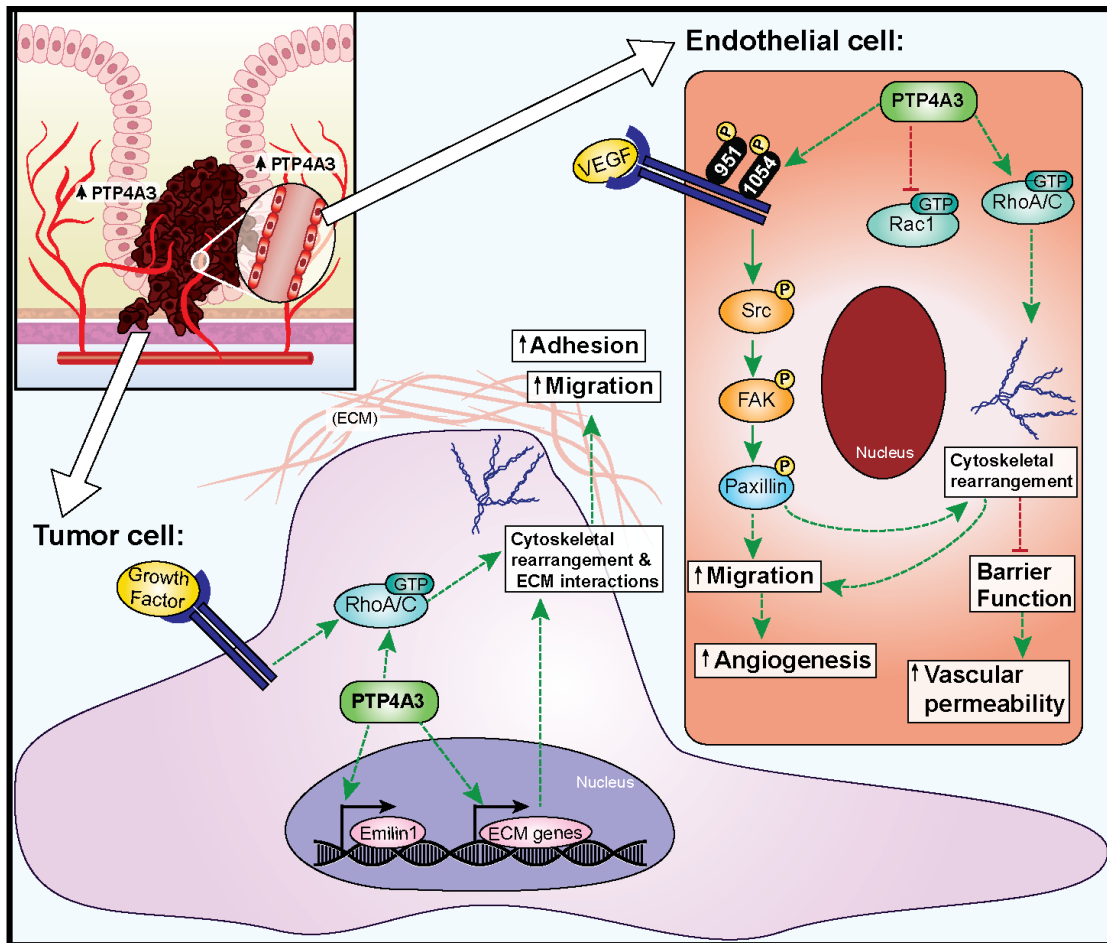
Figure 6-1 The impact of PTP4A3 on tumor and endothelial cell signaling and behavior.

A summary of the cumulative results of the experiments described in this thesis dissertation are depicted. This model was developed based on the impact of both genetic loss and pharmacological inhibition of PTP4A3 phosphatase inhibition. Dashed arrows represent indirect relationships, while solid arrows represent indirect relationships.

CRC remains one of the deadliest cancers worldwide, and the incidence of the disease continues to increase[7]. PTP4A3 mRNA and protein overexpression in metastatic CRC have been noted by others[9,44] and we found an increase in PTP4A3 mRNA expression in 14% of the CRC tumors sequenced in the TCGA database. Furthermore, it is becoming clear that PTP4A3 can functionally contribute to multiple aspects of malignant disease including tumor formation, metastasis, and angiogenesis[13,46,109]. Metastatic CRC was the first cancer for which antiangiogenic therapies were approved, underscoring the efficacy of targeting the vasculature in this disease[170]. Therefore, the impact of PTP4A3 expression and inhibition in the vasculature presents the unique opportunity to target both the tumor vasculature and tumor cells by inhibiting a single protein. Despite the relatively low *in vitro* catalytic activity of PTP4A with artificial substrates, the catalytic domain is functionally or structurally relevant in oncogenesis because cells that express the phosphatase-deficient mutant protein are unable to form tumors[222]. The generation of a PTP4A-targeted small molecule tool set should help to uncover the mechanism by which PTP4A phosphatases alter cancer cell biology and confirm cellular effects observed with PTP4A3 genetic manipulation.

Studies using transient PTP4A3 overexpression systems implicate a number of signaling molecules and cellular pathways; however, we do not have a solid understanding of the mechanism by which PTP4A3 influences these signaling mechanisms and subsequent cellular responses. It appears that, within these transient expression systems, PTP4A3 has a central role in regulating the phosphorylation status of important intracellular signaling proteins yet, paradoxically, hyper- rather than hypo-phosphorylation of tyrosines, serines, and threonines has been observed in cells with

elevated levels of PTP4A3[223]. Such results imply that the observed changes in the

phosphorylation status of the signaling proteins are an indirect effect of PTP4A3

activity[131]. This may be, at least in part, due to the action of Src kinase seen in the

presence of PTP4A3[128,131]. Moreover, these transient overexpression systems can suffer

from experimental artifacts associated with the expression of super-physiological levels

of PTP4A3. Since the PTP4A3^{fl/fl} cells endogenously express detectable PTP4A3 protein,

PTP4A3 function and physiological substrates may be more directly identified. Coupling

this cell line with its paired PTP4A3^{-/-} cell line partner provides a controlled experimental

system to further delineate the functionality of PTP4A3 phosphatase and its role in

cellular signaling.

JMS-053 is the most potent and specific known PTP4A family inhibitor[190,208] and

a considerable improvement upon thienopyridone, the previously described small

molecule pan-PTP4A inhibitor[138]. As a pan-PTP4A inhibitor, JMS-053 is a useful

chemical probe for the PTP4A subfamily and can be used to determine functional roles of

the individual PTP4A family members[138,190]. For example, our results suggest PTP4A3,

and not PTP4A1 or PTP4A2, is the major family member determinant of migration and

invasion in the PTP4A3^{fl/fl} CRC cells, based on the observation that treatment of

PTP4A3^{-/-} cells with JMS-053 produced no further changes in these processes. Thus,

JMS-053, coupled with our loss-of-function paired CRC cell lines, provides us with

complementary orthogonal methods to interrogate and confirm PTP4A3 phosphatase

functionality.

One of the more well-characterized PTP4A3 cellular roles is as a regulator of

cancer cell proliferation. Specifically, studies using PTP4A3 overexpression or transient

suppression systems[73,116,127] led to the general conclusion that PTP4A3 overexpression

increased cell proliferation while reduction of PTP4A3 either had no effect[11,93] or reduced

cell proliferation[100]. Similarly, using *Ptp4a3* wildtype CRC cells grown on the lethally

irradiated rat LA7 mammary epithelial cells, with their attendant heterotypic interactions,

we observed a faster proliferation rate compared to the *Ptp4a3* null cells[45]. However,

once the feeder layer was eliminated and the cells were grown independently on plastic,

the resulting PTP4A3^{fl/fl} and PTP4A3^{-/-} cell lines shared similar growth rates. These

results suggest the ECM and hetero- or homotypic interactions influence aspects of cell's

phenotype with in a PTP4A3 expression-dependent manner. Our observation that

PTP4A3^{-/-} cells display a marked inhibition in their ability to form spheroids also

suggests a functional role for PTP4A3 in mediating homotypic cellular interactions.

Homotypic and heterotypic tumor cell interactions with the ECM are pivotal

components of the epithelial-mesenchymal transition and the subsequent metastatic

process. As tumor cells evade programmed cell death induced by loss of anchorage, they

are able to alleviate their necessity to adhere to the ECM, and subsequently migrate to

and invade distant sites[224]. PTP4A3 is a regulator of the epithelial-mesenchymal

transition[225] so it is perhaps unsurprising that PTP4A3 is a regulatory element of the

cell's interaction with the ECM. However, the scope of PTP4A3 involvement in the

regulation of the ECM was previously unknown. Our PCR microarray screen suggests

that at least ten ECM-related genes are regulated by PTP4A3. The most provocative is

Emilin 1, a member of the *Emilin* family of proteins, which binds specifically to elastin

and is a key component of the ECM in tumor tissue[204,205]. Previous studies demonstrated

that when *Emilin 1* is absent, it alters cell-ECM interactions and enriches the opportunity

for migration and invasion. This suggests that *Emilin 1* functions as a tumor

suppressor[226]. We demonstrate that upon genetic ablation or pharmacological inhibition

of PTP4A3 we enhance *Emilin 1* gene expression. Thus, overexpression of PTP4A3 may

override cellular control mechanisms leading to tumor migration and metastasis.

Similarly, *Fbln 1* is reported to function as a tumor suppressor[227]. *Fbln 1* is involved in

matrix reorganization, and high expression correlates with improved patient prognosis.

PTP4A3 may be acting to reduce the amount of *Fbln 1* present, thereby disrupting the

matrix organization leading to an altered interaction of the cells with the ECM. A more

detailed investigation into these changes should provide valuable insight into the actions

of PTP4A3 in CRC.

The mechanism by which PTP4A3 alters the mRNA levels of protein components

of the ECM is unclear and addressing this question is complicated by PTP4A3s complex

role in cancer biology, the anonymity of its direct substrate(s), and limited available tools

for PTP4A3 as well as target genes. Consequently, new cellular models and cell active,

well-credentialed, chemical probes, such as JMS-053, provide valuable reagents to help

clarify PTP4A3 function. Not only does PTP4A3 have a profound effect on the ability to

migrate, but also, PTP4A3 is driving this phenotype through interactions with the ECM.

This is exemplified in the changes in integrin (*Itgb2*) and matrix metalloproteinase

expression *(Mmp1a)*. In this same vein, the changes in the cells ability to adhere can be

traced back to changes in expression of these key genes. The integrins function to both

bind and respond to the ECM surrounding the cell, and changing the expression of these

genes alters the cellular response to differing matrix types. MMPs are essential enzymes

for the breakdown and turnover of specific matrix proteins. Given that the expression of

proteins within these families were altered, it is unsurprising that the genetic and

pharmacologic inhibition of PTP4A3 resulted in differences in the strength of the

adhesion of the cells to plastic. This may be because of the way these cells interact with

the self-produced matrix due to a decrease in the level of *Mmp1a* and an increase in

Itgb2.

I cannot exclude a role for RhoA GTPase in mediating the effects of PTP4A3.

RhoA is activated by growth factors and integrins, and has a central role in controlling

the transmembrane ECM-cytoskeleton interactions and focal adhesions[228]. The present

study and others[134] demonstrate RhoA activity can be controlled by PTP4A3. In studies

using ovarian cancer cells, reported in Appendix A, I found that treatment with JMS-053

resulted in a concentration-dependent reduction in GTP-bound (active) RhoA (Figure A-

1A). Moreover, knockdown of PTP4A3 with targeted shRNA reduced RhoA activation

and JMS-053 (500 nM) caused no further reduction in RhoA activation consistent with

PTP4A3 target engagement (Figure A- 1B). Furthermore, in the paired PTP4A3^{fl/fl} and

PTP4A3^{-/-} CRC cell lines there was significantly reduced RhoA activation and treatment

of the PTP4A3^{fl/fl} cells with JMS-053 caused a concentration dependent reduction,

described in Appendix B. With small G-proteins, including RhoA, the rate of nucleotide

exchange is regulated by nucleotide-bound magnesium, which regulates the biological

activity of the GTPase[229]. The magnesium-based regulation of RhoA is particularly

relevant given recent work suggesting that PTP4A phosphatases bind the magnesium

transporter cyclin M/ancient conserved domain protein (CNNM3) via the PTP4A

phosphatase active site, thereby increasing intracellular magnesium transport[74]. Thus,

PTP4A binds to CNNM3 and causes an increase in intracellular magnesium. This

increase in magnesium then causes a decrease in the dissociation rate of GTP from RhoA, resulting in an increase in RhoA GTPase activity.

The lack of significant difference between the tumor formation caused by the feeder layer-independent PTP4A3$^{fl/fl}$ and PTP4A3$^{-/-}$ cells was unanticipated in light of the soft agar colony formation assay (Figure 3-4C), an *in vitro* indication of tumorigenicity. The *in vitro* assay suggested PTP4A3$^{-/-}$ cells should be significantly less tumorigenic than PTP4A3$^{fl/fl}$ cells, while the *in vivo* assay (Figure 3-10) did not support this conclusion. The dissonance may be explained by a number of factors. First, with the original *Ptp4a3$^{-/-}$* cells, the *in vitro* limiting dilution analysis revealed that as the cells increased in passage number their colony forming ability improved, despite maintaining a significantly reduced colony forming ability as compared to *Ptp4a3$^{fl/fl}$* cells[45]. The PTP4A3$^{-/-}$ cells have been in culture for a longer period of time than the original *Ptp4a3$^{-/-}$* cells, therefore, it is possible that the colony forming ability of the cells improved to a point that the number of tumor cells injected greatly exceeded the minimal tumor formation dosage.

Another explanation for the lack of significant difference could be the use of bilateral injections of different cell types in a single animal. The PTP4A3 present in the PTP4A3$^{fl/fl}$ tumor cells may be influencing the contralateral PTP4A3$^{-/-}$ tumor cells in a way that enhanced their ability to form a tumor and grow. It has been reported that increased PTP4A3 expression in malignant tumors results in a change in the secretion of cytokines that regulate both NF-κB and Jak2-STAT3 pathways[223]. The secretion of these cytokines by the PTP4A3$^{fl/fl}$ cells may therefore be enhancing these pro-oncogenic

pathways in the PTP4A3$^{-/-}$ tumor cells present in the same mouse, which are less active when the PTP4A3$^{-/-}$ tumor cells are grow independently.

The growth of the PTP4A3$^{-/-}$ tumor cells in the immunocompromised mice may have also been supported by PTP4A3 expressed in the stromal cells. As discussed in the introduction, PTP4A3 over expression in tumor cells can induce angiogenic behavior in endothelial cells (Section 1.2.3). The data presented in CHAPTER 5: also provide evidence for the role of PTP4A3 in endothelial cell signaling, therefore, the PTP4A3 expressing cells may be causing changes in the vascular cells that are advantageous to the PTP4A3$^{-/-}$ tumor. Moreover, the athymic nude mice are deficient in T cell function but still have fully functioning macrophages. This is important as PTP4A3 expression in tumor cells has been shown to change cytokines secreted by tumor-associated macrophages influencing the gene-expression and behavior of tumor cells. In light of this, the PTP4A3$^{fl/fl}$ cells may be causing changes in the macrophages in the mouse that, in turn, are supportive of the growth of the PTP4A3$^{-/-}$ tumor[142]. While I believed bilateral injection of PTP4A3$^{fl/fl}$ and PTP4A3$^{-/-}$ cells in a single mouse would provide a sound biological control, the impact of PTP4A3 expression in a contralateral PTP4A3$^{fl/fl}$ tumor on both the non-malignant and PTP4A3$^{-/-}$ cells may have influenced the results. Additional studies on mice receiving only one cell type should help clarify this issue.

Finally, I cannot exclude the possibility that the lack of tumorigenicity seen in the original feeder layer-independent *Ptp4a3*$^{-/-}$ cells was due, at least in part, to a difference in the mutational profile induced by the AOM treatment of the *Ptp4a3*$^{fl/fl}$ and *Ptp4a3*$^{-/-}$ mice. Ergo, by using the same *Ptp4a3*$^{fl/fl}$ cell pool with the same baseline mutagen-induced genetic alterations in my studies, I uncovered evidence to disprove our original

conclusion[45] that PTP4A3 levels influence colon tumor formation at least in this

xenograft model. This type of *in vivo* experiment, however, may not be the best way to

address how PTP4A3 is affecting tumor growth and progression, and further studies are

warranted. The study in CHAPTER 3 is simply looking at what happens when the tumor

cells are injected into predetermined site and does not look at the ability of the tumor

cells to actually find a site and establish a tumor. The primary effect of PTP4A3 may be

on metastasis as opposed to the growth of a primary tumor. Therefore, future *in vivo*

studies may see differences by modeling experimental metastasis through tail-vein

injection (which commonly used and would likely establish lesions in the lungs) or

splenic injection (which would more closely model the local dissemination of CRC and

likely establish lesions in the liver). Experimental metastasis models, however, would

also have their drawbacks because they would not reflect the first steps in the metastatic

cascade including local invasion through the breakdown of the basement membrane and

invasion of the into the proximal ECM and intravasation wherein the tumor cells enter

circulation. The evidence presented with regard to PTP4A3 control of ECM interacting

genes in tumor cells and vascular permeability in endothelial cells support a potential role

of PTP4A3 in these initial phases of the metastatic cascade.

In contrast to the *in vivo* results obtained using the PTP4A3$^{fl/fl}$ and PTP4A3$^{-/-}$

cells, an ovarian cancer nude mouse tumor model demonstrated that JMS-053

administration significantly reduces the tumor weight with no overt toxicity (Figure A-

2). The potential benefits of inhibition of PTP4A3 suggested by the work presented in

this dissertation, as well as the advancement of the targeted biological therapy PRL3-

ZUMAB to phase 1 clinical trials, advocate the *in vivo* testing of the JMS-053 for the

treatment of CRC. For future *in vivo* studies investigating JMS-053 treatment of CRC, the use of the PTP4A3^{fl/fl} and PTP4A3^{-/-} cells combined with compound treatment could test on-target anti-tumor, or anti-metastatic effects of PTP4A3 phosphatase inhibition.

Endothelial cells mirrored the PTP4A3 phosphatase-dependent reduction in migration displayed by CRC cells. The results presented here suggest that several proteins, notably Src, FAK, paxillin, and RhoA, were affected by the absence or inhibition of PTP4A3. The current results suggest that Src is a downstream effector of PTP4A3 in endothelial cells, as *Ptp4a3*-null cells completely lost the ability to increase Src activation following VEGF exposure. VEGFR2 is known to be regulated by intracellular tyrosine phosphorylation on multiple sites including Tyr951, Tyr1054, Tyr1059, Tyr1175, and Tyr1214[210]. VEGFR2 phosphorylation on Tyr951 facilitates binding of VEGFR2 to the Src homology-2 domain of T cell-specific adaptor, TSAd, which increases VEGF-induced activation of Src kinase. Additionally, VEGFR2 Tyr1059 can bind to Src allowing the phosphorylation of other Tyr residues of VEGFR2[210]. It is therefore significant that loss of PTP4A3 resulted in a reduction of phospho-Tyr951 and 1059[75]. This presumably indirect effect implies that increased PTP4A3 expression in the endothelium may increase VEGFR2 Tyr951 and 1059 phosphorylation and may therefore contribute enhanced TSAd-mediated Src activation and enhanced phosphorylation of VEGFR2 by Src. Moreover, it was recently shown that VEGF-induced permeability and vascular leakage depend upon the signaling initiated by the phosphorylation of VEGFR2 Tyr951[215]. Blocking this VEGFR2 Tyr951 phosphorylation prevented the metastatic spread of glioblastoma[215]. This means that the modest reduction in Tyr951 seen in the

PTP4A3 null cells may contribute to the reduced vascular permeability seen in the null

mice.

In endothelial cells the cycling between inactive, GDP-, and active, GTP-bound

configurations of RhoA and Rac1 is essential for the regulation of endothelial barrier

function. GTPase activating proteins, which increase the intrinsic rate of GTP hydrolysis

and guanine nucleotide exchange factors, and in turn promote GTPases into the GTP-

bound state are responsible for regulating this cycle[150]. Different patterns of cytoskeletal

and cellular contact remodeling are induced by the opposing effects of Rac1 and RhoA

on endothelial barrier function[154]. The effects exerted by Rac1 are often protective of

endothelial barrier function while those exerted by RhoA lead to endothelial barrier

dysfunction[230]. Activation of RhoA by inflammatory mediators, including LPS, activates

ROCK1/2, which consequently leads to the phosphorylation of myosin light chain kinase

and causes actomyosin contraction, actin stress fiber formation, and disruption of

endothelial barrier integrity[132]. Dysfunction of the endothelial barrier can lead to vascular

permeability presenting invading tumor cells with the opportunity to disseminate. The

inhibition of RhoA and activation of Rac1 by either JMS-053 or Compound 43 are

significant in that they not only protect the endothelial barrier, but can also restore the

barrier integrity. The *in vivo* reduction in vascular permeability in *Ptp4a3*$^{-/-}$ mice in

combination with the *in vitro* barrier function data provides evidence that inhibition of

PTP4A3 phosphatase activity can reduce vascular permeability.

PTP4A3 is an enigmatic phosphatase. Some investigators have even suggested

that PTP4A3 is not a phosphatase but rather acts as a pseudophosphatase[74]. The

implications of alterations in the expression levels of phosphatases reach far beyond any

individual direct substrate and understanding the impact of changes in these networks is essential to understanding how these molecules drive oncogenic phenotypes. The cellular and pharmacological reagents developed should assist in the process of understanding how this intracellular protein communicates with the ECM. In addition, given the impact of PTP4A3 on both cell types, the relationship between tumor and endothelial cell PTP4A3 expression should be explored further in the context of tumor formation and metastasis.

In conclusion, while I have begun to elucidate the contribution of PTP4A3 to CRC pathogenesis and its importance in tumor and vascular cells, much remains to be discovered regarding its biological function. Future studies such as an in depth analysis of the genetic differences in the paired cell lines by RNASeq, *in vivo* experimental metastasis comparisons using both the paired cell lines and JMS-053, and evaluation of JMS-053 binding to PTP4A3 by NMR would be very beneficial to the continued investigation of PTP4A3. The opportunities for continuing this research are plentiful and continued investigation has the potential to impact the development of future therapies for the treatment of CRC. This has implications not only for CRC, but the numerous other cancer types that exhibit PTP4A3 overexpression.

APPENDIX A: PTP4A3 INHIBITION BY JMS-053 TO TARGET OVARIAN CANCER

This appendix depicts the efficacy of JMS-053 in ovarian cancer cell lines and an *in vivo* model for tumor growth using ovarian cancer cell lines. There were elevated levels of PTP4A3 phosphatase in 79% of human ovarian tumor samples, with significant overexpression in tumor endothelium and pericytes. Based on this data as well as evidence presented in the literature[10,68,88,89], the benefit of pharmacological inhibition of PTP4A3 in ovarian cancer was investigated.

A.1   Materials and Methods

A.1.1 Human ovarian cancer cell culture

HeyA8 and HeyA8-MDR cells were obtained from Dr. Anil Sood (MD Anderson Cancer Center, Houston, TX) and have been described previously. The cell line was authenticated by short tandem repeat DNA profiling prior to experimental studies. Cells were maintained in RPMI (Life Technologies, Grand Island, NY) supplemented with 10% FBS, with no antibiotics, and were passaged <20 times.

A.1.2 Nude mouse tumor studies

For *in vivo* antitumor experiments with JMS-053, HeyA8-MDR cells in exponential growth phase were detached from the monolayer with 0.25% trypsin and 20

μg/mL EDTA in PBS and resuspended in 10% FBS-containing RPMI, pelleted, and

resuspended in serum-free RPMI at a concentration of 5 x 10^6 cells/mL Female athymic

nude mice (Envigo, Dublin, VA) were injected intraperitoneally (IP) (200 μL/injection)

with cells and after one week mice (n = 10 per group) were randomized for treatment

with vehicle (20% 1-methyl-2-pyrrolididone, 25% Kolliphor HS 15, and 55% 1X

phosphate buffered saline) or with vehicle plus 10 mg/kg JMS-053. Mice were treated IP

daily (100 μL/ injection) for 5 days with a 2-day holiday followed by 4 additional days of

treatment before being sacrificed. All tumors were excised and weighed. All *in vivo*

procedures were performed using the University of Virginia approved IACUC protocols.

Animal care was administered in accordance to guidelines established by the American

Association for Accreditation of Laboratory Animal Care.

A.2   Results

A.2.1   JMS-053 suppresses RhoA activation in ovarian cancer cells

RhoA activation is known to be integral to the promotion of growth, migration,

and dissemination of tumor cells[132], and elevated PTP4A3 expression levels are reported

to increase RhoA activity[98,132,134]. Therefore, the impact of JMS-053 treatment on the

activation of RhoA in HeyA8 cells was investigated. HeyA8 cells were serum-starved

overnight and then pre-treated with JMS-053 (0.1-1 μM) or vehicle for 30 min followed

by a 30 min exposure to medium supplemented with 10% FBS to stimulate RhoA

activation in the presence of either JMS-053 or vehicle. JMS-053 treatment caused a

significant inhibition of RhoA activation at all concentrations tested with an IC_{50} of 0.6

µM (Figure A-2A). Treatment of HeyA8 cells with the control compound JMS-038 (1

µM) had no significant effect compared to the DMSO vehicle control. Treatment with

PTP4A3 targeted shRNA reduced RhoA activation and JMS-053 (500 nM) caused no

further reduction in RhoA activation consistent with PTP4A3 target engagement (Figure

A-2B).
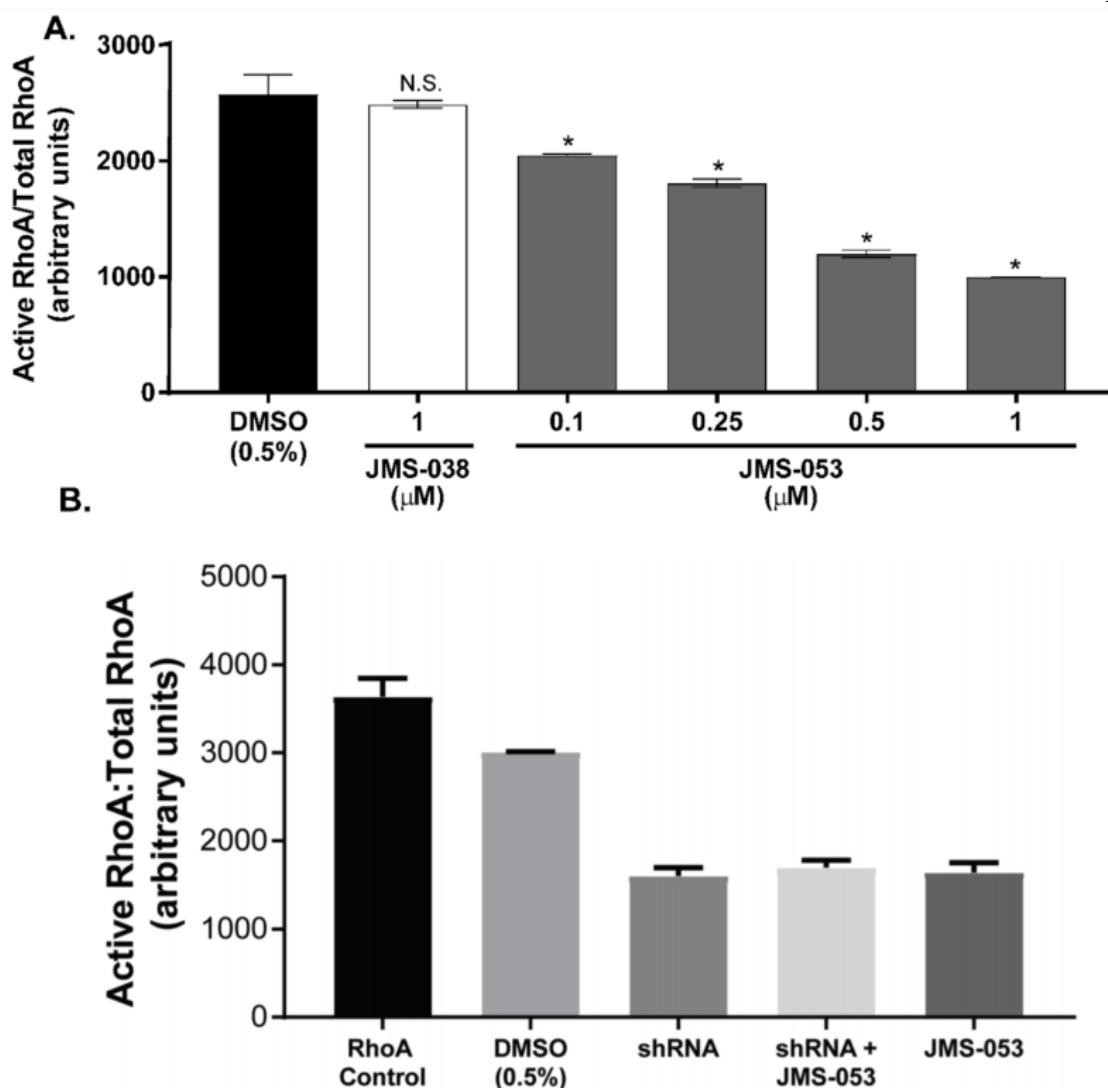
Figure A- 1 JMS-053 inhibits RhoA activation in HeyA8 cells via PTP4A3.

A) Cells were starved in serum-free RPMI 1640 for 24 h, then activation of RhoA was induced by exposure to 10% serum. Cells were pre-treated with indicated concentrations of compounds for 30 min prior to serum stimulation and for 30 min while being stimulated with medium containing 10% FBS. GTP bound RhoA in equal amounts of total lysate was quantified by a luminescence-based G-LISA RhoA activation assay. Treatment with 0.1-1 μM JMS-053. Constitutively active RhoA was used as a positive control for the binding of GTP-RhoA to G-LISA. The data were expressed as relative

luminescence units (RLU) and were the mean $\pm$ SEM ($N = 4$). Statistical significance was

determined by one-way ANOVA and Tukey's multiple comparison test. *=P < 0.05, n.s.

= not significant. **B)** HeyA8 cells were treated with PTP4A3-targeted shRNA for 24 h in

complete medium. Cells were starved in serum-free RPMI 1640 for 24 h, then activation

of RhoA was induced by exposure to 10% serum. Cells were pre-treated with 500 nM

JMS-053 or vehicle control (0.5% DMSO) for 30 min prior to serum stimulation and for

30 min while being stimulated with medium containing 10% FBS. GTP bound RhoA in

equal amounts of total lysate was quantified by G-LISA RhoA Activation assay.

Constitutively active RhoA was used as a positive control for binding of GTP-RhoA to

G-LISA. The data were expressed in arbitrary units relative to total RhoA present in cells

with the mean $\pm$ SEM (N=2).

A.2.2 JMS-053 treatment inhibits drug-resistant ovarian cancer tumor growth in vivo.

Drug resistance remains a challenging aspect of ovarian cancer treatment. Therefore, the *in vivo* activity of JMS-053 was examined using a HeyA8-MDR nude mouse tumor model. Mice readily tolerated an IP dose of 10 mg/kg of JMS-053 and, based on an independent pharmacokinetic study by SAI Life Sciences, the maximum plasma concentration was reached within 30 min and plasma concentrations of 225 ng/mL (879 nM) were present 8 h after the injection. The area under the plasma concentration curve (AUC) was 4.425 h*µg/mL, which indicated a sustained presence of compound. Female nu/nu mice bearing IP HeyA8-MDR tumors were used, because IP site is very representative of the human disease[231]. Tumor bearing mice were treated with vehicle or 10 mg/kg JMS-053 over a nine-day period. We observed IP ovarian cancer tumors in all vehicle treated mice and in 7 of 9 JMS-053 treated mice. The tumors from the mice treated with JMS-053 for nine days weighed 45% less than those from the vehicle treated group (Figure A-3A). There was no significant difference in the body weights of the mice in the two treatment groups (Figure A-3B).
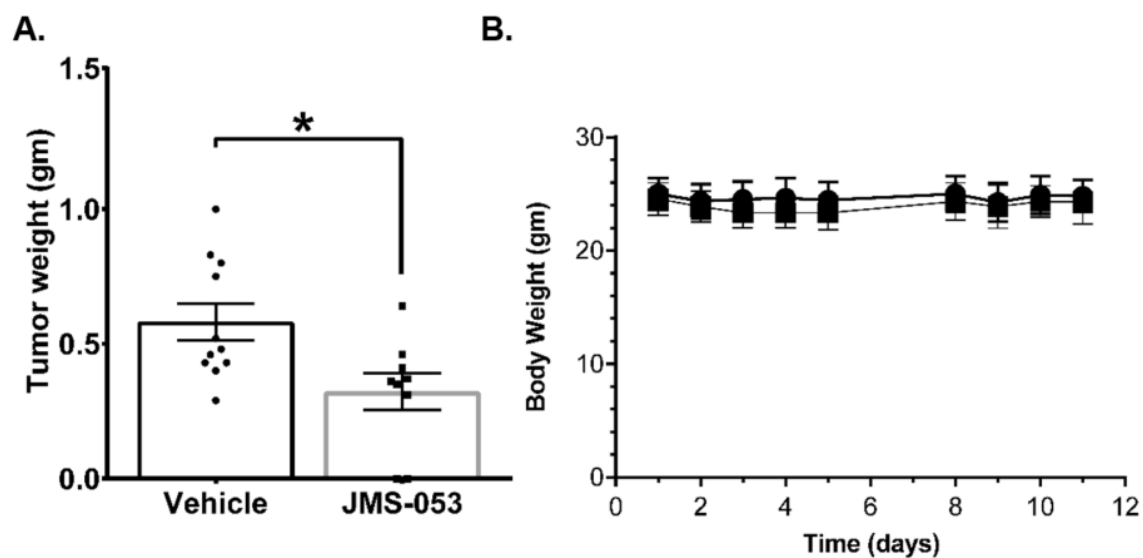
Figure A- 2 JMS-053 has antitumor activity against ovarian cancer.

A) Female, athymic nude mice with HeyA8-MDR tumors were injected IP with vehicle or JMS-053 (10 mg/kg) daily for 5 days followed by two days without treatment and four additional daily treatments (10 mg/kg). Error bars=SEM. *=P < 0.05 (Mann-Whitney).

B) Body weight monitoring for 12 days indicates that JMS-053 treatment did not cause significant weight loss.

APPENDIX B: IMPACT OF PTP4A3 LOSS OR INHIBITION ON RHOA ACTIVATION IN MURINE CRC CELLS

This appendix depicts the effect of genetic loss and pharmacological inhibition of PTP4A3 in the paired murine CRC cells lines described in CHAPTER 3. Based on the findings regarding RhoA activation in endothelial cells as well as ovarian cancer cell lines, the impact of PTP4A3 protein loss and treatment with JMS-053 on the activation of RhoA were investigated.

B.1   Materials and Methods

RhoA activation in murine CRC cells was detected by the luminescence formatted RhoA G-LISA Activation Assay (Cytoskeleton Inc., Denver, CO), according to manufacturer's instructions. Following a 24 h serum starvation in DMEM/F12 supplemented with L-glutamine, murine tumor cells at ~50% confluence were pretreated in serum-free medium for 1 h with compounds in a final DMSO concentration of 0.5%, as was the vehicle control. Cells were then stimulated for 30 min with DMEM/F12 containing 10 ng/ml PDGFβ with treatment in a final DMSO concentration of 0.5%. Cells were harvested on ice and snap-frozen in liquid nitrogen. Total protein was determined using Precision Red Advanced protein assay reagent (Cytoskeleton Inc.). Twenty-five µg of protein per Rho-GTP affinity well were incubated at 4°C for 30 min on an orbital shaker to facilitate binding. As a positive control, 1 ng of purified recombinant RhoA was bound to the affinity well. The provided primary and secondary antibodies were used at a 1:250 and 1:500 dilution, respectively. Luminescence data were

captured on a SpectraMax M5 multimode plate reader set to 25 msec integration time following 2 min incubation with luminescence detection reagent. Data were normalized to total RhoA as determined by the total RhoA ELISA (Cytoskeleton Inc.).

B.2 Genetic loss or treatment with JMS-053 suppresses RhoA activation

RhoA GTPase has well defined roles in the regulation cytoskeletal dynamics, which are essential for cancer cell migration, invasion, and metastasis[132]. We previously demonstrated that JMS-053 caused a significant inhibition of FBS-stimulated RhoA activation in ovarian cancer cells[208]. PDGFβ is potent inducer of cell migration, which is mediated by RhoA activation and the resultant cytoskeletal rearrangement[232]. A 30 min exposure of PTP4A3$^{fl/fl}$ cells to PDGFβ (10 ng/ml) caused a 1.7-fold activation of RhoA but no activation in PTP4A3$^{-/-}$ cells (Figure B-1), confirming the central role of PTP4A3 in mediating RhoA activation by PDGFβ. JMS-053 (2.5-5 µM) markedly inhibited the PDGFβ-mediated RhoA activation in PTP4A3$^{fl/fl}$ cells. In contrast, the inactive congener JMS-038 at 5 µM failed to inhibit PDGFβ-mediated RhoA activation in PTP4A3$^{fl/fl}$ cells. We observed no effect on RhoA activation with JMS-053 or JMS-038 in PTP4A3$^{-/-}$ cells (Figure B-1).
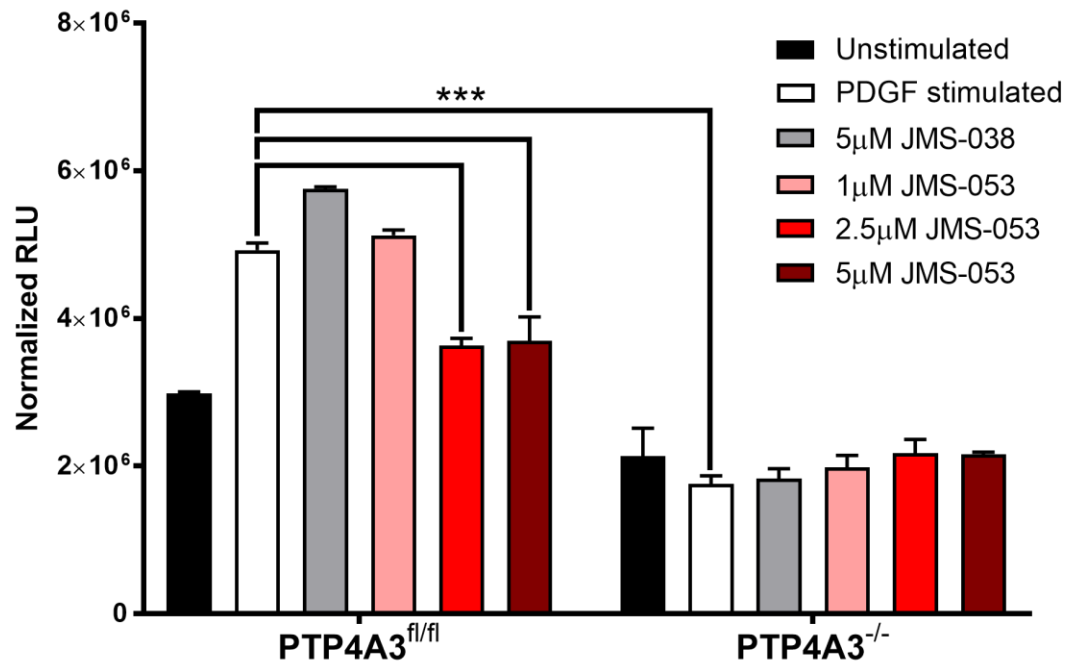
Figure B-1 Loss of PTP4A3 or Inhibition of PTP4A3 phosphatase activity with JMS-053 reduces RhoA activation.

PDGFβ (10 ng/µl) activated RhoA in PTP4A3$^{fl/fl}$ but not cells PTP4A3$^{-/-}$ and JMS-053 inhibited RhoA activation. N=3, error bars=SEM. ***=p<0.0001.

PUBLICATIONS RESULTING FROM THIS WORK

McQueeney KE, Salamoun JM, Ahn J, Pekic P, Blanco IK, Struckman H, Sharlow ER, Wipf P, Lazo JS. *A chemical genetics approach identifies PTP4A3 as a regulator of colon cancer cell adhesion*. FASEB J. Manuscript submitted.

McQueeney KE, Salamoun JM, Burnett JC, Barabutis N, Pekic P, Lewandowski SL, Llaneza DC, Cornelison R, Bai Y, Zhang ZY, Catravas, JD, Landen CN, Wipf P, Lazo JS, Sharlow ER. *Targeting ovarian cancer and endothelium with an allosteric PTP4A3 phosphatase inhibitor*. Oncotarget. DOI: 10.18632/oncotarget.23787, 2017.

Salamoun JM, **McQueeney KE**, Patil K, Geib SJ, Sharlow ER, Lazo JS, Wipf P. *Photooxygenation of an amino-thienopyridone yields a more potent PTP4A3 inhibitor.* Org Biomol Chem. 14:6398-402, 2016.

Zimmerman MW, **McQueeney KE**, Isenberg JS, Pitt BR, Wasserloos KA, Homanics GE, Lazo JS. *Protein-tyrosine phosphatase 4A3 (PTP4A3) promotes vascular endothelial growth factor signaling and enables endothelial cell motility*. J Biol Chem. 289:5904-5913, 2014.

ADDITIONAL PUBLICATIONS

Lazo JS, **McQueeney KE**, Burnett JC, Wipf P, Sharlow ER. *Small molecule targeting of PTPs in cancer.* (Invited Review). Int J Biochem Cell Biol. 10.1016/j.biocel.2017.09.011, 2017.

Lazo JS, **McQueeney KE**, Sharlow, ER. *New approaches to difficult drug targets: The phosphatase story.* (Invited Review). SLAS Discov. 40:345-370, 2017.

Bauer ST, **McQueeney KE**, Patel T, Morris MT. *Localization of a trypanosome peroxin to the endoplasmic reticulum.* J Eukaryot Microbiol. 10.1111/jeu.12343, 2016.

Eaton JM, Takkellapati S, Lawrence RT, **McQueeney KE**, Boroda S, Mullins GR, Sherwood SG, Fink BN, Villén J, Harris TE. *Lipin 2 binds phosphatidic acid by the electrostatic hydrogen bond switch mechanism independent of phosphorylation.* J Biol Chem. 10.1074/jbc.M114.547604, 2014.

Sharlow ER, Wipf P, **McQueeney KE**, Bakan A, Lazo JS. *Investigational inhibitors of PTP4A3 phosphatases as antineoplastic agents*. (Invited Review). Exp Opin Investig Drugs. 23:661-673, 2014.

REFERENCES

1   Santos, R. *et al.* A comprehensive map of molecular drug targets. *Nat Rev Drug Discov* **16**, 19-34, doi:10.1038/nrd.2016.230 (2017).

2   Julien, S. G., Dube, N., Hardy, S. & Tremblay, M. L. Inside the human cancer tyrosine phosphatome. *Nat Rev Cancer* **11**, 35-49, doi:10.1038/nrc2980 (2011).

3   Lazo, J. S. & Sharlow, E. R. Drugging undruggable molecular cancer targets. *Annu Rev Pharmacol Toxicol* **56**, 23-40, doi:10.1146/annurev-pharmtox-010715-103440 (2016).

4   Dang, C. V., Reddy, E. P., Shokat, K. M. & Soucek, L. Drugging the 'undruggable' cancer targets. *Nat Rev Cancer* **17**, 502-508, doi:10.1038/nrc.2017.36 (2017).

5   National Cancer Institute. *Cancer Statistics*, <https://www.cancer.gov/about-cancer/understanding/statistics> (2017).

6   National Cancer Institute. *SEER Cancer Stat Facts: Colon and Rectum Cancer*, <http://seer.cancer.gov/statfacts/html/colorect.html> (2016).

7   Siegel, R. L. *et al.* Colorectal cancer statistics, 2017. *CA Cancer J Clin* **67**, 177-193, doi:10.3322/caac.21395 (2017).

8   Connell, L. C., Mota, J. M., Braghiroli, M. I. & Hoff, P. M. The rising incidence of younger patients with colorectal cancer: Questions about screening, biology, and treatment. *Curr Treat Options Oncol* **18**, 23, doi:10.1007/s11864-017-0463-3 (2017).

9   Saha, S. *et al.* A phosphatase associated with metastasis of colorectal cancer. *Science* **294**, 1343-1346, doi:10.1126/science.1065817 (2001).

10   Guzinska-Ustymowicz, K. & Pryczynicz, A. PRL-3, an emerging marker of carcinogenesis, is strongly associated with poor prognosis. *Anticancer Agents Med Chem* **11**, 99-108 (2011).

11   Liang, F. *et al.* PRL3 promotes cell invasion and proliferation by down-regulation of Csk leading to Src activation. *J Biol Chem* **282**, 5413-5419, doi:10.1074/jbc.M608940200 (2007).

12   Yu, Z. H. & Zhang, Z. Y. Regulatory mechanisms and novel therapeutic targeting strategies for protein tyrosine phosphatases. *Chem Rev* **50**, 122-129, doi:10.1021/acs.chemrev.7b00105 (2017).

13   Xu, J. *et al.* VEGF promotes the transcription of the human PRL-3 gene in HUVEC through transcription factor MEF2C. *PLoS ONE* **6**, e27165, doi:10.1371/journal.pone.0027165 (2011).

14   Rouleau, C. *et al.* Protein tyrosine phosphatase PRL-3 in malignant cells and endothelial cells: expression and function. *Mol Cancer Ther* **5**, 219-229, doi:10.1158/1535-7163.MCT-05-0289 (2006).

15   Alonso, A. & Pulido, R. The extended human PTPome: a growing tyrosine phosphatase family. *Febs j* **283**, 1404-1429, doi:10.1111/febs.13600 (2016).

16   Alonso, A. *et al.* Protein tyrosine phosphatases in the human genome. *Cell* **117**, 699-711, doi:10.1016/j.cell.2004.05.018 (2004).

17   Charbonneau, H. *et al.* Human placenta protein-tyrosine-phosphatase: amino acid sequence and relationship to a family of receptor-like proteins. *Proc Natl Acad Sci U S A* **86**, 5252-5256 (1989).

18   Tonks, N. K., Diltz, C. D. & Fischer, E. H. Characterization of the major protein-tyrosine-phosphatases of human placenta. *J Biol Chem* **263**, 6731-6737 (1988).

19   Tonks, N. K., Charbonneau, H., Diltz, C. D., Fischer, E. H. & Walsh, K. A. Demonstration that the leukocyte common antigen CD45 is a protein tyrosine phosphatase. *Biochemistry* **27**, 8695-8701 (1988).

20   Chen, M. J., Dixon, J. E. & Manning, G. Genomics and evolution of protein phosphatases. *Sci Signal* **10**, doi:10.1126/scisignal.aag1796 (2017).

21   den Hollander, P. *et al.* Phosphatase PTP4A3 promotes triple-negative breast cancer growth and predicts poor patient survival. *Cancer Res* **76**, 1942-1953, doi:10.1158/0008-5472.CAN-14-0673 (2016).

22   Bollu, L. R., Mazumdar, A., Savage, M. I. & Brown, P. H. Molecular pathways: Targeting protein tyrosine phosphatases in cancer. *Clin Cancer Res* **23**, 2136-2142, doi:10.1158/1078-0432.CCR-16-0934 (2017).

23   Tonks, N. K. Protein tyrosine phosphatases--from housekeeping enzymes to master regulators of signal transduction. *Febs j* **280**, 346-378, doi:10.1111/febs.12077 (2013).

24   Hollander, M. C., Blumenthal, G. M. & Dennis, P. A. PTEN loss in the continuum of common cancers, rare syndromes and mouse models. *Nat Rev Cancer* **11**, 289-301, doi:10.1038/nrc3037 (2011).

25   Kinross, K. M. *et al.* An activating Pik3ca mutation coupled with Pten loss is sufficient to initiate ovarian tumorigenesis in mice. *J Clin Invest* **122**, 553-557, doi:10.1172/JCI59309 (2012).

26   Petrocelli, T. & Slingerland, J. M. PTEN deficiency: a role in mammary carcinogenesis. *Breast Cancer Res* **3**, 356-360 (2001).

27   Song, M. S., Salmena, L. & Pandolfi, P. P. The functions and regulation of the PTEN tumour suppressor. *Nat Rev Mol Cell Biol* **13**, 283-296, doi:10.1038/nrm3330 (2012).

28   Tarcic, G. *et al.* An unbiased screen identifies DEP-1 tumor suppressor as a phosphatase controlling EGFR endocytosis. *Curr Biol* **19**, 1788-1798, doi:10.1016/j.cub.2009.09.048 (2009).

29   Kovalenko, M. *et al.* Site-selective dephosphorylation of the platelet-derived growth factor beta-receptor by the receptor-like protein-tyrosine phosphatase DEP-1. *J Biol Chem* **275**, 16219-16226 (2000).

30   Zhai, X. *et al.* Dual specificity phosphatase 6 suppresses the growth and metastasis of prostate cancer cells. *Mol Med Rep* **10**, 3052-3058, doi:10.3892/mmr.2014.2575 (2014).

31   Bunda, S. *et al.* Inhibition of SHP2-mediated dephosphorylation of Ras suppresses oncogenesis. *Nat Commun* **6**, 8859, doi:10.1038/ncomms9859 (2015).

32   Dance, M., Montagner, A., Salles, J. P., Yart, A. & Raynal, P. The molecular functions of Shp2 in the Ras/Mitogen-activated protein kinase (ERK1/2) pathway. *Cell Signal* **20**, 453-459, doi:10.1016/j.cellsig.2007.10.002 (2008).

33   Xu, R. *et al.* Overexpression of Shp2 tyrosine phosphatase is implicated in leukemogenesis in adult human leukemia. *Blood* **106**, 3142-3149, doi:10.1182/blood-2004-10-4057 (2005).

34   Zhou, X., Coad, J., Ducatman, B. & Agazie, Y. M. SHP2 is up-regulated in breast cancer cells and in infiltrating ductal carcinoma of the breast, implying its involvement in breast oncogenesis. *Histopathology* **53**, 389-402, doi:10.1111/j.1365-2559.2008.03103.x (2008).

35   Zhou, X. D. & Agazie, Y. M. Inhibition of SHP2 leads to mesenchymal to epithelial transition in breast cancer cells. *Cell Death Differ* **15**, 988-996, doi:10.1038/cdd.2008.54 (2008).

36   Krishnan, N. *et al.* Targeting the disordered C terminus of PTP1B with an allosteric inhibitor. *Nat Chem Biol* **10**, 558-566, doi:10.1038/nchembio.1528 (2014).

37   Bentires-Alj, M. & Neel, B. G. Protein-tyrosine phosphatase 1B is required for HER2/Neu-induced breast cancer. *Cancer Res* **67**, 2420-2424, doi:10.1158/0008-5472.CAN-06-4610 (2007).

38   Hoekstra, E. *et al.* Increased PTP1B expression and phosphatase activity in colorectal cancer results in a more invasive phenotype and worse patient outcome. *Oncotarget* **7**, 21922-21938, doi:10.18632/oncotarget.7829 (2016).

39   Wang, J. *et al.* PTP1B expression contributes to gastric cancer progression. *Med Oncol* **29**, 948-956, doi:10.1007/s12032-011-9911-2 (2012).

40   Wiener, J. R. *et al.* Overexpression of the tyrosine phosphatase PTP1B is associated with human ovarian carcinomas. *Am J Obstet Gynecol* **170**, 1177-1183 (1994).

41   Wu, C. W., Kao, H. L., Li, A. F., Chi, C. W. & Lin, W. C. Protein tyrosine-phosphatase expression profiling in gastric cancer tissues. *Cancer Lett* **242**, 95-103, doi:10.1016/j.canlet.2005.10.046 (2006).

42   Fujikawa, A. *et al.* Small-molecule inhibition of PTPRZ reduces tumor growth in a rat model of glioblastoma. *Sci Rep* **6**, 20473, doi:10.1038/srep20473 (2016).

43   Fujikawa, A. *et al.* Targeting PTPRZ inhibits stem cell-like properties and tumorigenicity in glioblastoma cells. *Sci Rep* **7**, 5609, doi:10.1038/s41598-017-05931-8 (2017).

44   Bardelli, A. *et al.* PRL-3 expression in metastatic cancers. *Clin Cancer Res* **9**, 5607-5615 (2003).

45   Cramer, J. M. *et al.* Deletion of Ptp4a3 reduces clonogenicity and tumor-initiation ability of colitis-associated cancer cells in mice. *Stem Cell Res* **13**, 164-171, doi:10.1016/j.scr.2014.05.004 (2014).

46   Zimmerman, M. W., Homanics, G. E. & Lazo, J. S. Targeted deletion of the metastasis-associated phosphatase Ptp4a3 (PRL-3) suppresses murine colon cancer. *PLoS ONE* **8**, e58300, doi:10.1371/journal.pone.0058300 (2013).

47   Lazo, J. S., McQueeney, K. E. & Sharlow, E. R. New approaches to difficult drug targets: The phosphatase story. *SLAS Discov*, 2472555217721142, doi:10.1177/2472555217721142 (2017).

48   Zeng, Q. *et al.* Prenylation-dependent association of protein-tyrosine phosphatases PRL-1, -2, and -3 with the plasma membrane and the early endosome. *J Biol Chem* **275**, 21444-21452, doi:10.1074/jbc.M000453200 (2000).

49   Diamond, R. H., Cressman, D. E., Laz, T. M., Abrams, C. S. & Taub, R. PRL-1, a unique nuclear protein tyrosine phosphatase, affects cell growth. *Mol Cell Biol* **14**, 3752-3762 (1994).

50   Zeng, Q., Hong, W. & Tan, Y. H. Mouse PRL-2 and PRL-3, two potentially prenylated protein tyrosine phosphatases homologous to PRL-1. *Biochem Biophys Res Commun* **244**, 421-427, doi:10.1006/bbrc.1998.8291 (1998).

51   Sharlow, E. R., Wipf, P., McQueeney, K. E., Bakan, A. & Lazo, J. S. Investigational inhibitors of PTP4A3 phosphatase as antineoplastic agents. *Expert Opinion on Investigational Drugs* **23**, 661-673, doi:10.1517/13543784.2014.892579 (2014).

52   Sun, J. P. *et al.* Structure and biochemical properties of PRL-1, a phosphatase implicated in cell growth, differentiation, and tumor invasion. *Biochemistry* **44**, 12009-12021, doi:10.1021/bi0509191 (2005).

53   Gulerez, I. *et al.* Phosphocysteine in the PRL-CNNM pathway mediates magnesium homeostasis. *EMBO Rep* **17**, 1890-1900, doi:10.15252/embr.201643393 (2016).

54   Kozlov, G. *et al.* Structural insights into molecular function of the metastasis-associated phosphatase PRL-3. *J Biol Chem* **279**, 11882-11889, doi:10.1074/jbc.M312905200 (2004).

55   Jeong, D. G. *et al.* Trimeric structure of PRL-1 phosphatase reveals an active enzyme conformation and regulation mechanisms. *J Mol Biol* **345**, 401-413, doi:10.1016/j.jmb.2004.10.061 (2005).

56   Bai, Y. *et al.* Novel anticancer agents based on targeting the trimer interface of the PRL phosphatase. *Cancer Res* **76**, 4805-4815, doi:10.1158/0008-5472.CAN-15-2323 (2016).

57   Sun, J. P. *et al.* Phosphatase activity, trimerization, and the C-terminal polybasic region are all required for PRL1-mediated cell growth and migration. *J Biol Chem* **282**, 29043-29051, doi:10.1074/jbc.M703537200 (2007).

58   Pascaru, M. *et al.* Analysis of molecular determinants of PRL-3. *J Cell Mol Med* **13**, 3141-3150, doi:10.1111/j.1582-4934.2008.00591.x (2009).

59   Krndija, D. *et al.* The phosphatase of regenerating liver 3 (PRL-3) promotes cell migration through Arf-activity-dependent stimulation of integrin alpha5 recycling. *J Cell Sci* **125**, 3883-3892, doi:10.1242/jcs.104885 (2012).

60   Dumaual, C. M., Sandusky, G. E., Crowell, P. L. & Randall, S. K. Cellular localization of PRL-1 and PRL-2 gene expression in normal adult human tissues. *J Histochem Cytochem* **54**, 1401-1412, doi:10.1369/jhc.6A7019.2006 (2006).

61   Matter, W. F. *et al.* Role of PRL-3, a human muscle-specific tyrosine phosphatase, in angiotensin-II signaling. *Biochem Biophys Res Commun* **283**, 1061-1068, doi:10.1006/bbrc.2001.4881 (2001).

62   Bai, Y. *et al.* Role of phosphatase of regenerating liver 1 (PRL1) in spermatogenesis. *Sci Rep* **6**, 34211, doi:10.1038/srep34211 (2016).

63   Kobayashi, M. *et al.* PRL2/PTP4A2 phosphatase is important for hematopoietic stem cell self-renewal. *Stem Cells* **32**, 1956-1967, doi:10.1002/stem.1672 (2014).

64   Dong, Y. *et al.* Phosphatase of regenerating liver 2 (PRL2) is essential for placental development by down-regulating PTEN (Phosphatase and Tensin Homologue Deleted on Chromosome 10) and activating Akt protein. *J Biol Chem* **287**, 32172-32179, doi:10.1074/jbc.M112.393462 (2012).

65   Hardy, S., Wong, N. N., Muller, W. J., Park, M. & Tremblay, M. L. Overexpression of the protein tyrosine phosphatase PRL-2 correlates with breast tumor formation and progression. *Cancer Res* **70**, 8959-8967, doi:10.1158/0008-5472.Can-10-2041 (2010).

66   Kato, H. *et al.* High expression of PRL-3 promotes cancer cell motility and liver metastasis in human colorectal cancer: a predictive molecular marker of metachronous liver and lung metastases. *Clin Cancer Res* **10**, 7318-7328, doi:10.1158/1078-0432.CCR-04-0485 (2004).

67   Wang, Q., Holmes, D. I., Powell, S. M., Lu, Q. L. & Waxman, J. Analysis of stromal-epithelial interactions in prostate cancer identifies PTPCAAX2 as a potential oncogene. *Cancer Lett* **175**, 63-69 (2002).

68   Polato, F. *et al.* PRL-3 phosphatase is implicated in ovarian cancer growth. *Clinical Cancer Research* **11**, 6835-6839, doi:10.1158/1078-0432.Ccr-04-2357 (2005).

69   Fang, X. Y. *et al.* PRL-3 promotes the malignant progression of melanoma via triggering dephosphorylation and cytoplasmic localization of NHERF1. *J Invest Dermatol* **135**, 2273-2282, doi:10.1038/jid.2015.154 (2015).

70   Zhou, J. B. *et al.* Phosphatase of regenerating liver-3 is regulated by signal transducer and activator of transcription 3 in acute myeloid leukemia.

Experimental Hematology **42**, 1041-1052, doi:10.1016/j.exphem.2014.08.001 (2014).

71   Hao, R. T. *et al.* Prognostic and metastatic value of phosphatase of regenerating liver-3 in invasive breast cancer. *J Cancer Res Clin Oncol* **136**, 1349-1357, doi:10.1007/s00432-010-0786-y (2010).

72   Yamashita, S. *et al.* Down-regulation of the human PRL-3 gene is associated with the metastasis of primary non-small cell lung cancer. *Ann Thorac Cardiovasc Surg* **13**, 236-239 (2007).

73   Slordahl, T. S. *et al.* The phosphatase of regenerating liver-3 (PRL-3) is important for IL-6-mediated survival of myeloma cells. *Oncotarget* **7**, 27295-27306, doi:10.18632/oncotarget.8422 (2016).

74   Kostantin, E. *et al.* Inhibition of PRL-2.CNNM3 protein complex formation decreases breast cancer proliferation and tumor growth. *J Biol Chem* **291**, 10716-10725, doi:10.1074/jbc.M115.705863 (2016).

75   Zimmerman, M. W. *et al.* PTP4A3 phosphatase promotes VEGF signaling and enables endothelial cell motility. *J Biol Chem* **289**, 5904-5913 (2014).

76   Fiordalisi, J. J., Dewar, B. J., Graves, L. M., Madigan, J. P. & Cox, A. D. Src-mediated phosphorylation of the tyrosine phosphatase PRL-3 is required for PRL-3 promotion of Rho activation, motility and invasion. *PLoS ONE* **8**, e64309, doi:10.1371/journal.pone.0064309 (2013).

77   Wang, L. *et al.* PTP4A3 is a target for inhibition of cell proliferatin, migration and invasion through Akt/mTOR signaling pathway in glioblastoma under the regulation of miR-137. *Brain Res* **1646**, 441-450, doi:10.1016/j.brainres.2016.06.026 (2016).

78   Hassan, N. M. *et al.* Increased expression of the PRL-3 gene in human oral squamous cell carcinoma and dysplasia tissues. *Asian Pac J Cancer Prev* **12**, 947-951 (2011).

79   Dong, Q., Ding, X., Chang, B., Wang, H. & Wang, A. PRL-3 promotes migration and invasion and is associated with poor prognosis in salivary adenoid cystic carcinoma. *J Oral Pathol Med* **45**, 111-118, doi:10.1111/jop.12331 (2016).

80   Stevenson, W. S. *et al.* DNA methylation of membrane-bound tyrosine phosphatase genes in acute lymphoblastic leukaemia. *Leukemia* **28**, 787-793, doi:10.1038/leu.2013.270 (2014).

81   Kobayashi, M. *et al.* Phosphatase of regenerating liver in hematopoietic stem cells and hematological malignancies. *Cell Cycle* **13**, 2827-2835, doi:10.4161/15384101.2014.954448 (2014).

82   Park, J. E. *et al.* Oncogenic roles of PRL-3 in FLT3-ITD induced acute myeloid leukaemia. *EMBO Mol Med* **5**, 1351-1366, doi:10.1002/emmm.201202183 (2013).

83   Zhou, J. *et al.* PRL-3, a metastasis associated tyrosine phosphatase, is involved in FLT3-ITD signaling and implicated in anti-AML therapy. *PLoS ONE* **6**, e19798, doi:10.1371/journal.pone.0019798 (2011).

84   Jin, S. *et al.* Oncogenic function and prognostic significance of protein tyrosine phosphatase PRL-1 in hepatocellular carcinoma. *Oncotarget* **5**, 3685-3696, doi:10.18632/oncotarget.1986 (2014).

85   Mayinuer, A. *et al.* Upregulation of protein tyrosine phosphatase type IVA member 3 (PTP4A3/PRL-3) is associated with tumor differentiation and a poor prognosis in human hepatocellular carcinoma. *Ann Surg Oncol* **20**, 305-317, doi:10.1245/s10434-012-2395-2 (2013).

86   Zhao, W. B., Li, Y., Liu, X., Zhang, L. Y. & Wang, X. Evaluation of PRL-3 expression, and its correlation with angiogenesis and invasion in hepatocellular carcinoma. *Int J Mol Med* **22**, 187-192 (2008).

87   Stephens, B., Han, H., Hostetter, G., Demeure, M. J. & Von Hoff, D. D. Small interfering RNA-mediated knockdown of PRL phosphatases results in altered Akt phosphorylation and reduced clonogenicity of pancreatic cancer cells. *Mol Cancer Ther* **7**, 202-210, doi:10.1158/1535-7163.MCT-07-0542 (2008).

88   Liu, H. G. *et al.* PRL-3 suppresses c-FOS and integrin a2 expression in ovarian cancer cells. *BMC Cancer* **13**, 80 (2013).

89   Reich, R., Hadar, S. & Davidson, B. Expression and clinical role of protein of regenerating liver (PRL) phosphatases in ovarian carcinoma. *Int J Mol Sci* **12**, 1133-1145, doi:10.3390/ijms12021133 (2011).

90   Yeh, H. C. *et al.* Overexpression of PTP4A3 is associated with metastasis and unfavorable prognosis in bladder cancer. *World J Urol* **34**, 835-846, doi:10.1007/s00345-015-1698-x (2016).

91   Foy, M., Anezo, O., Saule, S. & Planque, N. PRL-3/PTP4A3 phosphatase regulates integrin beta1 in adhesion structures during migration of human ocular melanoma cells. *Exp Cell Res* **353**, 88-99, doi:10.1016/j.yexcr.2017.03.012 (2017).

92   Laurent, C. *et al.* High PTP4A3 phosphatase expression correlates with metastatic risk in uveal melanoma patients. *Cancer Res* **71**, 666-674, doi:10.1158/0008-5472.CAN-10-0605 (2011).

93   Qian, F. *et al.* PRL-3 siRNA inhibits the metastasis of B16-BL6 mouse melanoma cells in vitro and in vivo. *Mol Med* **13**, 151-159, doi:10.2119/2006-00076.Qian (2007).

94   Pathak, M. K. *et al.* Pentamidine is an inhibitor of PRL phosphatases with anticancer activity. *Mol Cancer Ther* **1**, 1255-1264 (2002).

95   Strilic, B. & Offermanns, S. Intravascular survival and extravasation of tumor cells. *Cancer Cell* **32**, 282-293, doi:10.1016/j.ccell.2017.07.001 (2017).

96   Hwang, J. J. *et al.* Altered expression of phosphatase of regenerating liver gene family in non-small cell lung cancer. *Oncol Rep* **27**, 535-540, doi:10.3892/or.2011.1495 (2012).

97   Wang, Y. & Lazo, J. S. Metastasis-associated phosphatase PRL-2 regulates tumor cell migration and invasion. *Oncogene* **31**, 818-827, doi:10.1038/onc.2011.281 (2012).

98   Ming, J., Liu, N., Gu, Y., Qiu, X. & Wang, E. H. PRL-3 facilitates angiogenesis and metastasis by increasing ERK phosphorylation and up-regulating the levels and activities of Rho-A/C in lung cancer. *Pathology* **41**, 118-126, doi:10.1080/00313020802579268 (2009).

99   Achiwa, H. & Lazo, J. S. PRL-1 tyrosine phosphatase regulates c-Src levels, adherence, and invasion in human lung cancer cells. *Cancer Res* **67**, 643-650, doi:10.1158/0008-5472.CAN-06-2436 (2007).

100   Gari, H. H., DeGala, G. D., Lucia, M. S. & Lambert, J. R. Loss of the oncogenic phosphatase PRL-3 promotes a TNF-R1 feedback loop that mediates triple-negative breast cancer growth. *Oncogenesis* **5**, e255, doi:10.1038/oncsis.2016.50 (2016).

101   Gari, H. H., DeGala, G. D., Ray, R., Lucia, M. S. & Lambert, J. R. PRL-3 engages the focal adhesion pathway in triple-negative breast cancer cells to alter actin structure and substrate adhesion properties critical for cell migration and invasion. *Cancer Lett* **380**, 505-512, doi:10.1016/j.canlet.2016.07.017 (2016).

102   Flores-Perez, A. *et al.* Suppression of cell migration is promoted by miR-944 through targeting of SIAH1 and PTP4A1 in breast cancer cells. *BMC Cancer* **16**, 379, doi:10.1186/s12885-016-2470-3 (2016).

103   Zhao, D. *et al.* The prognostic significance of protein tyrosine phosphatase 4A2 in breast cancer. *Onco Targets Ther* **8**, 1707-1717, doi:10.2147/OTT.S85899 (2015).

104   Radke, I. *et al.* Expression and prognostic impact of the protein tyrosine phosphatases PRL-1, PRL-2, and PRL-3 in breast cancer. *Br J Cancer* **95**, 347-354, doi:10.1038/sj.bjc.6603261 (2006).

105   Yeh, H. C. *et al.* PTP4A3 independently predicts metastasis and survival in upper tract urothelial carcinoma treated with radical nephroureterectomy. *J Urol* **194**, 1449-1455, doi:10.1016/j.juro.2015.05.101 (2015).

106   Li, J. *et al.* Generation of PRL-3- and PRL-1-specific monoclonal antibodies as potential diagnostic markers for cancer metastases. *Clin Cancer Res* **11**, 2195-2204, doi:10.1158/1078-0432.CCR-04-1984 (2005).

107   Andersen, S. *et al.* Expression of phosphatase of regenerating liver (PRL)-3, is independently associated with biochemical failure, clinical failure and death in prostate cancer. *PLoS ONE* **12**, e0189000, doi:10.1371/journal.pone.0189000 (2017).

108   Vandsemb, E. N. *et al.* Phosphatase of regenerating liver 3 (PRL-3) is overexpressed in human prostate cancer tissue and promotes growth and migration. *J Transl Med* **14**, 71, doi:10.1186/s12967-016-0830-z (2016).

109   Xiong, J. *et al.* PRL-3 promotes the peritoneal metastasis of gastric cancer through the PI3K/Akt signaling pathway by regulating PTEN. *Oncol Rep* **36**, 1819-1828, doi:10.3892/or.2016.5030 (2016).

110   Ooki, A. *et al.* Therapeutic potential of PRL-3 targeting and clinical significance of PRL-3 genomic amplification in gastric cancer. *BMC Cancer* **11**, 122, doi:10.1186/1471-2407-11-122 (2011).

111   Bessette, D. C., Qiu, D. & Pallen, C. J. PRL PTPs: mediators and markers of cancer progression. *Cancer Metastasis Rev* **27**, 231-252, doi:10.1007/s10555-008-9121-3 (2008).

112   Thura, M. *et al.* PRL3-zumab, a first-in-class humanized antibody for cancer therapy. *JCI Insight* **1**, e87607, doi:10.1172/jci.insight.87607 (2016).

113   Kim, N. W. *et al.* Correlation between liver metastases and the level of PRL-3 mRNA expression in patients with primary colorectal cancer. *J Korean Soc Coloproctol* **27**, 231-236, doi:10.3393/jksc.2011.27.5.231 (2011).

114   Mollevi, D. G. *et al.* PRL-3 is essentially overexpressed in primary colorectal tumours and associates with tumour aggressiveness. *Br J Cancer* **99**, 1718-1725, doi:10.1038/sj.bjc.6604747 (2008).

115   Wang, Y. *et al.* Expression of the human phosphatases of regenerating liver (PRLs) in colonic adenocarcinoma and its correlation with lymph node metastasis. *Int J Colorectal Dis* **22**, 1179-1184, doi:10.1007/s00384-007-0303-1 (2007).

116   Wang, H. *et al.* PRL-3 down-regulates PTEN expression and signals through PI3K to promote epithelial-mesenchymal transition. *Cancer Res* **67**, 2922-2926, doi:10.1158/0008-5472.CAN-06-3598 (2007).

117   Abdollahi, P. *et al.* Src family kinases are regulated in multiple myeloma cells by phosphatase of regenerating liver-3. *Mol Cancer Res* **15**, 69-77, doi:10.1158/1541-7786.MCR-16-0212 (2017).

118   Jiang, Y. *et al.* Phosphatase PRL-3 is a direct regulatory target of TGFbeta in colon cancer metastasis. *Cancer Res* **71**, 234-244 (2011).

119   Massague, J. TGFbeta in Cancer. *Cell* **134**, 215-230, doi:10.1016/j.cell.2008.07.001 (2008).

120   Basak, S. *et al.* The metastasis-associated gene Prl-3 is a p53 target involved in cell-cycle regulation. *Mol Cell* **30**, 303-314, doi:10.1016/j.molcel.2008.04.002 (2008).

121   Zheng, P. *et al.* Snail as a key regulator of PRL-3 gene in colorectal cancer. *Cancer Biol Ther* **12**, 742-749, doi:10.4161/cbt.12.8.15981 (2011).

122   Liu, Y. *et al.* PRL-3 promotes epithelial mesenchymal transition by regulating cadherin directly. *Cancer Biol Ther* **8**, 1352-1359 (2009).

123   Yu, H. & Jove, R. The STATs of cancer--new molecular targets come of age. *Nat Rev Cancer* **4**, 97-105, doi:10.1038/nrc1275 (2004).

124   Wang, H. *et al.* PCBP1 suppresses the translation of metastasis-associated PRL-3 phosphatase. *Cancer Cell* **18**, 52-62, doi:10.1016/j.ccr.2010.04.028 (2010).

125   Rubio, T. & Kohn, M. Regulatory mechanisms of phosphatase of regenerating liver (PRL)-3. *Biochem Soc Trans* **44**, 1305-1312, doi:10.1042/BST20160146 (2016).

126   Choi, M. S. *et al.* The essential role of FKBP38 in regulating phosphatase of regenerating liver 3 (PRL-3) protein stability. *Biochem Biophys Res Commun* **406**, 305-309, doi:10.1016/j.bbrc.2011.02.037 (2011).

127   Xing, C. *et al.* Ubiquitin-specific protease 4-mediated deubiquitination and stabilization of PRL-3 is required for potentiating colorectal oncogenesis. *Cancer Res* **76**, 83-95, doi:10.1158/0008-5472.CAN-14-3595 (2016).

128   Liang, F. *et al.* Translational control of C-terminal Src kinase (Csk) expression by PRL3 phosphatase. *J Biol Chem* **283**, 10339-10346, doi:10.1074/jbc.M708285200 (2008).

129   Orsatti, L. *et al.* 2-D Difference in gel electrophoresis combined with Pro-Q Diamond staining: a successful approach for the identification of kinase/phosphatase targets. *Electrophoresis* **30**, 2469-2476, doi:10.1002/elps.200800780 (2009).

130   Al-Aidaroos, A. Q. *et al.* Metastasis-associated PRL-3 induces EGFR activation and addiction in cancer cells. *J Clin Invest* **123**, 3459-3471, doi:10.1172/JCI66824 (2013).

131   Walls, C. D. *et al.* Phosphatase of regenerating liver 3 (PRL3) provokes a tyrosine phosphoproteome to drive prometastatic signal transduction. *Mol Cell Proteomics* **12**, 3759-3777, doi:10.1074/mcp.M113.028886 (2013).

132   Orgaz, J. L., Herraiz, C. & Sanz-Moreno, V. Rho GTPases modulate malignant transformation of tumor cells. *Small GTPases* **5**, e29019, doi:10.4161/sgtp.29019 (2014).

133   Parri, M. & Chiarugi, P. Rac and Rho GTPases in cancer cell motility control. *Cell Commun Signal* **8**, 23, doi:10.1186/1478-811X-8-23 (2010).

134   Fiordalisi, J. J., Keller, P. J. & Cox, A. D. PRL tyrosine phosphatases regulate rho family GTPases to promote invasion and motility. *Cancer Res* **66**, 3153-3161, doi:10.1158/0008-5472.CAN-05-3116 (2006).

135   Huang, Y. H. *et al.* A role of autophagy in PTP4A3-driven cancer progression. *Autophagy* **10**, 1787-1800, doi:10.4161/auto.29989 (2014).

136   Sun, Z. H. & Bu, P. Downregulation of phosphatase of regenerating liver-3 is involved in the inhibition of proliferation and apoptosis induced by emodin in the SGC-7901 human gastric carcinoma cell line. *Exp Ther Med* **3**, 1077-1081, doi:10.3892/etm.2012.516 (2012).

137   Sun, W. *et al.* Increased expression of GATA zinc finger domain containing 1 via gene amplification promotes liver cancer by directly inducing PRL3. *Hepatology*, doi:10.1002/hep.29750 (2017).

138   Daouti, S. *et al.* A selective phosphatase of regenerating liver phosphatase inhibitor suppresses tumor cell anchorage-independent growth by a novel

mechanism involving p130Cas cleavage. *Cancer Res* **68**, 1162-1169, doi:10.1158/0008-5472.CAN-07-2349 (2008).

139   Casanova, I. *et al.* Celecoxib induces anoikis in human colon carcinoma cells associated with the deregulation of focal adhesions and nuclear translocation of p130Cas. *Int J Cancer* **118**, 2381-2389, doi:10.1002/ijc.21662 (2006).

140   Min, S. H. *et al.* Downregulation of p53 by phosphatase of regenerating liver 3 is mediated by MDM2 and PIRH2. *Life Sci* **86**, 66-72, doi:10.1016/j.lfs.2009.11.010 (2010).

141   Lian, S. *et al.* PRL-3 activates NF-κB signaling pathway by interacting with RAP1. *Biochem Biophys Res Commun* **430**, 196-201 (2012).

142   Xu, H. *et al.* Tumor-associated macrophage-derived IL-6 and IL-8 enhance invasive activity of LoVo cells induced by PRL-3 in a KCNN4 channel-dependent manner. *BMC Cancer* **14**, 330, doi:10.1186/1471-2407-14-330 (2014).

143   Maacha, S. *et al.* Protein tyrosine phosphatase 4A3 (PTP4A3) promotes human uveal melanoma aggressiveness through membrane accumulation of matrix metalloproteinase 14 (MMP14). *Invest Ophthalmol Vis Sci* **57**, 1982-1990, doi:10.1167/iovs.15-18780 (2016).

144   Peng, L. *et al.* PRL-3 promotes the motility, invasion, and metastasis of LoVo colon cancer cells through PRL-3-integrin beta1-ERK1/2 and-MMP2 signaling. *Mol Cancer* **8**, 110, doi:10.1186/1476-4598-8-110 (2009).

145   Lee, S. K. *et al.* Phosphatase of regenerating liver-3 promotes migration and invasion by upregulating matrix metalloproteinases-7 in human colorectal cancer cells. *Int J Cancer* **131**, E190-203, doi:10.1002/ijc.27381 (2012).

146   Radke, I. *et al.* Expression of PRL-3 regulates proliferation and invasion of breast cancer cells in vitro. *Arch Gynecol Obstet* **296**, 1153-1160, doi:10.1007/s00404-017-4542-2 (2017).

147   Peng, L. *et al.* Identification of integrin alpha1 as an interacting protein of protein tyrosine phosphatase PRL-3. *Biochem Biophys Res Commun* **342**, 179-183, doi:10.1016/j.bbrc.2006.01.102 (2006).

148   Tian, W. *et al.* Phosphatase of regenerating liver-3 directly interacts with integrin beta1 and regulates its phosphorylation at tyrosine 783. *BMC Biochem* **13**, 22, doi:10.1186/1471-2091-13-22 (2012).

149   Forte, E. *et al.* Ezrin is a specific and direct target of protein tyrosine phosphatase PRL-3. *Biochim Biophys Acta* **1783**, 334-344, doi:10.1016/j.bbamcr.2007.11.004 (2008).

150   Khanna, C. *et al.* The membrane-cytoskeleton linker ezrin is necessary for osteosarcoma metastasis. *Nat Med* **10**, 182-186, doi:10.1038/nm982 (2004).

151   McParland, V. *et al.* The metastasis-promoting phosphatase PRL-3 shows activity toward phosphoinositides. *Biochemistry* **50**, 7579-7590, doi:10.1021/bi201095z (2011).

152   Khapare, N. *et al.* Plakophilin3 loss leads to an increase in PRL3 levels promoting K8 dephosphorylation, which is required for transformation and metastasis. *PLoS ONE* **7**, e38561, doi:10.1371/journal.pone.0038561 (2012).

153   Mizuuchi, E., Semba, S., Kodama, Y. & Yokozaki, H. Down-modulation of keratin 8 phosphorylation levels by PRL-3 contributes to colorectal carcinoma progression. *Int J Cancer* **124**, 1802-1810, doi:10.1002/ijc.24111 (2009).

154   Lamouille, S., Xu, J. & Derynck, R. Molecular mechanisms of epithelial-mesenchymal transition. *Nat Rev Mol Cell Biol* **15**, 178-196, doi:10.1038/nrm3758 (2014).

155   Hardy, S. *et al.* The protein tyrosine phosphatase PRL-2 interacts with the magnesium transporter CNNM3 to promote oncogenesis. *Oncogene* **34**, 986-995, doi:10.1038/onc.2014.33 (2015).

156   Zhang, H. *et al.* PRL3 phosphatase active site is required for binding the putative magnesium transporter CNNM3. *Sci Rep* **7**, 48, doi:10.1038/s41598-017-00147-2 (2017).

157   Hirata, Y., Funato, Y., Takano, Y. & Miki, H. Mg2+-dependent interactions of ATP with the cystathionine-beta-synthase (CBS) domains of a magnesium transporter. *J Biol Chem* **289**, 14731-14739, doi:10.1074/jbc.M114.551176 (2014).

158   Funato, Y. *et al.* Membrane protein CNNM4-dependent Mg2+ efflux suppresses tumor progression. *J Clin Invest* **124**, 5398-5410, doi:10.1172/JCI76614 (2014).

159   Wolf, F. I. & Trapani, V. Magnesium and its transporters in cancer: a novel paradigm in tumour development. *Clin Sci (Lond)* **123**, 417-427, doi:10.1042/CS20120086 (2012).

160   Castiglioni, S. & Maier, J. A. Magnesium and cancer: a dangerous liason. *Magnes Res* **24**, S92-100, doi:10.1684/mrh.2011.0285 (2011).

161   Xu, H. *et al.* PRL-3 improves colorectal cancer cell proliferation and invasion through IL-8 mediated glycolysis metabolism. *Int J Oncol* **51**, 1271-1279, doi:10.3892/ijo.2017.4090 (2017).

162   Hanahan, D. & Weinberg, R. A. Hallmarks of cancer: the next generation. *Cell* **144**, 646-674, doi:10.1016/j.cell.2011.02.013 (2011).

163   Ye, Z. *et al.* PRL-3 activates mTORC1 in cancer progression. *Sci Rep* **5**, 17046, doi:10.1038/srep17046 (2015).

164   Parker, B. S. *et al.* Alterations in vascular gene expression in invasive breast carcinoma. *Cancer Res* **64**, 7857-7866, doi:10.1158/0008-5472.CAN-04-1976 (2004).

165   Folkman, J. Tumor angiogenesis: therapeutic implications. *N Engl J Med* **285**, 1182-1186, doi:10.1056/NEJM197111182852108 (1971).

166   Folkman, J. & Shing, Y. Angiogenesis. *J Biol Chem* **267**, 10931-10934 (1992).

167   Hicklin, D. J. & Ellis, L. M. Role of the vascular endothelial growth factor pathway in tumor growth and angiogenesis. *J Clin Oncol* **23**, 1011-1027, doi:10.1200/JCO.2005.06.081 (2005).

168   Hanahan, D. & Weinberg, R. A. The hallmarks of cancer. *Cell* **100**, 57-70 (2000).

169   Ferrara, N. Vascular endothelial growth factor: basic science and clinical progress. *Endocr Rev* **25**, 581-611, doi:10.1210/er.2003-0027 (2004).

170   Hurwitz, H. *et al.* Bevacizumab plus irinotecan, fluorouracil, and leucovorin for metastatic colorectal cancer. *N Engl J Med* **350**, 2335-2342, doi:10.1056/NEJMoa032691 (2004).

171   Marques, I., Araujo, A. & de Mello, R. A. Anti-angiogenic therapies for metastatic colorectal cancer: current and future perspectives. *World J Gastroenterol* **19**, 7955-7971, doi:10.3748/wjg.v19.i44.7955 (2013).

172   Wu, P., Nielsen, T. E. & Clausen, M. H. Small-molecule kinase inhibitors: an analysis of FDA-approved drugs. *Drug Discov Today* **21**, 5-10, doi:10.1016/j.drudis.2015.07.008 (2016).

173   Wang, Z. *et al.* Mutational analysis of the tyrosine phosphatome in colorectal cancers. *Science* **304**, 1164-1166, doi:10.1126/science.1096096 (2004).

174   Feldhammer, M., Uetani, N., Miranda-Saavedra, D. & Tremblay, M. L. PTP1B: a simple enzyme for a complex world. *Crit Rev Biochem Mol Biol* **48**, 430-445, doi:10.3109/10409238.2013.819830 (2013).

175   Zhu, S., Bjorge, J. D. & Fujita, D. J. PTP1B contributes to the oncogenic properties of colon cancer cells through Src activation. *Cancer Res* **67**, 10129-10137, doi:10.1158/0008-5472.CAN-06-4338 (2007).

176   Ran, H., Tsutsumi, R., Araki, T. & Neel, B. G. Sticking it to cancer with molecular glue for SHP2. *Cancer Cell* **30**, 194-196, doi:10.1016/j.ccell.2016.07.010 (2016).

177   Gagne-Sansfacon, J. *et al.* SHP-2 phosphatase contributes to KRAS-driven intestinal oncogenesis but prevents colitis-associated cancer development. *Oncotarget* **7**, 65676-65695, doi:10.18632/oncotarget.11601 (2016).

178   Hui, E. *et al.* T cell costimulatory receptor CD28 is a primary target for PD-1-mediated inhibition. *Science* **355**, 1428-1433, doi:10.1126/science.aaf1292 (2017).

179   Chen, Y. N. *et al.* Allosteric inhibition of SHP2 phosphatase inhibits cancers driven by receptor tyrosine kinases. *Nature* **535**, 148-152, doi:10.1038/nature18621 (2016).

180   Lazo, J. S., McQueeney, K. E., Burnett, J. C., Wipf, P. & Sharlow, E. R. Small molecule targeting of PTPs in cancer. *Int J Biochem Cell Biol*, doi:10.1016/j.biocel.2017.09.011 (2017).

181   Han, Y. M. *et al.* Emodin inhibits migration and invasion of DLD-1 (PRL-3) cells via inhibition of PRL-3 phosphatase activity. *Bioorg Med Chem Lett* **22**, 323-326, doi:10.1016/j.bmcl.2011.11.008 (2012).

182   Min, G. *et al.* Rhodanine-based PRL-3 inhibitors blocked the migration and invasion of metastatic cancer cells. *Bioorg Med Chem Lett* **23**, 3769-3774, doi:10.1016/j.bmcl.2013.04.092 (2013).

183   Ahn, J. H. *et al.* Synthesis and biological evaluation of rhodanine derivatives as PRL-3 inhibitors. *Bioorg Med Chem Lett* **16**, 2996-2999, doi:10.1016/j.bmcl.2006.02.060 (2006).

184   Xia, X. *et al.* Image-based chemical screening identifies drug efflux inhibitors in lung cancer cells. *Cancer Res* **70**, 7723-7733, doi:10.1158/0008-5472.CAN-09-4360 (2010).

185   Choi, S. K. *et al.* Biflavonoids inhibited phosphatase of regenerating liver-3 (PRL-3). *Nat Prod Res* **20**, 341-346, doi:10.1080/14786410500463312 (2006).

186   Hoeger, B., Diether, M., Ballester, P. J. & Kohn, M. Biochemical evaluation of virtual screening methods reveals a cell-active inhibitor of the cancer-promoting phosphatases of regenerating liver. *Eur J Med Chem* **88**, 89-100, doi:10.1016/j.ejmech.2014.08.060 (2014).

187   Bai, Y., Yu, Z. H. & Zhang, Z. Y. Discovery and evaluation of PRL trimer disruptors for novel anticancer agents. *Methods Mol Biol* **1447**, 121-138, doi:10.1007/978-1-4939-3746-2_8 (2016).

188   Kaelin, W. G., Jr. Common pitfalls in preclinical cancer target validation. *Nat Rev Cancer* **17**, 425-440, doi:10.1038/nrc.2017.32 (2017).

189   Catravas, J. D. *et al.* Harvesting, identification and barrier function of human lung microvascular endothelial cells. *Vascul Pharmacol* **52**, 175-181, doi:10.1016/j.vph.2009.12.009 (2010).

190   Salamoun, J. M. *et al.* Photooxygenation of an amino-thienopyridone yields a more potent PTP4A3 inhibitor. *Org Biomol Chem* **14**, 6398-6402, doi:10.1039/c6ob00946h (2016).

191   Burnett, J. C. *et al.* A threonine turnstile defines a dynamic amphiphilic binding motif in the AAA ATPase p97 allosteric binding site. *Org Biomol Chem* **15**, 4096-4114, doi:10.1039/c7ob00526a (2017).

192   George Rosenker, K. M. *et al.* Synthesis and biological evaluation of 3-aminoisoquinolin-1(2H)-one based inhibitors of the dual-specificity phosphatase Cdc25B. *Bioorg Med Chem* **23**, 2810-2818, doi:10.1016/j.bmc.2015.01.043 (2015).

193   Almo, S. C. *et al.* Structural genomics of protein phosphatases. *J Struct Funct Genomics* **8**, 121-140, doi:10.1007/s10969-007-9036-1 (2007).

194   St-Denis, N. *et al.* Phenotypic and interaction profiling of the human phosphatases identifies diverse mitotic regulators. *Cell Rep* **17**, 2488-2501, doi:10.1016/j.celrep.2016.10.078 (2016).

195   Huynh, K. & Partch, C. L. Analysis of protein stability and ligand interactions by thermal shift assay. *Curr Protoc Protein Sci* **79**, 28 29 21-14, doi:10.1002/0471140864.ps2809s79 (2015).

196   Barabutis, N. *et al.* p53 protects against LPS-induced lung endothelial barrier dysfunction. *Am J Physiol Lung Cell Mol Physiol* **308**, L776-787, doi:10.1152/ajplung.00334.2014 (2015).

197   Barabutis, N. *et al.* LPS induces pp60c-src-mediated tyrosine phosphorylation of Hsp90 in lung vascular endothelial cells and mouse lung. *Am J Physiol Lung Cell Mol Physiol* **304**, L883-893, doi:10.1152/ajplung.00419.2012 (2013).

198   Chen, J. & Huang, X. F. The signal pathways in azoxymethane-induced colon cancer and preventive implications. *Cancer Biol Ther* **8**, 1313-1317 (2009).

199   De Robertis, M. *et al.* The AOM/DSS murine model for the study of colon carcinogenesis: From pathways to diagnosis and therapy studies. *J Carcinog* **10**, 9, doi:10.4103/1477-3163.78279 (2011).

200   Saiga, T., Ohbayashi, T., Tabuchi, K. & Midorikawa, O. A model for
        tumorigenicity and metastatic potential: growth in 1.0% agar cultures. *In Vitro*
        Cell Dev Biol **23**, 850-854 (1987).

201   Zanoni, M. *et al.* 3D tumor spheroid models for in vitro therapeutic screening: a
        systematic approach to enhance the biological relevance of data obtained.
        Scientific Reports **6**, 19103, doi:ARTN 19103
10.1038/srep19103 (2016).

202   Chambers, A. F., Groom, A. C. & MacDonald, I. C. Dissemination and growth of
        cancer cells in metastatic sites. *Nat Rev Cancer* **2**, 563-572, doi:10.1038/nrc865
        (2002).

203   Hynes, R. O. The extracellular matrix: not just pretty fibrils. *Science* **326**, 1216-
        1219, doi:10.1126/science.1176009 (2009).

204   Zanetti, M. *et al.* EMILIN-1 deficiency induces elastogenesis and vascular cell
        defects. *Mol Cell Biol* **24**, 638-650 (2004).

205   Rabajdova, M. *et al.* The crucial role of emilin 1 gene expression during
        progression of tumor growth. *J Cancer Res Clin Oncol* **142**, 2397-2402,
        doi:10.1007/s00432-016-2226-0 (2016).

206   Cimmperman, P. *et al.* A quantitative model of thermal stabilization and
        destabilization of proteins by ligands. *Biophys J* **95**, 3222-3231,
        doi:10.1529/biophysj.108.134973 (2008).

207   Jeong, K. W. *et al.* Structure and backbone dynamics of vanadate-bound PRL-3:
        comparison of 15N nuclear magnetic resonance relaxation profiles of free and
        vanadate-bound PRL-3. *Biochemistry* **53**, 4814-4825, doi:10.1021/bi5003844
        (2014).

208   McQueeney, K. E. *et al.* Targeting ovarian cancer and endothelium with an
        allosteric PTP4A3 phosphatase inhibitor. *Oncotarget* **9**, 8223-8240,
        doi:10.18632/oncotarget.23787 (2018).

209   Tyurina, Y. Y. *et al.* Oxidative lipidomics of gamma-radiation-induced lung
        injury: mass spectrometric characterization of cardiolipin and phosphatidylserine
        peroxidation. *Radiat Res* **175**, 610-621, doi:10.1667/RR2297.1 (2011).

210   Sun, Z. *et al.* VEGFR2 induces c-Src signaling and vascular permeability in vivo via the adaptor protein TSAd. *J Exp Med* **209**, 1363-1377, doi:10.1084/jem.20111343 (2012).

211   Weis, S., Cui, J., Barnes, L. & Cheresh, D. Endothelial barrier disruption by VEGF-mediated Src activity potentiates tumor cell extravasation and metastasis. *J Cell Biol* **167**, 223-229, doi:10.1083/jcb.200408130 (2004).

212   Rafikov, R. *et al.* Lipopolysaccharide-induced lung injury involves the nitration-mediated activation of RhoA. *J Biol Chem* **289**, 4710-4722, doi:10.1074/jbc.M114.547596 (2014).

213   Nagy, J. A., Dvorak, A. M. & Dvorak, H. F. Vascular hyperpermeability, angiogenesis, and stroma generation. *Cold Spring Harb Perspect Med* **2**, a006544, doi:10.1101/cshperspect.a006544 (2012).

214   Eliceiri, B. P. *et al.* Selective requirement for Src kinases during VEGF-induced angiogenesis and vascular permeability. *Mol Cell* **4**, 915-924 (1999).

215   Li, X. *et al.* VEGFR2 pY949 signalling regulates adherens junction integrity and metastatic spread. *Nat Commun* **7**, 11017, doi:10.1038/ncomms11017 (2016).

216   Garcia-Roman, J. & Zentella-Dehesa, A. Vascular permeability changes involved in tumor metastasis. *Cancer Lett* **335**, 259-269, doi:10.1016/j.canlet.2013.03.005 (2013).

217   Miles, A. A. & Miles, E. M. Vascular reactions to histamine, histamine-liberator and leukotaxine in the skin of guinea-pigs. *J Physiol* **118**, 228-257 (1952).

218   Auerbach, R., Akhtar, N., Lewis, R. L. & Shinners, B. L. Angiogenesis assays: problems and pitfalls. *Cancer Metastasis Rev* **19**, 167-172 (2000).

219   Adam, A. P., Lowery, A. M., Martino, N., Alsaffar, H. & Vincent, P. A. Src family kinases modulate the loss of endothelial barrier function in response to TNF-α: Crosstalk with p38 signaling. *PLoS ONE* **11**, e0161975, doi:10.1371/journal.pone.0161975 (2016).

220   Mollevi, D. G. *et al.* PRL-3 is essentially overexpressed in primary colorectal tumours and associates with tumour aggressiveness. *Br J Cancer* **99**, 1718-1725, doi:10.1038/sj.bjc.6604747 (2008).

221   Bardelli A, S. S., Sager JA, Romans KE, Xin B, Markowitz SD, Lengauer C, Velculescu VE, Kinzler KW, Vogelstein B. PRL-3 expression in metastatic cancers. *Clin Cancer Res* **9**, 5607-5615 (2003).

222   Song, R. *et al.* Phosphatase of regenerating liver-3 localizes to cyto-membrane and is required for B16F1 melanoma cell metastasis in vitro and in vivo. *PLoS ONE* **4**, e4450, doi:10.1371/journal.pone.0004450 (2009).

223   Yang, Y., Lian, S., Meng, L., Qu, L. & Shou, C. Antibody array revealed PRL-3 affects protein phosphorylation and cytokine secretion. *PLoS ONE* **12**, e0169665, doi:10.1371/journal.pone.0169665 (2017).

224   Taddei, M. L., Giannoni, E., Fiaschi, T. & Chiarugi, P. Anoikis: an emerging hallmark in health and diseases. *J Pathol* **226**, 380-393, doi:10.1002/path.3000 (2012).

225   Lai, W. *et al.* KCNN4 channels participate in the EMT induced by PRL-3 in colorectal cancer. *Med Oncol* **30**, 566, doi:10.1007/s12032-013-0566-z (2013).

226   Danussi, C. *et al.* An EMILIN1-negative microenvironment promotes tumor cell proliferation and lymph node invasion. *Cancer Prev Res (Phila)* **5**, 1131-1143, doi:10.1158/1940-6207.CAPR-12-0076-T (2012).

227   Xu, Z., Chen, H., Liu, D. & Huo, J. Fibulin-1 is downregulated through promoter hypermethylation in colorectal cancer: a CONSORT study. *Medicine (Baltimore)* **94**, e663, doi:10.1097/MD.0000000000000663 (2015).

228   Geiger, B., Bershadsky, A., Pankov, R. & Yamada, K. M. Transmembrane crosstalk between the extracellular matrix--cytoskeleton crosstalk. *Nat Rev Mol Cell Biol* **2**, 793-805, doi:10.1038/35099066 (2001).

229   Zhang, B., Zhang, Y., Wang, Z. & Zheng, Y. The role of Mg2+ cofactor in the guanine nucleotide exchange and GTP hydrolysis reactions of Rho family GTP-binding proteins. *J Biol Chem* **275**, 25299-25307, doi:10.1074/jbc.M001027200 (2000).

230   Dejana, E., Orsenigo, F. & Lampugnani, M. G. The role of adherens junctions and VE-cadherin in the control of vascular permeability. *J Cell Sci* **121**, 2115-2122, doi:10.1242/jcs.017897 (2008).

231   Shaw, T. J., Senterman, M. K., Dawson, K., Crane, C. A. & Vanderhyden, B. C. Characterization of intraperitoneal, orthotopic, and metastatic xenograft models of human ovarian cancer. *Mol Ther* **10**, 1032-1042, doi:10.1016/j.ymthe.2004.08.013 (2004).

232   DeDonatis, A. *et al.* Proliferaition versus migration in platelet-derived growth factor signaling. *J Biol Chem* **283**, 19948-19956 (2008).